NON-FARADAIC ELECTROCHEMICAL MODIFICATION OF CATALYTIC ACTIVITY

(NEMCA) OF PROPANE OXIDATION ON Pt/YSZ THIN FILM CELL

Mr. Wanchana Lelalertsupakul

A Thesis Submitted in Partial Fulfillment of the Requirements

for the Degree of Master of Engineering in Chemical Engineering

Department of Chemical Engineering

Faculty of Engineering

Chulalongkorn University

Academic Year 2019

การปรับปรุงความว่องไวของตัวเร่งปฏิกิริยาด้วยวิธีทางไฟฟ้าเคมีที่ไม่เป็นไปตามกฎของฟาราเดย์
ของการออกซิชันโพรเพนบนแพลทินัม/ชั้น YSZ บาง

นายวันชนะ ลีลาเลิศศุภกุล

Thesis Title	NON-FARADAIC ELECTROCHEMICAL MODIFICATION OF CATALYTIC ACTIVITY (NEMCA) OF PROPANE OXIDATION ON Pt/YSZ THIN FILM CELL
By	Mr. Wanchana Lelalertsupakul
Field of Study	Chemical Engineering
Thesis Advisor	Assistant Professor Palang Bumroongsakulsawat, Ph.D.

Accepted by the Faculty of Engineering, Chulalongkorn University in Partial Fulfillment of the Requirement for the Master of Engineering

-- Dean of the Faculty of Engineering

(Professor SUPOT TEACHAVORASINSKUN, D.Eng.)

THESIS COMMITTEE

-- Chairman

(CHUTIMON SATIRAPIPATHKUL, D.Eng.)

-- Thesis Advisor

(Assistant Professor Palang Bumroongsakulsawat, Ph.D.)

-- Examiner

(Pattaraporn Kim, Ph.D.)

-- External Examiner

(Associate Professor Monrudee Phongaksorn, Ph.D.)

วันชนะ ลีลาเลิศศุภกุล : การปรับปรุงความว่องไวของตัวเร่งปฏิกิริยาด้วยวิธีทางไฟฟ้าเคมีที่ไม่เป็นไปตามกฎ
ของฟาราเดย์ของการออกซิซันโพรเพนบนแพลทินัม/ชั้น YSZ บาง . (NON-FARADAIC ELECTROCHEMICAL
MODIFICATION OF CATALYTIC ACTIVITY (NEMCA) OF PROPANE OXIDATION ON Pt/YSZ THIN FILM
CELL) อ.ที่ปรึกษาหลัก : ผศ. ดร.พลัง บำรุงสกุลสวัสดิ์

ในงานวิจัยนี้ทำการศึกษาการปรับปรุงความว่องไวของตัวเร่งปฏิกิริยาด้วยวิธีทางไฟฟ้าเคมีที่ไม่เป็นไปตามกฎ
ของฟาราเดย์ (ปราฏการณ์เนมคา) ของการออกซิซันโพรเพนเหนือแพลทินัม /อิตเทียสเตบิไลซ์เซอร์โคเนีย (YSZ) ฟิล์มบางบน
วัสดุฐานรองอะลูมินา ในขั้นแรก YSZ ฟิล์มบางถูกเตรียมด้วยวิธีจุ่มเคลือบและเผาในอุณหภูมิต่ำที่ 800 องศาเซลเซียส การ
ออกซิเดชันโพรเพนที่อุณหภูมิในช่วง 300-500 องศาเซลเซียสแสดงปรากฏการณ์เนมคาให้เห็นได้อย่างชัดเจน อัตราส่วนการ
เสริมอัตราการเกิดปฏิกิริยามากที่สุดมีค่าเข้าใกล้ 3 ที่การให้ศักย์ไฟฟ้า 1.0 โวลต์และอุณหภูมิทำปฏิกิริยาที่ 400 องศาเซลเซียส
สำหรับประสิทธิภาพในการส่งผ่านประจุมีค่ามากกว่า 10,000 การให้ศักย์ไฟฟ้า 0.2 โวลต์และอุณหภูมิทำปฏิกิริยาที่ 300 องศา
เซลเซียส แต่อย่างไรก็ตามปราฏการณ์เนมคาไม่ถูกพบที่อุณหภูมิ 200 องศาเซลเซียส ถึงแม้ว่าจะเป็นเช่นนั้นก็ตาม
ความสามารถในการทำซ้ำของเซลค่อนข้างแย่เนื่องจากการยึดเกาะที่ไม่แข็งแรงระหว่าง YSZ ฟิล์มกับวัสดุฐานรองอะลูมินาเกิด
จากอุณหภูมิการเผาที่ต่ำสำหรับฟิล์ม YSZ และไม่สามารถใช้อุณหภูมิที่สูงขึ้นได้เนื่องจากพบว่าขั้วทองคำซึ่งใช้เป็นขั้วช่วยไฟฟ้า
ได้แพร่ลงไปยังวัสดุฐานรองรับอะลูมินาที่อุณหภูมิสูงขึ้นและสูญเสียสภาพนำไฟฟ้า ด้วยเหตุนี้ YSZ ฟิล์มบางที่ทำขึ้นมานี้จึงยึด
เกาะกับวัสดุฐานรองอะลูมินาอย่างไม่แข็งแรง และมีค่าการนำไฟฟ้าที่ต่ำเนื่องจากโครงสร้างที่มีรูพรุน คอปเปอร์เจือบิสมัทวานา
เดต (BICUVOX.10) ซึ่งเป็นตัวช่วยซินเทอร์ถูกเติมลงไปในสูตรสำหรับเตรียม YSZ ฟิล์มบางเพื่อลดอุณหภูมิในการเผาฟิล์ม ผง
BICUVOX.10 ถูกเตรียมและวิเคราะห์คุณลักษณะด้วย เทคนิคการเลี้ยวเบนของรังสีเอ็กซ์ สเปคโตรสโคปีของอนุภาคอิเล็กตรอน
ที่ถูกปลดปล่อยด้วยรังสีเอกซ์ และเทคนิคดิฟเฟอเรนเชียลสแกนนิงแคลอริมิเตอร์ ดิฟเฟรคโตแกรมจากเทคนิคการเลี้ยวเบนของ
รังสีเอ็กซ์และกราฟจากทคนิคดิฟเฟอเรนเชียลสแกนนิงแคลอริมิเตอร์ได้ยืนยันถึงการมีอยู่ของเฟสที่เกิดขึ้นใหม่ ฟิล์มของวัสดุ
ผสม BICUVOX.10 และ YSZ ถูกทำขึ้นด้วยวิธีพิมพ์สกรีนและเผาที่อุณหภูมิ 800 องศาเซลเซียส การวิเคราะห์ด้วยเทคนิคการ
เลี้ยวเบนของรังสีเอ็กซ์แสดงให้เห็นว่าไม่มีการเกิดปฏิกิริยาสถานะของแข็งระหว่าง YSZ และ BICUVOX.10 ภาพถ่ายระดับ
จุลภาคของผิวหน้าฟิล์มบางแสดงให้เห็นว่าการเพิ่มขึ้นของความเข้มข้นของ BICUVOX.10 ช่วยเพิ่มโครงสร้างที่เกาะกันแน่นขึ้น
ของ YSZ ฟิล์มบาง แม้กระนั้นการเติม BICUVOX.10 ทำให้อัตราการเกิดปฏิกิริยาที่สภาวะวงจรเปิดลดลงเนื่องจากการลดลง
ของพื้นที่ผิวของฟิล์มบาง อย่างไรก็ตามการเพิ่มความเข้มข้นของ BICUVOX.10 ในแผ่นฟิล์มบางนั้นส่งผลให้ความไวของอัตรา
การเกิดปฏิกิริยาสูงขึ้นตามการให้ศักย์ไฟฟ้าในช่วงแอโนดิกโพลาไรเซชันโดยประสิทธิภาพส่งผ่านประจุมีค่าสูงสุดที่ 2.5%
BICUVOX.10

สาขาวิชา	วิศวกรรมเคมี	ลายมือชื่อนิสิต ....
ปีการศึกษา	2562	ลายมือชื่อ อ.ที่ปรึกษาหลัก ....

6070309121 : MAJOR CHEMICAL ENGINEERING

KEYWORD: NEMCA, propane oxidation, thin film, platinum catalyst

Wanchana Lelalertsupakul : NON-FARADAIC ELECTROCHEMICAL MODIFICATION OF CATALYTIC ACTIVITY (NEMCA) OF PROPANE OXIDATION ON Pt/YSZ THIN FILM CELL. Advisor: Asst. Prof. Palang Bumroongsakulsawat, Ph.D.

In this work, non-Faradaic Electrochemical Modification of Catalytic Activity (NEMCA) of propane oxidation over Pt/yttria-stabilized zirconia (YSZ) thin films on alumina substrates has been studied. YSZ thin films were initially prepared by slurry dip coating and calcined at a relatively lower temperature of 800 $^{\circ}$C. Propane oxidation at temperatures in a range of 300-500 $^{\circ}$C clearly exhibited NEMCA. The maximum rate enhancement ratio was close to 3 at an applied potential of 1.0 V and a reaction temperature of 400 $^{\circ}$C. The maximum faradaic efficiency was higher than 10,000 at an applied potential of 0.2 V and 300°C. However, NEMCA was not observed at 200 $^{\circ}$C. Nevertheless, the reproducibility of this cell was poor mainly because of weak adhesion between the YSZ film and the alumina substrate. This was caused by the low calcination temperature for the YSZ film. A higher temperature could not be used because the gold counter electrode had been found to diffuse into the alumina substrate at higher temperatures and lost its conductivity. For this reason, fabricated YSZ thin films adhered only weakly to alumina substrates and had a low-conductivity, highly porous structure. Copper doped bismuth vanadate (BICUVOX.10), which is a sintering aid, was added to the recipe for YSZ thin films to lower the films' sintering temperature. The BICUVOX.10 powder was prepared and characterized with XRD, XPS and DSC. The obtained XRD diffractogram and DSC curve confirmed the existence of a new phase transition. Composite films of YSZ and BICUVOX.10 were fabricated by screen printing and calcination 800 $^{\circ}$C. XRD analysis showed no solid-state reaction between YSZ and BICUVOX.10. Surface micrographs of thin film showed that increasing the BICUVOX.10 concentration resulted in a denser structure of the composite films. However, the addition of BICUVOX.10 decreased the open-circuit reaction rate due to the reduced surface areas of thin films. Nevertheless, increasing the concentration of BICUVOX.10 in thin films resulted in higher sensitivity of the reaction rate to the applied potential under anodic polarization region. The highest faradaic efficiency was obtained at 2.5 % BICUVOX.10.

Field of Study:	Chemical Engineering	Student's Signature	
Academic Year:	2019	Advisor's Signature	

ACKNOWLEDGEMENTS

Primary, I would like to express my sincere gratitude and great appreciation to my adviser, Asst. Prof. Palang Bumroongsakulsawat who give valuable guidance. without his suggestion, support and attentiveness, this thesis would not have been possible complete. The author would also be grateful to Dr. Chutimon Satirapipatthkul as chairman, Dr. Pattaraporn Kim, and Assoc. Prof. Monrudee Phongaksorn as a member of the thesis committee. Later, everyone would like to thankfulness all those who have helped, supported, suggested and encouraged me through the time spent on this study, especially research staff, all my friends. Finally, I would like to thank my beloved family including mother and old sisters who graciously helped, supported, countenanced and all ears for my problem. That is to say; I cannot achieve success in this work without encouragement from these authors.

Besides, I would like to acknowledge the Thailand Research Fund (TRF, MRG6080245) for financial supporting in this research.

Wanchana Lelalertsupakul

TABLE OF CONTENTS

LIST OF TABLES

จุฬาลงกรณ์มหาวิทยาลัย

CHULALONGKORN UNIVERSITY

LIST OF FIGURES

CHAPTER 1

INTRODUCTION

1.1 Background

Propane (C_3H_8) known as saturated light hydrocarbon product from natural processing and the crude oil refining. Usually, propane is found compression and storage as a liquid. The domestic and industrial applications of propane used in many ways, such as water heating, cooking, agricultural product drying, and fuel in the automotive engine [1, 2].

The essential chemical reaction for propane application is catalytic combustion or catalytic propane deep oxidation. This reaction is a necessary technology for both the improvement of energy resource and emission pollution control in an economically and environmentally friendly strategy[3]. Commonly, the catalytic combustion carried out with precious metal on oxide supports. However, these kinds of catalysts have limitations. Short catalytic lifetime, incapability of controlling the catalytic performance during operation are a few examples. Previous works, many researchers tried to improve catalytic activity by focusing on studies; developed support material[4], optimized active metal [5]or catalyst structure[6], modified catalyst by addition promoters[7] and increased amount of active phase dispersion[8].

Recently, a new concept of catalytic promotion named electrochemical promotion of catalysis (EPOC) or non-Faradaic electrochemical modification of catalytic activity (NEMCA) that was discovered by C. G. Vayanas and co-workers in 1980s. NEMCA has been studied widely for more than 70 reaction systems[9]. However, the catalytic hydrocarbon oxidation reaction is the most interesting alternation for electrochemical promotion of catalysis [10-15], they are a capability phenomenon that could bring to a furtherance in developments on catalytic converters. After all this time, researchers have improved NEMCA promising to its commercialization.

NEMCA effect refers to the process which when electric current or potential were applied between two electrodes and separated by a solid electrolyte that causes controlled reversible spillover of ions from the solid electrolyte on the metal surface and leads to a short time activated state. The NEMCA cell consists of a catalyst (working) electrode, a reference electrode, a counter electrode, and a solid electrolyte[9].

Yttria-stabilized zirconia (YSZ) is a universal thermal oxygen ion-conducting electrolyte material. YSZ is used in a wide range of applications: fuel cell[16], gas sensor[17], gas emission control[18]. However, this material is more expensive than ordinary supports used in the catalyst, e.g., alumina (Al_2O_3)[19-21], silica (SiO_2)[8, 22]. Traditionally, the NEMCA cells are ionic conducted on a relatively thick piece of YSZ[10, 11, 18, 23]. The economic worthiness is considered and found a way to save cost. The fabrication of thin-film can reduce the overall cost of YSZ in the solid electrolyte layer, while a cheaper support material is as a substrate.

Several methods have been employed to make YSZ thin films: radio frequency (RF) sputtering[24], DC reactive sputtering[25], pulsed laser deposition (PLD)[26], electrophoretic deposition (EPD)[27], spraying techniques[28, 29], spin coating[30-32], dip-coat techniques[33-35], chemical vapor deposition (CVD)[36] and atomic layer deposition (ALD)[37]. All those methods produced YSZ thin film at nanoscale to microscale or thick films. Nevertheless, dip-coat techniques are an intensive method for large-scale preparation and simple compared to other methods.

All the reasons mentioned above, leading to this work is focused on the NEMCA effect for propane oxidation at Pt/YSZ electrode. YSZ thin film was fabricated on the α-alumina substrate by the dip-coat technique in YSZ slurry. NEMCA phenomenon was observed in a continuous stirred reactor by stoichiometric condition and different applied cell voltages. Unfortunately, the NEMCA cell can be the observation of the NEMCA effect, but its repeatability and reproducibility are shallow. Many factors cause these reasons. For example, low contraction between the YSZ layer and the gold layer on a dense alumina substrate is considered. Alternatively, the low temperature of sintering leads to the porous structure of solid electrolyte film, resulting in poor ionic

conductivity. From this problem, the modification of YSZ thin film has occurred. Densification of YSZ thin film at low sintering temperature as the first goal in improvement. In this work, copper doped bismuth vanadate compound (BICUVOX.10) adopted as a sintering aid, which helps to produce dense YSZ thin film at a lower temperature. Second point, low adhesion between the interface layer was modified by change of YSZ slurry recipe and fabrication method.

1.2 Research objectives

1.2.1   To cast functioning YSZ thin film on alumina substrate.

1.2.2   To fabricate YSZ thin film at the low-temperature sintering by addition sintering aid.

1.2.3   To study NEMCA behavior on Pt/YSZ thin film for propane oxidation reaction.

1.2.4   To observe NEMCA effects of propane oxidation rate at different temperatures with fabricated electrochemical thin-film cell.

1.3 Research scopes

1.3.1   Effects of cell potential differences on CO_2 formation rates

1.3.2   Effects of operation temperature in the range of 200-500 $^{\circ}$C on CO_2 formation   rates

1.3.3   Effect of YSZ thin film at the low-temperature sintering on study NEMCA effect.

CHAPTER 2
THEORY

This chapter presents theories related to this thesis. Firstly, the catalytic propane oxidation is briefly discussed. In the next part, the fundamental conception of non-Faradaic electrochemical modification of catalytic activity (NEMCA), i.e., the principle of this phenomena, the composition of NEMCA cell, solid electrolyte, rules of the electrochemical promotion, basic experiment set up, type of reactor design are explained. Finally, it talks about the role of sintering additive in the high-temperature electrochemical field.

2.1 Propane oxidation with catalytic reaction

Propane is a gaseous product from natural gas and petroleum that its application is in heating and transportation energy; thus, propane is the kind of significant hydrocarbon. Furthermore, the catalytic deep oxidation of hydrocarbon has been widely employed for power generation and controlling emission pollutants from both stationary and mobile sources. While the precious metals, e.g., palladium (Pd), platinum (Pt), rhodium (Rh), and iridium (Ir), are recognized as highly reactive catalysts in this reaction for light alkanes even at low and high reaction temperature[19, 21, 38-40]. Nevertheless, palladium shows the best performance for only methane; platinum is the most active for heavier hydrocarbons in the conventional reactor

The overall reaction of propane oxidation may be represented by

$$C_3H_8 + 5O_2 \xrightarrow{\Delta} 3CO_2 + 4H_2O \qquad (2.1)$$
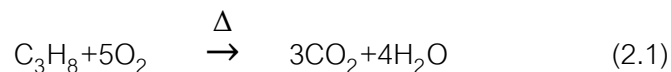
This equation is the empirical model, although the authenic reaction mechanism related to many free radical chain reactions. The usual pattern of hydrocarbon and CO catalytic combustion display in Figure 2.1. As the increase of temperature, the combustion rate started at a temperature that depends on the kind of catalysts and the class of hydrocarbon (area A). Even more, the rising of temperature in area B brings to exponential growth rate to the point where heat formed by combustion is much bigger

than heat supplied. In area C, the reaction rates are also determined with mass transfer limitation until the reactants are completed in area D. From this pattern, a significant increase in catalyst temperature due to the heat generated from the rapidly complete conversion of reactants Consequences, the thermal stabilization of catalysts at high temperatures should be considered [41].

Moreover, one crucial factor that should be considered in catalytic combustion is "light off." This factor refers to the temperature in which mass transfer limitation represents the reaction rate-determining step (area C in Figure 2.1). For the experiments, the definition of light off is the temperature at hydrocarbon convert to CO_2 reaches 50%, and the time it takes to bring up to light off should be reduced for enhanced efficiency of exhaust emission control[42, 43]. Moreover, the shapes of catalysts and the porosity of catalyst material have a significant impact on the C region in the combustion pattern. In previously reported, platinum-based oxygen vacancy support can reduce the light-off temperature in catalytic propane oxidation better than conventional a catalyst (Pt/Al_2O_3)[44].
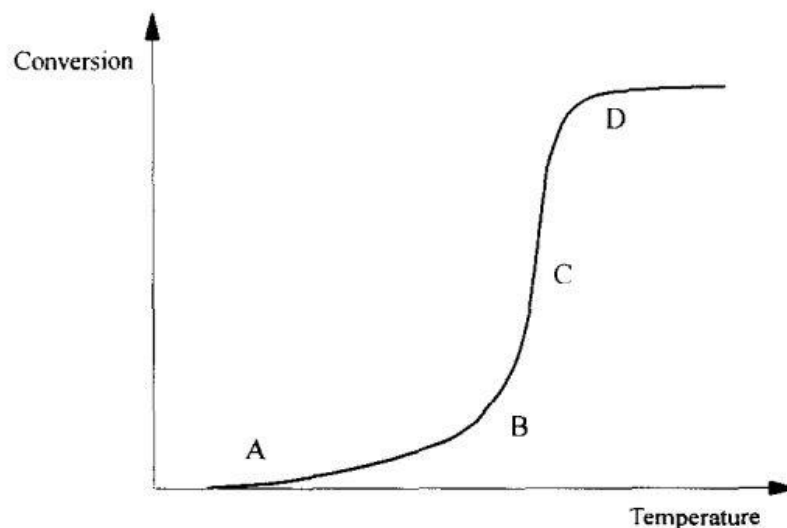
Figure 2. 1 *General pattern between conversion and temperature of catalytic combustion of hydrocarbon[41]*

2.2 Fundamental of Non-Faradaic Electrochemical Modification of Catalytic Activity (NEMCA)

The term non-Faradaic electrochemical modification of catalytic activity (NEMCA) known as in several synonyms, i.e., electrochemical promotion, electrochemical promotion of catalysis (EPOC), and in-situ controlled promotion (ICP). In the early 80s, NEMCA was observed in ethylene epoxidation on the Ag catalyst electrode by Professor C.G. Vayenas and his group. EPOC as a new electrochemically induced catalytic effect by applying a small current (1-10^4 μA/cm^2) and potential ($\pm$ 2 V) between working and counter electrode. The electrochemical promotion induced catalytic activity has been found to increase 400 times higher than the unpromoted catalytic activity[9, 45].

This phenomenon is connected to control back-spillover ion process or ion migration over the catalyst surface with an application of a little current or potential on the catalyst surface and inert metal film (counter electrode) that were separated by a dense solid electrolyte. The back-spillover ion performs as a "sacrificial promoter," which has many types of back-spillover ion such as $O^{\delta-}$ from oxide ion conductors or $Na^{\delta+}$ from sodium ion conductors. The rate of a catalytic reaction in an electrochemical cell enhanced beyond the rate that could be achieved was the reaction purely electrochemical during the passage of an electric current. Thus, the NEMCA effect on the catalyst electrode consists of two concurrently processes—a chemical and an electrochemical part. The major product is produced by the catalytic reaction pathway, which related the heterogeneous catalysis. control and modification of the electronic properties on catalyst surface is the essential role of electrochemical terms [9, 46-52]. Generally, this phenomenon is studied in wide range of catalytic reaction systems including oxidations [10, 12, 13, 15, 23, 53-55], hydrogenation [56, 57], dehydrogenation[58], isomerization[59], ammonia synthesis[60, 61], dimerization[62]

and many other types of electrolyte (acid or alkali aqueous, inorganic melts) have been achieved by electrochemical promotion.

A long time ago, the researchers were made inquiries as to the origin of the NEMCA phenomenon. The in-situ characterizations have provided a clear answer to this phenomenon. These include: (a) surface science techniques, e.g. Ultra-violet Photoelectron Spectroscopy (UPS), Photoelectron Emission Microscopy (PEEM), X-ray Photoelectron Spectroscopy (XPS), Temperature Programmed Desorption (TPD), (b) work function measurement via Kelvin probe technique (c) electrochemical experiment via Cyclic Voltammetry (CV), Electrochemical Impedance Spectroscopy (EIS) and Potential Programmed Reduction (PPR) and (d) catalytic testing e.g. analysis time of constants during transient[9, 47, 49-51] effect will help scientist understand it and bring to new knowledge for further performance improvement.

2.3 Spillover mechanism

From the previous literature reports, the NEMCA effect can be described that justified by the integration of catalytic science and electrochemistry. In Figure 2.2, the three possible pathways of the movement of ions during the polarization at three-phase boundaries (TPB) which is a region of a contract between three different phases (catalyst/solid electrolyte/gaseous reactant) as follow[9]

(a) Desorption to gaseous phase

(b) Reaction with co-adsorbed reaction

(c) Migration over the entire gas-exposed catalyst electrode surface (spillover)

It is clearly evident in case (a) that there is no effect of desorption on catalytic reaction whilst the reaction rate change (Δr) will be direct variation on Faraday's law (I/nF) in case (b). in last case (case (c)), the new species are generated and pumped onto the catalyst surface will interact with co-adsorbed reactant and will change catalytic properties. Consequently, case (a) and (b) will not be affected on NEMCA; nevertheless, Faraday's law does not control case (c).
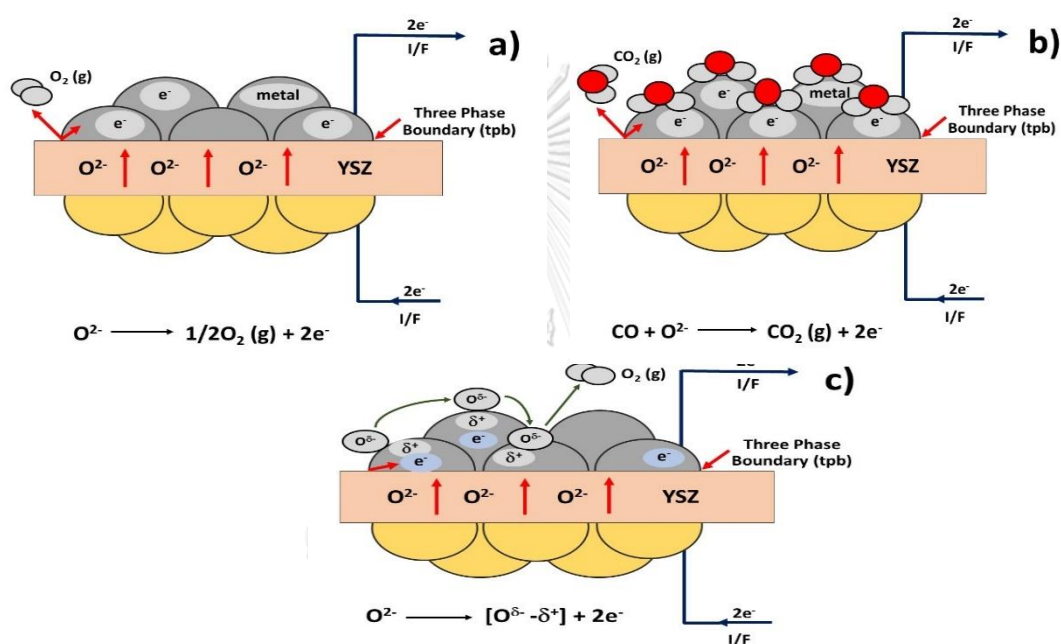
Figure 2. 2 Three possible pathways of oxygen-adsorbed species at three-phase boundary by current or potential application (a) desorption, (b) reaction, (c) back-spillover [9]

The effect of spillover represents a significant role in heterogeneous catalytic systems and was interestingly focused on research scopes recently. This effect can be clarified by the transportability of adsorbed species from one phase on which they easily adsorb (active phase, e.g., metal or oxide) to another phase where they do not directly adsorb (support). In this circumstance seems as though the inert material such as support in the catalyst can obtain catalytic activity. In the early 1990s, C.G. Vayenas has proposed a mechanism that has widely accepted for EPOC. The particular case of

spillover can call "back-spillover," which is the main of this mechanism. Figure 2.3 represents back-spillover of metal catalyst electrode on ionic conducting electrolyte, i.e., YSZ or β'' Al_2O_3 during electrochemical polarization conditions, where sacrificed ions with their counter charges on the metal ($O^{\delta-}$-$\delta+$, $Na^{\delta+}$-$\delta-$), move over the entire gas reveal surface after polarization. Thus, the promoting species transported from the electrolyte to the metal surface is controlled by current or potential. This process leads to the generation of an effective double layer that its density varies during the different potential. The effective double layer forms an intense dipole moment on the catalyst surface, getting into an alteration of bond strength of adsorbed molecules with catalysts by electronegative adsorbate (repulsive interaction) or electropositive adsorbate (attractive interaction) with promoting spillover species. These two types of interactions are believed to impact the activation energy for the step of surface reaction, in which changes can be detected from the different rates of reaction and selectivity[9, 49-51, 63].
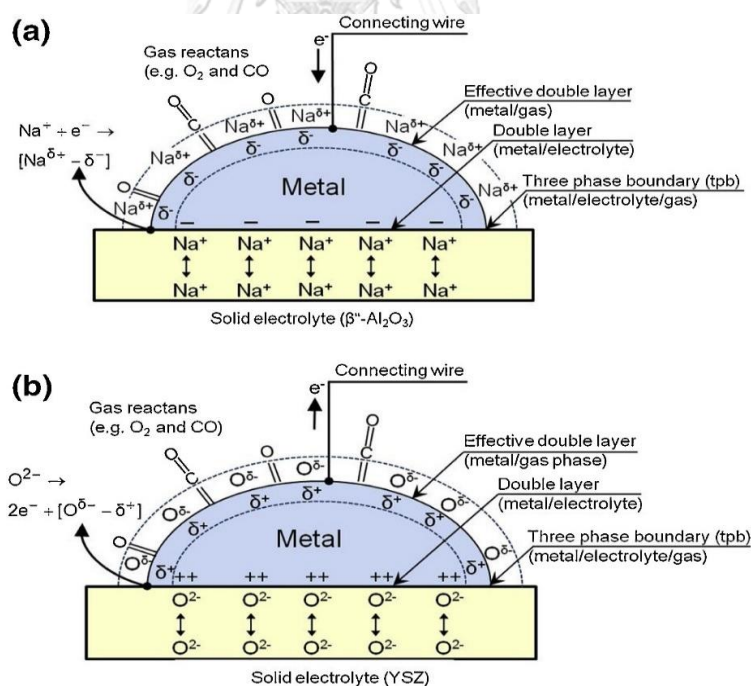
Figure 2. 3 Schematic description of the formation of the TPB, double layer created at metal-solid electrolyte interface and effective double layer forming at the metal-gas interface during polarization in case β''- Al_2O_3 (a) and YSZ (b) [63, 64]

2.3 Experiment set up

2.3.1 Reactor design for NEMCA

A typical reactor configuration for NEMCA studies show in Figure 2.4 (a) and (b). There are generally two types for reactor design including the fuel cell design and single pellet design[9, 49, 65].

1) Fuel-cell design or two-chamber system, feed of auxiliary gases, reactant, and product, are exposed with catalyst (working, W) electrode while reference (R) electrode and counter (C) electrode is exposed to reference gases mostly air. These two sections separated by a solid electrolyte wall of the reactor, as in Figure 2.4 (a).

2) Single pellet design of one chamber system, all electrodes are exposed to a mixture of co-feeding reactants and products, as shown in Figure 2.4 (b).

Both reactor configurations give similar results in NEMCA studies. The single pellet is a straightforward scale-up than the fuel-cell type but has the problem of reference electrode, which can effortlessly measure inaccuracies of potential compared to the two-chamber system.
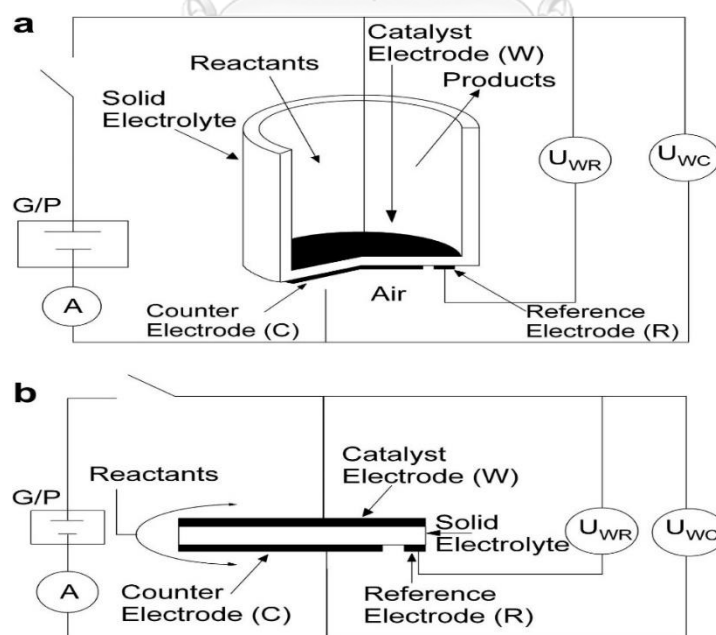
Figure 2. 4 Reactor configuration for NEMCA studies; (a) fuel-cell type configuration, (b) single pellet design [9].

2.3.2 NEMCA cell

An electrochemical cell for NEMCA experiments consists of the catalyst also execute as the working electrode, which is a subject area for surface reaction. The second, catalytically inert material is used for the counter electrode and reference electrode. Furthermore, the middle part of the cell is segregated by the solid electrolyte. As also shown in Figure 2.5, there are description following[10, 66, 67];

1) A catalyst or working electrode need to enough porosity so that reactant or product gas-exposed. The porosity and surface area on the electrochemical cell is control by the sintering temperature and catalyst preparation method. The catalyst films have been recent reports in several techniques such as screen printing, thin-film coating by metal paste, thermal evaporation and impregnation, etc.

2) A counter and reference electrode deposited on the opposite side of the solid electrolyte. Typically, the same material is unpopular used as a catalyst electrode. Both the two electrodes must be non-polarizable and electrocatalytic property.

3) A quasi-reference electrode is used to call the counter and reference electrode in a single pellet design. These electrodes are made from inert material because they exposed to reactive gas (reactant and product). The best choice for the satisfactory quasi-reference electrode is gold (Au) due to their potential that has been found to fluctuate little by changing the gaseous composition when fixed p_{O2} condition.
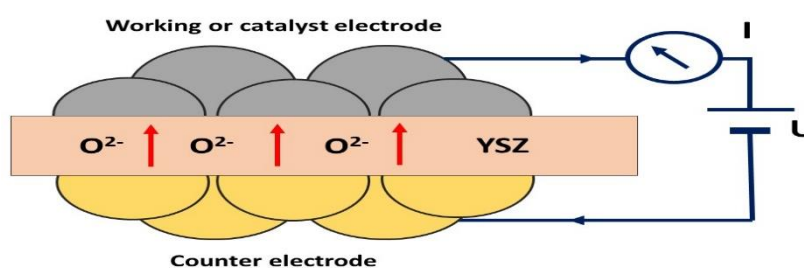
Figure 2. 5 Schematic diagram of the NEMCA cell in YSZ (oxide conductor) case

2.4 Solid electrolyte

The first observation about solid electrolyte occurred in 1834 by Michael Faraday when heated to PbF_2 at 500 ^{o}C becomes electric conductor. The solid electrolytes have been an enthusiastic area of science and engineering researches of this century, such as fuel cell, gas sensor, etc. There are classified of category according to ionic transportation in their structure for as follow[9]:

1) Oxide ion conductors: The ceramics are displacement of divalent or trivalent metal oxides in quadrivalent metal oxides Calcia- or Yttria-stabilized zirconia (YSZ) as an example for this type of solid electrolyte which are extensively used in oxygen sensor and solid oxide fuel cell (SOFC).

2) Protonic conductors: The material class allows for protonic conduction by changing the charge carrier to the more mobile proton. Of particular applications are Proton Exchange Membranes (PEM) such as Nafion 117, which demonstrate factual conductivity at room temperature. The prototypical examples of ceramic include acceptor-doped barium zirconate or barium ceranate compounds, which are steam permeable ceramics and recognize that is electrolyte in a fuel cell. Also, proton conductors are displayed by cesium hydrogen sulfate ($CsHSO_4$) and H-substituted β"-Al_2O_3.

3) Sodium ionic conductors: The general sodium ionic electrolytes are β'- and β"-alumina, which are non-stoichiometric compounds correlating to $Na_{1+x}Al_{11}O_{17+x/2}$ and $Na_{1+x}M_xAl_{11-x}O_{17}$ respectively, where M is used to describe superseding of a divalent cation such as Zn^{2+}, Mg^{2+} or Ni^{2+}. Another type, this material as known NASICON which is a crystalline structure in the rhombohedral family with genetic formula AMP_3O_{12}. Recently, the potential application of both types in sodium-ion conductors in battery and electrochemical fields.

4) Other cationic ceramics conductors: this class includes K^+, Cs^+, Rb^+, and Tl^+ that they replace sodium ion in β'- and β"-alumina, their application on similar field of sodium ion conductors.

Although several solid electrolytes are used to NEMCA studies. Since these solid ionic conductors have different operating temperatures. They exist in Table 2.1 [9, 63]:

Table 2. 1 Example of solid electrolyte in NEMCA experiment including ionic transport and operating temperature

Solid electrolyte	Type of conductor	Ion transport	Operating temperature (^{o}C)
YSZ	Oxide	O^{2-}	280-650
β"-alumina	Sodium	Na^{+}	180-400
NASICON			
$CsHSO_4$	Proton	H^{+}	25-150
$CaZr_{0.9}In_{0.1}O_{3-\alpha}$			
Nafion			
Aqueous	Acid	Cation	25-60
	Alkali	Anion	
CaF_2	Anion	F^{-}	550-700
$CeO-TiO_2$	Mixed ionic-electronic	O^{2-}, e^{-}	≈ 500
$V_2O_5-K_2S_2O_7$	Molten salt	O^{2-}	460

2.5 Yttria-stabilized zirconia (YSZ) [68-70]
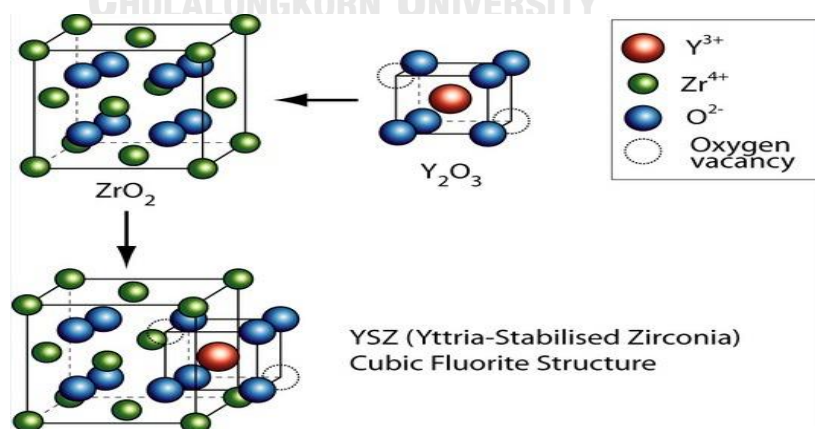
Figure 2. 6 Yttria-stabilize zirconia cubic crystalline structure[71]

Yttria-stabilized zirconia (YSZ) is a useful solid oxide electrolyte. YSZ has the fluorine crystal structure that this structure is a face center cubic (fcc). Zirconia (ZrO_2) display low ionic transport performance, and only rearrange the cubic fluorite phase above 2300 °C. Stabilization of the cubic structure at lower temperatures and increase the concentration of oxygen vacancies. The addition of di or trivalent oxides like calcia (CaO), magnesia (MgO), or yttria (Y_2O_3) assists stabilization of fluorite cubic structure at high temperature. It avoids the transformation to the monoclinic-tetrahedral structure. It is well known that adding an 8-9% mole of yttria is enough to stabilize the cubic phase of zirconia in Figure 2.6. The displacement of zirconium ion (Zr^{4+}) with yttrium ion (Y^{3+}) causes an oxygen vacancy, which may move through the lattice, thus providing electric conductivity by the transport of electric charge. In the Kröger and Vink notation, the equation can explain this incorporation reaction of Y_2O_3 as equation 2.2, which means two Y^{3+} ions form one vacancy on the anionic sublattice site. This facilitates moderate conductivity of YSZ for oxide ions high temperature. In practice, 8 mol.% of YSZ has been regarded as having the highest conductivity in the system.

$$Y_2O_3 \xrightarrow{ZrO_2} 2Y'_{Zr} + V_O^{\cdot\cdot} + 3O_O^x \qquad (2.2)$$

If discussing in advantages of YSZ, the first thing to think about is good ionic conductivity that this strong point is applied in the high-temperature electrochemical field. YSZ is high thermal stability; thus, it remains solid throughout; the electrolyte does not vaporize and minimal dry corrosion. From above, YSZ has many benefits; however, there are some limitations in the used of YSZ. The first, this material needs to operate in high temperatures, which can be expensive to the overall cost. Another thing, at high-temperature operation, leads to thermal expansion stress in this material. Due to the previous, thermal stress causes electrode fracturing too easily.

2.6 Copper doped bismuth vanadate compound (BICUVOX)

Abraham firstly discovered the bismuth vanadate compound (Bi_2O_3-V_2O_5) in 1988 [72]. This compound exhibits several properties, such as ferroelectricity, pyroelectricity, ionic conductivity, and active photocatalytic material. Bismuth vanadate was classified in the Aurivillius crystalline type which consists of alternating layers of $(Bi_2O_2)_n^{2n+}$ and vanadate perovskite layers $(VO_{3.5}\square_{0.5})_n^{2n-}$, where $\square$ represents oxygen vacancies in these layers. In the general structure of $(Bi_2O_2)_n^{2n+}$ has a square pyramid and coordination with four oxygen atoms. The perovskite layers exhibit bonding with oxygen atoms, which form VO_6 octahedra. Mobility of oxide ion hopping between vacancies in vanadate layers bring to ionic conductivity[73, 74]. Bismuth vanadate exhibit three polymorphs that depend on temperature. The first α-phase arrange monoclinic crystalline and appear in the range of room temperature to 430 $^\circ$C. Then the orthorhombic structure or β polymorph is stable temperature range between 430 $^\circ$C and 570 $^\circ$C. At high temperature (above 570 $^\circ$C), the γ phase form tetragonal structure which is the most ionic mobility at all polymorph[75]. The excellent ionic conductive performance at high temperature is a limitation of the bismuth vanadate compound. The solution to this problem is increasing the concentration of anion and disordering of vacancies within the perovskite layer. The partial substitution of cation which most of them are transition metal in the vanadium site can be stabilized γ phase at room temperature. The derivative bismuth vanadate compound is known as BIMEVOX, where BI: bismuth, V: vanadium, ME: dopant metal, and OX: oxygen. From previous work, selection substituted cations, and their molar ratio into the perovskite layer may affect structure and conductivity, and metal dopant with lower charge than vanadium ion brings to increasing oxygen vacancies [76].

Copper doped bismuth vanadate is compound in BIMEVOX family that has received interesting in studies and applications in oxide ion conductor devices such as solid electrolyte, composite in cathode layer for fuel cell technology or the high-temperature sensor. The optimum Cu concentration is at x=0.1, which, according to $Bi_2V_{0.9}Cu_{0.1}O_{5.35}$ (BICUVOX.10). The ionic conductivity at 300 $^\circ$C is the magnitude of 10^{-3}

Scm^{-1}, which is higher than any oxide ion conductors in this temperature region[77]. The comparison of ionic conductivity between BICUVOX.10 and another electrolyte was shown in Figure 2.7.
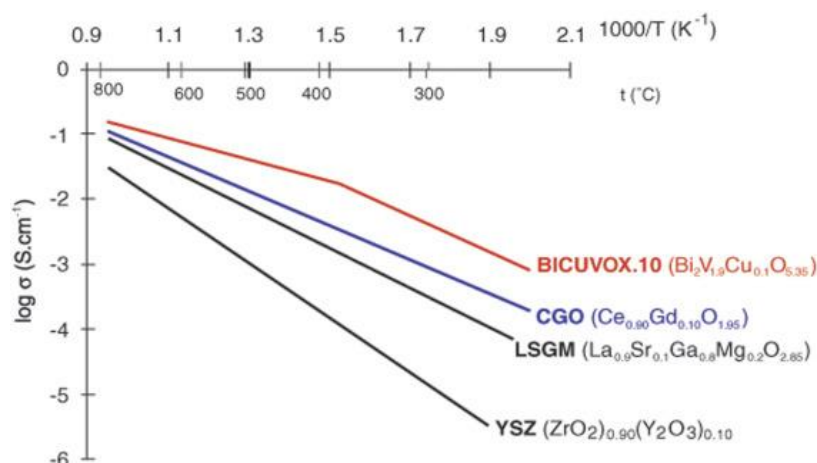
Figure 2. 7 Comparison of the ionic conductivity of general oxide ion conductors in Arrhenius plot By kind permission of Dr. R.-N. Vannier. [78]

2.7 Rules of promotional catalysis[9, 49-51, 63]

The chemisorption process is essential in heterogeneous catalysis. This process is the formation of bonding between adsorbate and adsorbed (metal). The formation of the chemisorption in ordinary relates either donation of electrons from the adsorbate to the metal or donation of electrons from the metal to the adsorbate (back donation). In term of thermodynamics, work function (Φ) is referred to minimum energy required to pull out an electron from the surface catalyst that concentration of each adsorption species on catalyst surface effects to work function change ($\Delta\Phi$). The measurement of Φ often used to study surface reaction and chemisorption species on the surface of the catalyst. Therefore, the adsorbates are classified into two types:

1) Electron acceptor adsorbates increase in general the work function of the substrate. The dipole generated by the chemisorption of oxygen atom has its negative end pointing to the vacuum; thus, an increase in Φ. Atomics oxygen is an example of this type.

2) Electron donor adsorbates decrease the work function of the substrate in general cases. The dipole formed by the adsorbate has its positive end pointing to the vacuum, thus, decreases Φ. The examples of this type include atomic hydrogen, alkalis, and olefins.

In terms of the electrochemical promotion of catalysis, the catalyst potential (U_{WR}), which is the applied potential between the working and reference electrode. The different catalyst potentials affect the catalytic rate (r). The significant variation of the catalytic rate was observed in comparison to the unpromoted rate of reaction (r_0) under open-circuit conditions. The study of effect of adsorbate on U_{WR} showed that electropositive (electron donor) adsorbates tend to decrease U_{WR} and Φ thus while electronegative adsorbates cause an increase in U_{WR} and Φ

From above, there can be four electrochemical promotion rules in terms of the chemisorption propensity of the electron acceptor and electron donor reactants (Figure 2.8). Therefore, four global electrochemical rules expressed in the term of global electrochemical rule, G1-G4 as follows,

G1: Electrophobic or Nucleophilic, referred to as the electron acceptor reactant, which strongly adsorbed on the catalyst surface. In Figure 2.8, the reaction rate rises when the application of potential increases.

G2: Electrophilic for the electron donor reactant, which strongly adsorbed on the catalyst surface than electron acceptor. From this chemisorbed pathway, the reaction rate tends to be inversely proportional to potential.

G3: Volcano-type, both electron acceptor and electron donor reactant can be strongly adsorbed on the catalyst surface. As a result, the maximum reaction rate is observed when there is a variation of potential from cathodic to anodic polarization.

G4: Inverted volcano-type, which both reactants form weakly bond strength. adsorbed on the catalyst surface. Under the influence of various potential, the minimum reaction appears.
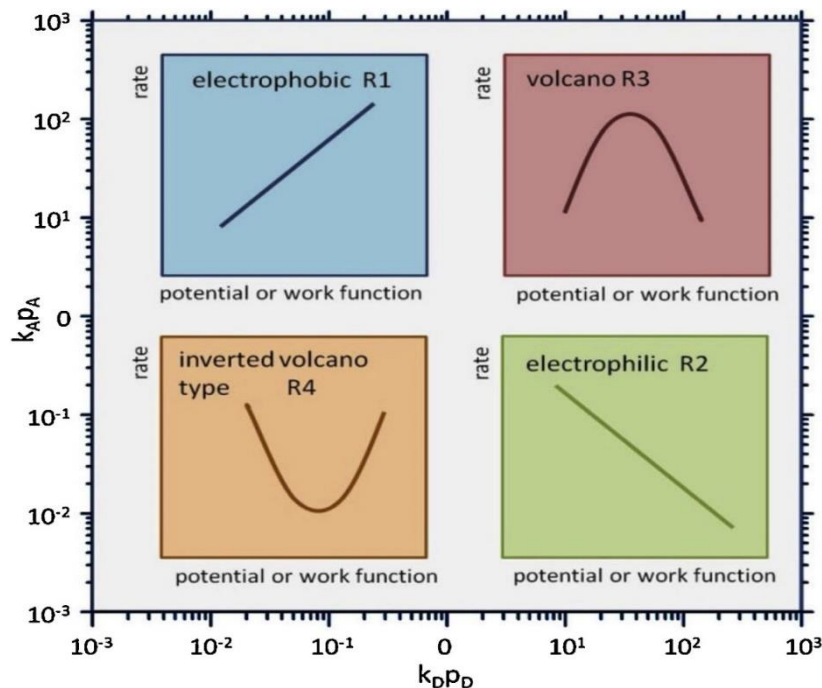
Figure 2. 8 Effect of adsorption equilibrium constants (k) and partial pressures (p) of the electron acceptor (A) and electron donor (D) reactant on the reaction rate versus potential (or work function) dependence of NEMCA behavior

2.8 Definitions and key parameters for NEMCA

Vayenas and Stoukides proposed the activity of O_2 adsorbed onto the surface of a silver metallic could be controlled by the applied potential for the partial oxidation of ethylene in the 1981s. Later, this activity was called back-spillover. When the reaction is charge transfer limited, the rate of oxygen supplied on the surface (r_f) follows Faraday's law[45, 79], shown by equation (2.2):

$$r_f = I/nF \qquad (2.3) .$$

Where I is the applied current (A)

F is Faraday's constant

n is the charge in promotion ion.
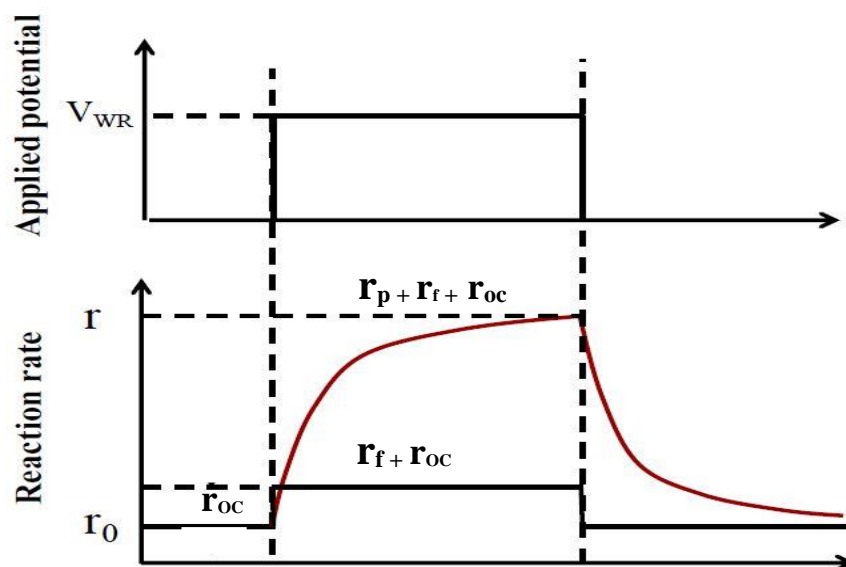
Figure 2. 9 Typical transient EPOC curve[80]

Astonishingly, Vayenas et al. found a phenomenon that the rate of a catalytic reaction in an electrochemical cell is enhanced beyond the rate that could be achieved was the reaction purely electrochemical during the passage of a potential. The typical transient EPOC curve has shown in Figure 2.9. The open-circuit, which means that there is no supply of electric current or potential. The catalytic rate refers to r_{OC}. When the application of electricity (current or potential) also known as closed-circuit condition. The total rate of reaction is greater than the sum of r_{OC} and r_f in theory. The difference in rate during polarization is affected by back-spillover species on the catalyst electrode.

The two parameters that are generally used to describe the magnitude of NEMCA effects are[10, 12-14, 53, 81, 82]:

1) The rate enhancement ratio (ρ) defined by:

$$\rho = {}^r\!/_{r_0} \qquad\qquad (2.4)$$

where r is the electro-promoted catalytic rate

r_0 is the open-circuit rate, i.e., non-promoted catalytic rate

2) The apparent Faradaic efficiency(Λ) defined by:

$$\Lambda = \frac{(r-r_0)}{I/_{nF}} \qquad (2.5)$$

where I is the applied current,

n is the charge of the promotion ion

F is Faraday's constant 96500 s $\cdot$ A /mol

A reaction performed NEMCA phenomenon when $|\Lambda| > 1$, while electrocatalysis is specified that $|\Lambda| \leq 1$. A reaction shows electrophobic behavior when $\Lambda > 1$, which explains that the reaction rate increases with catalyst potential and electrophilic behavior when $\Lambda < -1$, which explains that the rate decreases with catalyst potential. Faradaic efficiency used to describe the amount of product molecules generation per oxide ion flow during the polarization. Typical values of Λ are between 1 and 10^5. Therefore, NEMCA phenomenon demand low currents or potentials for activation of back-spillover promoter. Moreover, gaseous adsorption or chemical activation cannot generate sacrificial species such as O^{2-} or effective double layer [53, 68].

CHAPTER 3

LITERATURE REVIEWS

This chapter presents previous research involves the fabrication of solid electrolyte thin-film techniques, non-Faradaic electrochemical modification of catalytic activity (NEMCA) for several reaction types, and different types of electrode. The related kinds of literature are summarized in this chapter.

3.1 Fabrication of solid electrolyte thin-film techniques

Solid electrolyte thin films grown by several methods have been studied for use in solid oxide fuel cells (SOFCs) as thin ionic conductor layers, anode, and cathode. Fuel cells use in oxygen-ion conductors, such as stabilized zirconia or acceptor-doped ceria have been utilized for electric power generation and developed as future alternatives for vehicle power supplies.

There are a large number of preparations for solid electrolyte thin-film techniques that show their advantages and disadvantages according to Table 3.1

Table 3. 1 Comparison between the advantages and disadvantages of solid electrolyte fabrication techniques [83]

Fabrication techniques	Common applications	Advantages	Disadvantages
Chemical vapor deposition (CVD)	Cathode and electrolyte	- Make a uniform film - Gain a gas-tight	- Get to corrosive gas - Low deposition rates - Equipment costs are expensive
Sputtering	Cathode, anode, and electrolyte	- Can design composition and morphology of thin film - Acquire thin film at low temperature	- Easy to crack - Operating costs are expensive

Table 3.1 Comparison between advantages and disadvantages of solid electrolyte fabrication techniques (continues)[83]

Fabrication techniques	Common applications	Advantages	Disadvantages
Sol-gel	Electrolyte	- Can control dense or porous thin films	- Obtaining thin film at high temperature
Pulsed-laser deposition (PLD)	Cathode and electrolyte	- Obtaining thin film in nanoscale thickness	- suitable for fabrication in small area of substrates
Spin coating	Cathode and electrolyte	- Thin and dense film	- repeating several times to form a dense and pore-free thin
Tape casting	Anode and electrolyte	- Able to produce multi-layer cell - Scale-up easily	- Unsuitable for large cell area
Screen printing	Cathode, anode, and electrolyte	- Simple method - Low cost of fabrication - Scale-up easily	- Low adhesion with substrate -Cracking of some material
Painting	Electrode and electrolyte	- Simple method	- Difficult to scale-up - Poor reproducibility
Dry pressing	Anode and electrolyte	- Simple method - Cost-effective	- Requiring experiences skill - Difficult to scale-up
Dip coating	Cathode, electrolyte, and anode	- Simple method - Cost-effective - Scale-up easily	- Need to binder
Spray pyrolyze	Electrolyte	- High deposition rates	- hard to produce a dense film

Electrode and frequently utilize for dense or porous thin film and able to produce film various thicknesses. The benefits of both techniques are the common methods, uncomplicated to set-up, and able to produce on a large scale easily. For these reasons, dip-coating is the best choice for developing commercialization.

In preparation of YSZ film via slurry casting have several parameters that may significantly affect physical, chemical, and electrochemical properties.

3.1.1 Composition of slurry or paste

First of all, the slurry recipe must have an appropriate composition. The previous researches have been reported on the effect of composition in solid electrolyte slurry. In 2008, Zhenhua et al. [84] studied the effects of different slurry recipes that were modified for dip-coating YSZ electrolyte films on an anode substrate for intermediate temperature solid oxide fuel cells (IT-SOFCs). There are comparison of suitable solvent pairs, dispersant to powder ratio, solid loading and coating time for optimum condition in dip-coat YSZ thin film   The best YSZ slurry contains methylethylketone/ethanol (MEK/EtOH) as a solvent, triethanolamine (TEA) as dispersant and 0.364 g/ml for solid loading, to prepare YSZ thin film by dip-coating. As a result, YSZ thin film, which twice dip-coat, was shown to be a low ohmic loss and well adhesion with the supported anode. For electrochemical properties, this film represents open-circuit voltage (OCV) of 1. 01 V and obtains a maximum power density of 262 mWcm^{-2} under operating temperature at 800 ˚C. This research was successful in improvement solid content as high 30 wt.% while prior researches have low solid content.

Later, Libin et al. [35] prepared various modified slurry recipes for YSZ thin film on Ni/YSZ anode substrate. A 28 % YSZ loading in ethanol was added 1.9% polyvinyl butyral as a binder, TEA as dispersant, and polyethylene glycol-dioctyl phthalate as a plasticizer that enhanced the greatest of maximum power density at 800 ˚C. For physical properties, this slurry recipe provided dense film and crack-free between an anode and thin-film, which demonstrates that adhesion is excellence. The adding more binder

brings to the higher kinetic viscosity better than YSZ powder. Moreover, the increased viscosity also affects the film thickness, which is significant findings in this work.

On the other hand, the development of the screen print method is equally important. The morphology or other properties of ceramic films have influenced by ink composition. Paul et al. [85] investigated the effect of difference of organic vehicle on rheology and effect of YSZ loading on screen-printed film properties. His work reported that increasing of ceramic powder increase ink viscosity. Another thing, thickness, and roughness of film depends on solid loading while the density of the film is not. Furthermore, OCV of cell ranges (1.05-1.089 V) of close to theorem Nernst voltage at 1.10 V. In 2013, Somalu et al. [86] studied rheological of nickel/scandium stabilized zirconia (Ni/ScSZ) ink base on terpineol and texanol solvent with 1 to 3 wt.% of binder for screen printed anode film. The properties of ink and film were affected significantly by a binder more than solvent. Increasing of binder in ink has an influence on thickness and roughness of dried film and improving elastic properties in ink. In terms of electrochemical, DC electric conductivity also has the same trend as the other properties due to increasing binding content to improve the particle connectivity and density of film. The lowest total polarization of screen printed was observed in having 3% wt.% binder which is an optimized binder in this study.

3.1.2 Sintering temperature

Secondly, the sintering temperature is an important parameter that determines the properties of the ceramic film. In 2008, Wang Z. et al. [34] evaluate the densification process of the YSZ layer on NiO/YSZ via the dip-coat method in three temperatures. The sintered film at 1300 and 1400 $^{\circ}$C is smaller gain size than film at 1500 $^{\circ}$C, and the two layers between YSZ and anode were observed. While the sintered film at 1500 $^{\circ}$C was found Ni agglomerate formation in substrate on account to the over-sintering phenomena. In the electrochemical section, the conductivity and resistance of cell decrease and increase, respectively, when the co-fire sintering temperature increase. The fuel cell performances, OCV values at all sintered temperatures shown higher than

Nernst voltages. The best of all is the cell with the YSZ layer at 1300 $^{\circ}$C which obtains maximum power density at 800 $^{\circ}$C. Then Hanna T. et al. [87] present the effect of different temperatures of pre-sintering YSZ electrolyte layer on anode substrate by dip-coat process. This literature found that the defect of films such as pore and void appeared on the pre-sintered at high temperature. Besides, the sintering behavior was studied by the dilatometric method. The densification step of YSZ film began at 1000 $^{\circ}$C, and linear shrinkage decreased when the YSZ film was pretreated at high temperature. Recently, Hirofumi S. et al. [88] investigated micro defect in screen printed YSZ layer on supported anode at different sintering temperatures via in-situ X-ray stress measurement for non-destructive method. As a result, the internal compressive stress in the YSZ layer decrease with decreasing fire temperature. Although at 1200-1300 $^{\circ}$C shown low internal stress values, the cross-section area appeared micro-crack and pore which bring about gas and fuel leak. For the sintered film 1400 $^{\circ}$C. have a too much internal stress value. The suitable temperature for manufacturing at 1350 $^{\circ}$C and the micropore in thin film can be reduced the internal stress 50-100 MPa.

3.1.3 Thickness of film

The thickness of film is one factor for considering electric or ionic conductivity. The electrochemical performances of fuel cells also depend on the thickness of the electrolyte layer. As an example of previous research, Sun-Dong K. et al. [89] varied the thickness of YSZ layers that produced in the dip-coat method on the anode functional layer. This research records the relationship between thickness and maximum power density. The reducing of the thickness of the YSZ layer from 10.5 to 6.5 μm can increase maximum power density at 700 and 800 $^{\circ}$C up to 89.7% % and 51.4% respectively due to the decreasing of film resistance (Figure 3.1).
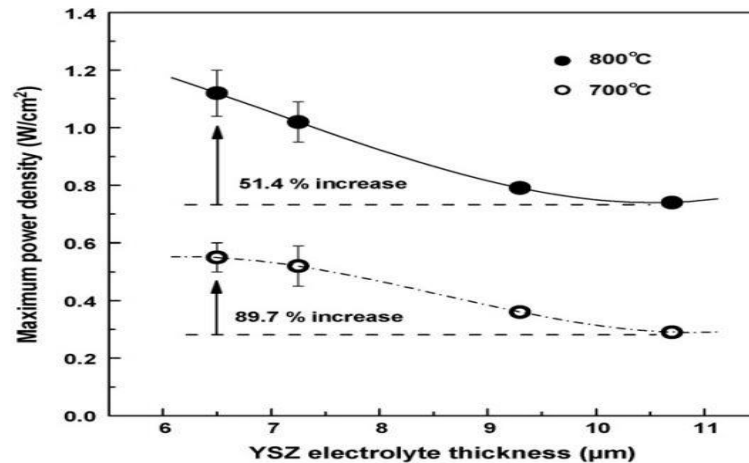
Figure 3. 1 Maximum power density of single cells for YSZ electrolyte thickness[89].

From the previous literature review can be summarized that several factors have affected microstructures and their properties like physical and electrochemical properties. The list of these factors includes the composition of slurries, step to sintering, sintering temperature, the thickness of thin-film, etc. The researchers are still studied and developed the dip-coat process to more efficient utilization.

3.2 NEMCA for light hydrocarbon oxidation reaction

The best known NEMCA was observed unexpectedly by Vayenas and Stoukides. The phenomenon based on the concept described earlier in sections 2.1, 2.2, and 2.6. NEMCA is a promising application mixed with many scientific and engineering fields, e.g., heterogeneous catalysis, fuel cell, electrolysis, and battery. It becomes crucial to be the exhaust gas treatment researches. The NEMCA is classified into four types following global electrochemical rules (Figure 3.2): purely electrophobic, purely electrophilic, volcano, and inverted-volcano, as maintained by changes in reaction rates concerning changes in catalyst potential. Commonly, reactions are seemingly able to show more than one type of the four behaviors base on reaction conditions and kind of catalysts. The NEMCA effect depends on several parameters follow:
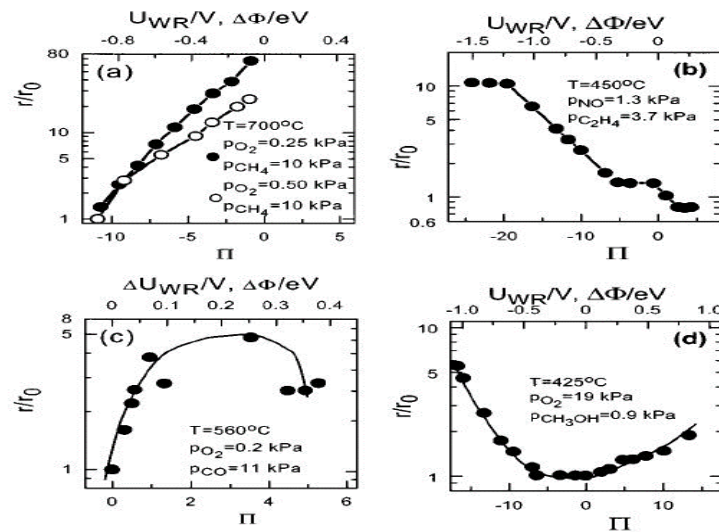
Figure 3. 2 Examples of the four types of NEMCA behaviors. r/r0 represents the ratio of the rate when a potential difference ΔUWR between the working electrode and the reference electrode work function ϕ, change (vs I = 0), and dimensionless catalyst potential $\Pi = F \Delta U_{WR} /RT$ on the rate of reaction[50].

The type of gas or gas ingredient has been reported to affect NEMCA behavior. Jiménez-Borja, C. et al.[14], has been reported the electrochemically promoted combustion of natural gas mainly comprised of methane, ethane, and propane at temperature 340 to 420 °C in a lean condition. The result in methane oxidation over this electrode exhibits electrophobic behavior that increases in alkane consumption rate under anodic polarization while ethane and propane have invert-volcano behavior. Then Peng-ont S. et al.[12], in this work, studies the NEMCA effect in methane and propane oxidation over sputtered-thin film of Pd supported YSZ disk under excess oxygen gas condition at temperatures from 320 to 450 °C. From this investigation, both methane and propane oxidation reaction over Pd film exhibit electrophobic type. Also, the XRD results point is clear evidence for the phase transformation of Pd to PdO after methane oxidation. This phase transformation stabilizes to activate the catalyst electrode for methane oxidation reaction. At last, Matei F. el al.[90], this work was successfully Pd thin film on porous-dense YSZ electrode for use in electrochemical promotion of methane combustion. These reactions were investigated at temperature range 350 to 430 °C under reducing, stoichiometric and oxidizing conditions. As a result, the porous

electrode is a quite increase in the rate of CO_2 generation with a higher NEMCA effect than the dense electrode. For porous electrode cases, reducing condition, at the lowest temperature (350 °C), exhibits electroprobic type while other temperatures appear invert-volcano behavior. Because in high temperatures under rich conditions, the methane oxidation is determined by competitive adsorption of methane and oxygen, leading to low coverage of both acceptor (O_{ads}) and donor (CH_4) on the catalyst surface. Weak adsorption of both reactant species on the surface causes an increased methane oxidation rate under both anod,ic and cathodic polarization. In parts of stoichiometric and oxidizing temperature perform electroprobic behavior.

3.3 NEMCA in propane oxidation reaction

3.3.1 Mechanism

In this section, there present the previous literature review for NEMCA in propane oxidation which focus on the evolution of this reaction, development of electrochemical cell and include the significant finding in their work.

Vernoux, P. et al.[91] investigated the mechanism of NEMCA in propane oxidation over Pt/YSZ electrode by isotopically labeling studies under open circuit and anodic polarization condition. This study shows three equation for open circuit (3.1), ^{18}O in reaction atmosphere react with propane on the platinum surface become $C^{18}O_2$. During electrochemical polarization, carbon dioxides are generated from three-way that shows in equation (3.1), (3.2), and (3.3).

$$C_3H_8(ads) + 10^{18}O^{2-}(ads) \rightarrow 3C^{18}O_2 + 4H_2^{18}O \quad\quad (3.1)$$

$$C_3H_8(ads) + 10^{16}O^{2-}(YSZ) \rightarrow 3C^{16}O_2 + 4H_2^{16}O + 20e^- \quad\quad (3.2)$$

$$C_3H_8(ads) + 5^{16}O^{2-}(YSZ) + 5^{18}O^{2-}(ads) \rightarrow 3C^{16}O\,^{18}O + 4H_2^{16}O\,^{18}O \quad (3.3)$$
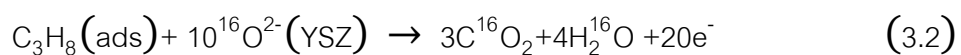
In (3.1), $C^{18}O_2$ formed the catalytic reaction. Adsorbed oxygen react with the carbon from propane adsorption. Then, the reaction of the electrochemical pathway produces $C^{16}O_2$. For this pathway, thermally supplied back-spillover species migrate on

the catalyst surface with propane (eq (3.2)). Finally, $C^{16}O^{18}O$ due to the controverting between the two oxygen species present on the catalyst surface according to the equation (3.3), which confirms anionic defect such as oxygen vacancies in YSZ, favor oxygen exchange reaction. Another thing that provides clear evidence of values of $\Delta rC^{16}O_2$ lay on around the line of $\Lambda=1$, confirming that the $C^{16}O_2$ production generated from the electrochemical oxidation of propane (Figure 3.3 a) and b)). However, important production of $C^{16}O^{18}O$ was displayed due to oxygen exchange reaction on Pt surface at three-phase boundaries, which shows to form sacrificial oxygen species.
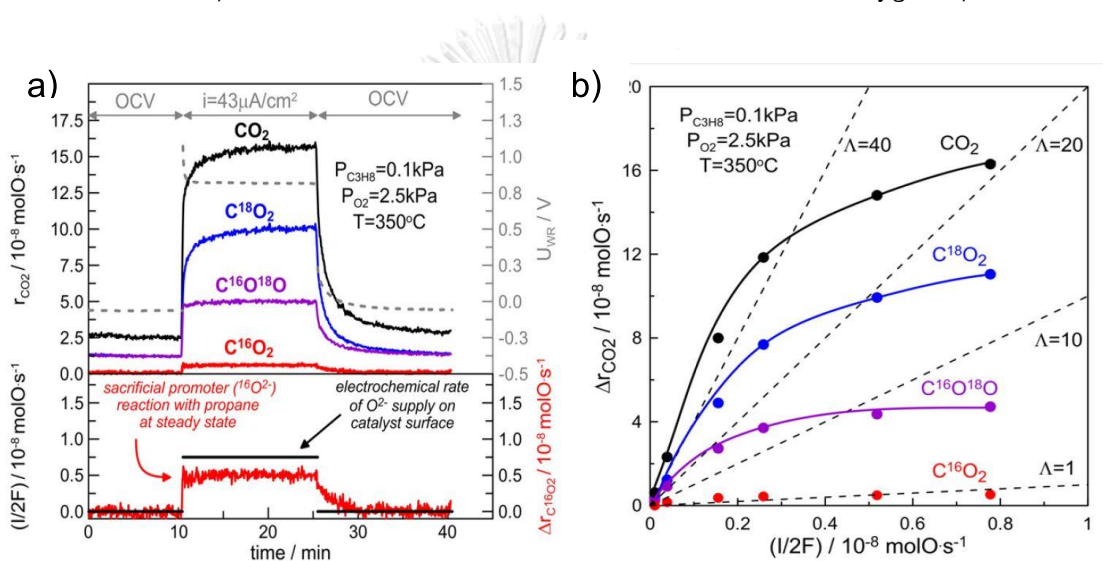
Figure 3. 3 *a) Transient response on the catalytic activity of propane deep oxidation and the catalyst potential (dashed line) during C_3H_8 oxidation on Pt/YSZ electrode. (bottom) Comparison between the electrochemical rate of O^{2-} supplied onto the Pt surface and the rate increase of $C^{16}O_2$ production. b) Effect of O^{2-} supply on the CO_2 formation rate increase. Dashed lines correspond to Λ [91].*

3.3.2 Effect of catalyst electrode

This topic focuses on specialized NEMCA cells, which are different from the traditional system. To begin with, Vernoux P. et al.[11], prepared Pt/YSZ composite electrodes by wet impregnation in two different Pt contents between 1 and 5 wt%, followed by isostatic pressing at 1000 °C. These electrodes are observed

electrochemical properties by using AC impedance spectroscopy at temperatures from 350 to 600 °C under He, O_2/He, and C_3H_8 /O_2//He atmosphere and NEMCA experiment for propane oxidation have been investigated in the same condition. Results indicate that Pt particles act as blocking of the ionic conductivity, and grain boundary was ascribed to the formation of PtOx layer of chemisorbed oxygen on Pt particles. The catalytic activity of porous Pt/YSZ composites electrodes for propane deep oxidation was higher than conventional Pt films deposited on a dense YSZ pellet. Unfortunately, NEMCA effects cannot detect in their operating conditions. The next, Lizarraga L. et al. [81] compare two preparation of Pt layer between DC magnetron sputtering and conventional paste painting on YSZ pellet. The sputtered Pt is a higher dispersion and OCV rate of reaction than Pt paste due to the nanometric structure of sputtered Pt. and Both type cells shown electrophobic behavior according to prior report. Then, Kabolis A. et al. successful prepared low Pt loading and highly dispersion in porous GDC/LSCF on dense GDC disc. The NEMCA effect was detected at low temperatures (267-338 °C) under positive polarization. Another thing, Peng-ont S. et al.[53], in this work, studies the NEMCA effect in propane oxidation over sputtered-thin film of Pd, Ir, and Ru supported YSZ disk under excess oxygen gas condition at temperatures from 320 to 450 °C. Under open-circuit conditions, the catalytic activity of fresh electrode was found to decrease in the series of Ru, Pd, and Ir; respectively however, for used electrode, the activity decreasing of series was Pd, Ru, and Ir. Respectively. In polarization, all three electrodes exhibit electrophobic type.

3.3.3 Effect of operating temperature

Table 3. 2 Comparison of faradaic efficiency, rate enhancement ratio and rule of promotion of propane oxidation reported in different previous research

Preparation method	Electrode	Temperature	Result	Promotional types
Sputtering[81]	Pt-YSZ	400 °C	$\Lambda = 1 \times 10^6$	Elecrophobic
Sputtering [92]	Pt-YSZ	350 °C	$\Lambda = 330$ $\rho = 5.6$	Elecrophobic
Pt Paste [93]	Pt-YSZ	420 -520 °C	$\Lambda = 2330$ $\rho = 1350$	Invert-volcano
Pt Paste [10]	Pt-YSZ	350–500 °C	$\rho = 1400$	Invert-volcano
Sputter-deposited Pd film on YSZ [12, 53]	Pd-YSZ	320–450 °C	$\Lambda = 250$ $\rho = 3$	Elecrophobic

Previous literature reviews in Table 3.2 are summarized that electrophobic behavior display at low to medium temperatures, the propane oxidation generally exhibits while at higher temperatures, usually higher than 450 °C, inverted-volcano behavior is detected for both anodic and cathodic region bring to an increase in catalytic activity. Also, isotopically labeling in the reaction was proposed oxygen exchange reaction generated in Pt/YSZ system.

3.4 Other the NEMCA configuration cell

Wring connection between the working electrode and the counter-electrode of a cell is common in the complication of NEMCA systems. A rare work focuses on to relieve this constraint by introducing alternative cell layouts. Marwood and Vayenas [94] achieve an isolated Pt electrode positioned between two Au electrodes between which potential differences were imposed (Figure 3.4). This cell configuration is called the

wireless of bipolar [95]. When potential or current were applied between two gold electrodes that one side electrode exhibits a positive charge while the opposite side electrode exhibits a negative charge. This phenomenon leads to effective double layer forming and induce to NEMCA phenomenon [9, 15].
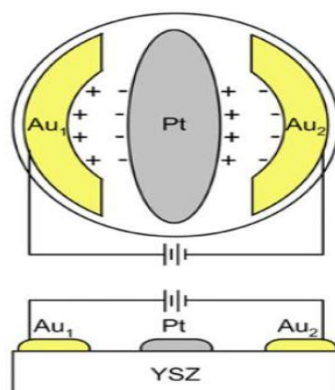
Figure 3. 4 *The bipolar configuration cell[94]*

Besides, the effect of platinum size on the bipolar cell was reported by Bumroongsakulsawat P. et al. [15] that studies NEMCA of propane oxidation on Pt disperses, which prepared by wet impregnation (WI) and strong electrostatic adsorption (SEA) on YSZ disks. The NEMCA cells which are wireless configuration was studied and compared in stoichiometric conditions. As a result, the Pt film that was prepared by SEA showed the enhancement ratio and faradaic yield higher than WI method. Since SEA method can be effective, Pt dispersion more than WI method leading to smaller Pt particles. The small Pt particle can be induced to the favorable condition of oxide migration on Pt surface better than larger particles (Figure 3.5).
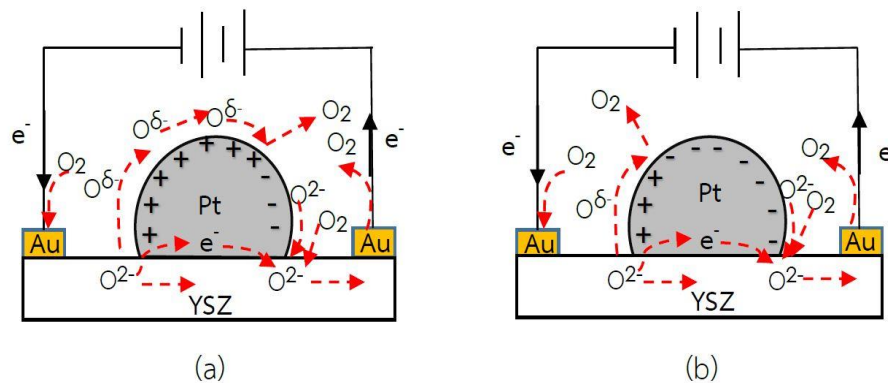
Figure 3. 5 *The migration of O^{2-} cover Pt in wireless configuration: favorable condition (a) and unfavorable condition (b) [15]*

3.5 sintering additive for YSZ

Dense YSZ membrane was produced approximately 1400 °C for excellent stability and perfectly ionic conductivity, but at a temperature above 1250 °C, YSZ can be reacted with the interface between YSZ and cathode and may lead to deactivation of activity in the electrochemical cell. Therefore, the solution to this problem is reducing sintering temperature. The densification of YSZ can be improved at lower temperature in two ways. First, the membrane made from nanoscale powder. However, the nano YSZ is lower thermal stability than micro YSZ, and high cost for preparation was considered. Second, the addition of metal or oxide into YSZ that this chemical increase grain connectivity and their chemical are called "sintering aid or sintering additive." One more advantage of reducing the densification temperature is production cost saving.

In the previous literature, sintering aids were reported as follows: to begin with, copper oxide (CuO) [96] was reported to reduce sintering temperature of YSZ at 1130 °C because of the generation of $CuO(Cu_2O)-Y_2O_3-ZrO_2$ eutectic liquid phase. However, the addition of CuO also decreases bulk and grain boundary conductivity [97]. Zinc oxide was studied in the role of sintering additive. Yang F. et al. [98] varied the amount of ZnO between 1-3% mole in the YSZ pellet. As a result, 2% mole of ZnO obtain dense YSZ at 1200 °C and increase total conductivity at 800 °C. Cobalt oxide was also interested in grain growth additive. The small amount of Co_3O_4 can reduce sintering

temperature approximately 1195 °C and still have electrochemical properties like pure YSZ, which sintering at higher temperatures [99]. Although these additives can improve the sinter-ability of YSZ, their performances are limited to 100-300 °C. Interestingly, Kim H. can produce dense YSZ at 900 °C in addition to bismuth oxide (Bi_2O_3) [100]. In reducing or vacuum, segregation of bismuth droplet on the surface in which the electrolyte becomes poor conductivity due to the reduction of bismuth oxide to metallic bismuth [101] Recently, Masahiro N. et al. [102] successive prepared YSZ pellet at 800 °C for sintering temperature by addition copper doped bismuth vanadate (BICUVOX.10). Their conductivity was slightly lower than pure YSZ which sintered at 1300 °C and under low oxygen partial pressure not affected to conductivity.
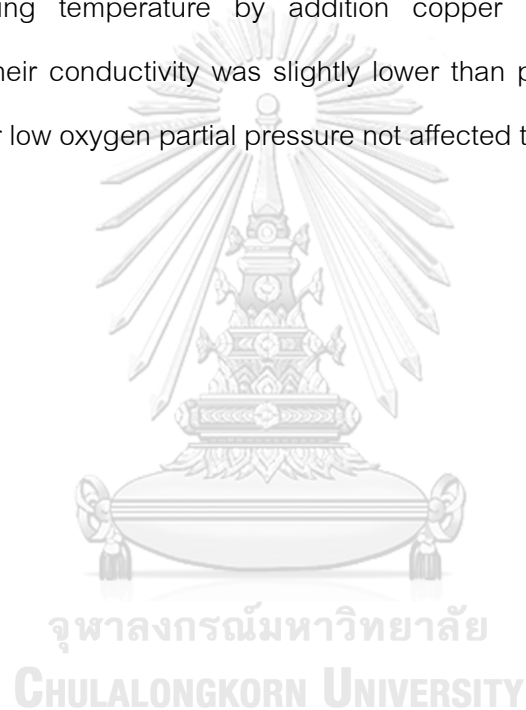
CHAPTER 4

METHODOLOGY

This chapter is divided into three-part. Firstly, the processes of preparation, characterization, and NEMCA observation of Pt/YSZ/Au thin film in which the YSZ layer was fabricated via dip-coating was described. The second part, general details for the synthesis method and characterization of BICUVOX.10 were explained. The last section will provide an experiment procedure about screen printed YSZ thin film in which BICUVOX.10 was added.

PART 1: The study of NEMCA behavior of Pt/YSZ/Au thin film on dense $A_{l2}O_3$ substrate

4.1 Electrode and electrolyte preparation

4.1.1 Preparation of YSZ slurries

YSZ slurries were prepared with 78 wt% xylene (Sigma-Aldrich) and 22 wt% butyraldehyde (Sigma-Aldrich) as a solvent and polyvinyl pyrrolidone (PVP, Sigma-Aldrich) as a dispersant. The amount of YSZ powder (TZ8Y, Tosoh Co.) was kept at 20 wt%. Poly-vinyl-butyral (PVB, Butvar B98, Santa Cruz Biotechnology) was selected as a binder, and polyethylene glycol (PEG-400, Merck) was used as a plasticizer.

The colloidal technique was used for the preparation of the coating slurry. In the first stage, the solvent dispersant and binder were mixed with YSZ powder under continuous stirring. Then the plasticizer was added into the mixture and stirred until a homogeneous mixture was obtained.

4.1.2 Fabrication of YSZ thin films by dip-coat technique and electrode preparation

The substrates were dense alumina discs of 20 mm in diameter and 1.2 mm in thickness (sliced from alumina rods, Coorstek Inc) by precision cutting machine (IsoMet® 1000, precision sectioning saw, BUEHLER). The gold counter-electrodes were sputtered on the alumina disks by sputtering (JOEL: JFC-1100E Ion sputtering). Then, the dip-coating process was carried out in slurries. YSZ layer was dried at room

temperature overnight before sintering at 800 °C for four h to obtain YSZ thin films. Finally, YSZ/Au on alumina discs were coated with Pt by sputtering. The NEMCA cell configuration as shown in Figure 4.1.
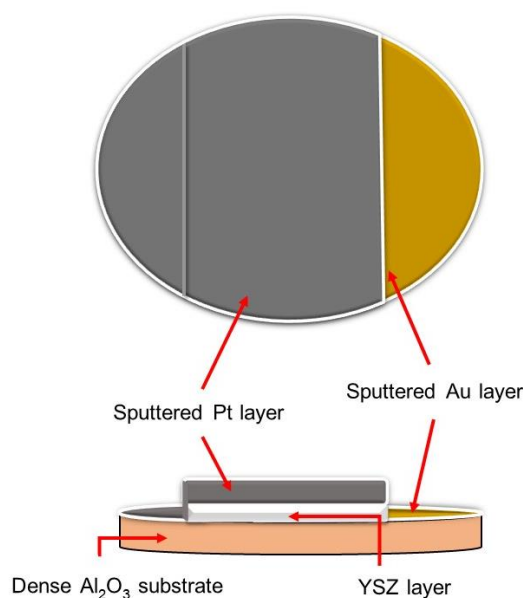
Figure 4. 1 *Top view and side view of NEMCA thin-film cell*

4.2 Catalytic activity measurements

NEMCA experiment of propane oxidation was studied in a continuous flow quartz reactor in which all two-electrode exposed the same reactive gas under a stoichiometric ratio of propane to oxygen. Mixtures of 3% C_3H_8 in He balance (Linde), 10% O_2 in He balance (Linde), and He (Linde, 99.995 % purity) as the vector gas were used under atmospheric pressure (C_3H_8: O_2: He ratio 16.67 cm^3: 25 cm^3:58.33 cm^3). Mass flow controllers controlled the gas compositions and fixed constant total gas flow rate of 100 cm^3 min^{-1}. For electric connection, sputtered gold joined with the gold wire as counter and reference electrode as well as the Pt layer on the opposite side but, Pt act as the catalyst electrode. The catalytic performance was investigated between 200 and 500 °C. The reaction temperature was monitored through a K-type thermocouple and controlled by SHINKO 100 FCD 100 series temperature controller.

The reaction products (CO_2) were analyzed by an online IR spectrometer (YOKOGAWA, IR200-JNGHFGHKNN-4TU). A potentiostat–galvanostat (Autolab, PGSTATE101) was used to apply, measure, and record both potentials and currents. Faradaic yields and rate enhancement ratios were calculated results by equation 2.4 and 2.5, respectively. The diagram of the experimental apparatuses are shown in Figure 4.2.
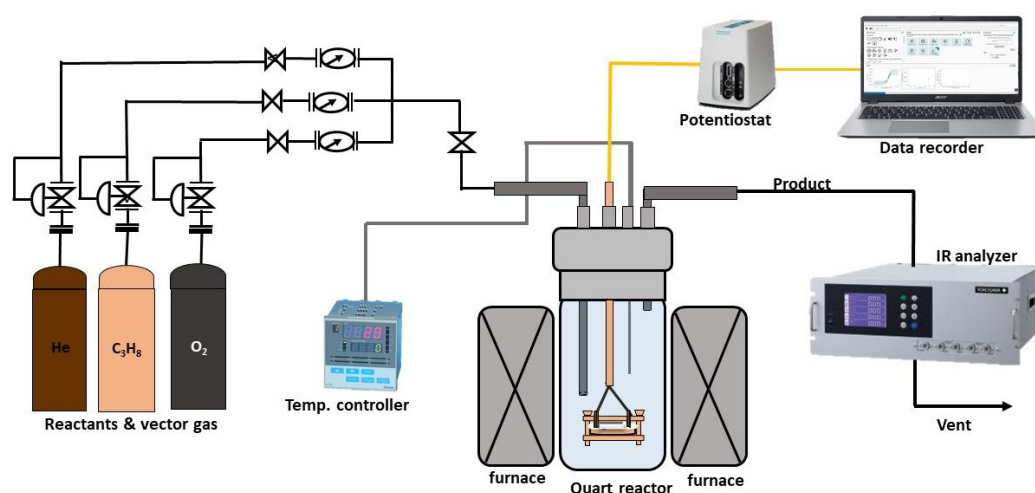
Figure 4. 2 Schematic diagram of the experimental apparatuses

4.3 Characterization of electrode

Firstly, the thermal decomposition behavior of organic additive in YSZ dip-coated film was studied by thermal gravimetric and differential thermal gravimetric method (TGA/DTG, Diamond thermogravimetry, and Differential Analyzer, TA Instrument SDT Q600). The thermal analysis is record at room temperature to 800 °C (film sintering temperature), heating ramp 5 °C/min under 100 ml/min of airflow. All electrode samples (fresh and used) were analyzed by scanning electron microscope (SEM, JEOL model JSM-5800LVand Link Isis Series 300 program) and energy-dispersive x-ray spectroscopy (EDX, EDAX APEX™ EDS Analysis Software) for the morphology and determination of elemental distribution. The crystalline phases of the platinum and its

YSZ support were examined by X-ray powder diffraction (XRD) performed in a Bruker D8 Advance powder X-ray diffractometer with CuKα source.

PART2: SYNTHESIS AND CHARACTERIZATION OF COPPER DOPED BISMUTH VANADATE COMPOUND ($Bi_2V_{0.9}Cu_{0.1}O_{5.35}$, BICUVOX.10) AS SINTERING ADDITIVE OF YSZ THIN FILM

4.4 Synthesis BICUVOX.10 via two steps solid-state reaction (SSR)

This process of synthesized powder has been according to previous literature by Masahiro et al. and modified detail in some steps [102]. The starting material used in the SSR method were bismuth oxide (Bi_2O_3, sigma Aldrich, 10μm, 99.9%), vanadium oxide (V_2O_5, sigma Aldrich, ≥98%) and copper (II) oxide (CuO, sigma Aldrich, ≥99.0%). Additionally, Bi_2O_3 powder was pretreated at 600 °C for 4 hours. This step is the decarbonization process, which is removed carbonate on the Bi_2O_3 surface. The stoichiometric ratio of each oxide was stabilized in ethanol and homogenized for 24 hours by using a plenary ball mill at 400 rpm with the ball to powder ratio (BPR) 10:1. After that, mixed oxide slurry was evaporated solvent at 120 °C until completely dry powder. Then mixed oxide powder was calcined in ambient air at 800 °C for 2 hours. Calcined powder was milled and fire again; However, the speed of milling was shortened to 200 rpm, and the reaction time in the furnace was elongated to 10 hours. The final product was reduced particle-sized by plenary ball mill at 200 rpm.

4.2 Characterization of BICUVOX.10 powder

The structure of powder was analyzed by X-ray powder diffraction (XRD) performed in a Bruker D8 Advance powder X-ray diffractometer with CuKα source. The diffractogram was recorded over 2θ range of 10-80°. The surface morphology and elemental dispersion was obtained by SEM (Jeol) and EDX (EDAX APEX™ EDS Analysis Software). The elements and chemical composition of synthesized oxide were determined through the standard calibration method by using inductively coupled plasma (ICP-OES spectrometer ICP-OES optima 2100 DV from Perkin Elmer). Chemical

state on the surface of synthesized powder was observed by X-ray photo photoelectron spectroscopy (XPS, AMICUS/ESCA-3400 XPS instrument, KRATOS ANALYTICAL, SHIMADZU COMPANY) which binding energy from analyzed samples represent oxidation state or molecule bond of element. Finally, thermal analysis confirms the highest ionic conductivity phase which is tetragonal γ phase by differential scanning calorimetry (DSC, Diamond thermogravimetry, and Differential Analyzer, TA Instrument SDT Q600).

PART3: FRABICATION OF YSZ-BICUVOX.10 THIN FILM VIA SCREEN PRINTING METHOD AND NEMCA OBSERVATION ON THIN FILM CELL

4.4 Preparation of YSZ-BICUVOX.10 powder and their paste

YSZ-BICUVOX.10 powder was prepared by the physical mixing method. The precise amount of BICUVOX.10 range 1.5-4.5 mole% was added in YSZ powder and blended in ethanol media for 24 hours. This slurry was dried at 120 °C overnight. For YSZ-BICUVOX.10 paste, the organic vehicle was made by dissolving 5 wt.% of PVB into 92 wt.% α-terpineol (Sigma-Aldrich). Besides, 3 wt. % of PEG 400 was added for improving plastic property of composite film Then the blended ceramics powder was mixed in the organic vehicle and continuously stirred until the ceramic paste is viscous and homogeneous. Moreover, TGA and DTG was investigated thermal decomposition of organic phase in ceramic paste during YSZ film was sintered in atmosphere condition by Diamond thermogravimetry and Differential Analyzer, TA Instrument SDT Q600 equipment. Finally, the observation of phase transition and solid-state reaction was investigated by XRD analysis (X-ray powder diffraction performed in a Bruker D8 Advance powder X-ray diffractometer with CuKα source). The composite powder was analyzed over 2θ range of 10-80°. The morphology of composite powder was determined by scanning electron microscope (SEM, JEOL model JSM-5800LVand Link Isis Series 300 program)

4.5 Cell configuration and catalytic measurement

The cell configuration and NEMCA experiments were, according to 4.1.2 and 4.2, respectively. Nevertheless, a different electrolyte coating layer, YSZ film was grown on sputtered Pt/ dense Al_2O_3 disc using the screen print method. The composite paste was pressed through a woodblock screen with 120 mesh by rubber squeegee (70 durometer) until the ceramics paste ensures complete coverage. This film was slowly dried at room temperature for two days. After that, the dried film was sintered at 800 °C for 4 hours. The surface morphology and structure of composite films were investigated via scanning electron microscopy (scanning electron microscope (SEM, JEOL model JSM-5800LVand Link Isis Series 300 program) and X-ray diffraction analysis (X-ray powder diffraction performed in a Bruker D8 Advance powder X-ray diffractometer with CuKαsource).
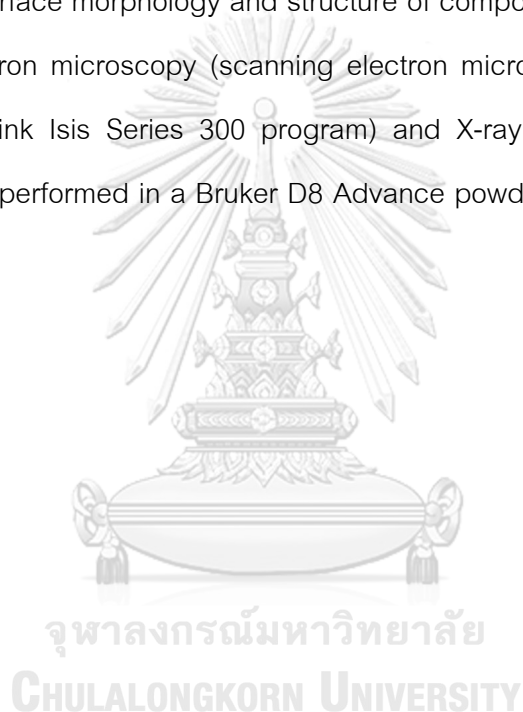
CHAPTER 5

RESULTS AND DISCUSSION

This chapter represents the electrochemical promotion of catalysis experiment in Pt/ YSZ thin electrode on the corundum substrate for propane combustion. To begin with, Pt/dip-coated YSZ/Au system was studied NEMCA effect including problems and limitation for this electrode was discussed to possible solution in this section. Secondly, BICUVOX.10, as sintering aid, was reported about characteristic properties. Finally, Pt/ YSZ thin electrode via screen printed YSZ was investigated and observed NEMCA behavior.

PART 1: The study NEMCA behavior of Pt/YSZ/Au thin film on dense $A_{l2}O_3$ substrate

5.1 Investigation of thermal decomposition of organic ingredient in dip-coated YSZ thin film

In general sintering process of YSZ pellet or film was operated at high temperature. However, this work use sputtered Au thin film as a counter electrode. The melting point of gold approximate 1064 $^\circ$C that is a limitation for the densification process of YSZ. Preparation of YSZ thin film at low temperature was taken into consideration. The thermal analysis was used to investigate the decomposition of the organic compounds in the slurry. The TGA and DTG curves display in Figure 5.1. The weight loss in the temperature range from 0 to 150 $^\circ$C was purported to the moisture dehydration, which absorbed on the surface of the thin film. Then the temperature between 150 to 200 $^\circ$C attribute production of butanoic acid, butanol and butyraldehyde from cyclic butyral [103]. The third peak of the DTG curve appears above 250 to 360 $^\circ$C, which indicates the degradation of the side chain of PVP and PVB [103, 104]. Another thing, PEG can decompose in the temperature range of 300 to 450 $^\circ$C[105]. This result confirms the entirely thermal degradation of the organic component from dip-coated YSZ thin film before 800 $^\circ$C which is sintering temperature.
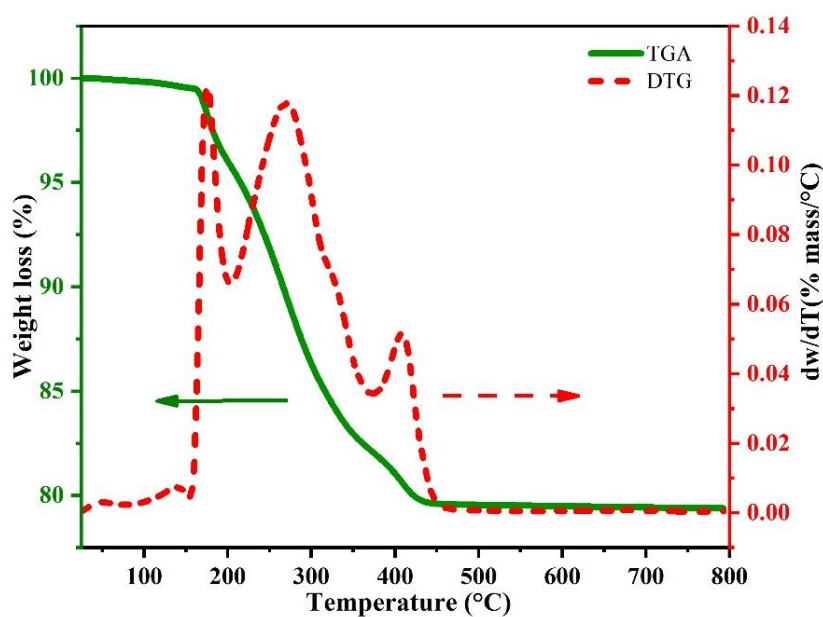
Figure 5. 1 TGA and DTG curve for thermal analysis of dip-coated YSZ thin film

5.2 Morphology of Pt/YSZ/Au on α-Al$_2$O$_3$ disc

SEM observed the surface morphology of the substrate and each layer in Figure 18a-e. In Figure 5.2a show top view surface of α-Al$_2$O$_3$ that present dense and roughness substrate. When Gold was sputtered on the substrate in Figure 5.2b, which perfectly covers and disperse on the alumina surface. For dip-coated YSZ before and after sintering at 800 °C represent in Figure 5.2c-d respectively. Both figures do not see a significant difference after sintering. The dip-coated YSZ performed a porous film similar to a sponge. The ion migration in the YSZ layer will not be suitable due to the poor connecting of the solid electrolyte. Lastly, the high dispersion of Pt was produced via ion-sputtering and displayed in Figure 5.2e. Pt particles thoroughly cover on the YSZ layer which was confirmed by EDS in Figure 5.2f-g. EDS mapping of Pt show 76.28% wt. of Pt on the working electrode.
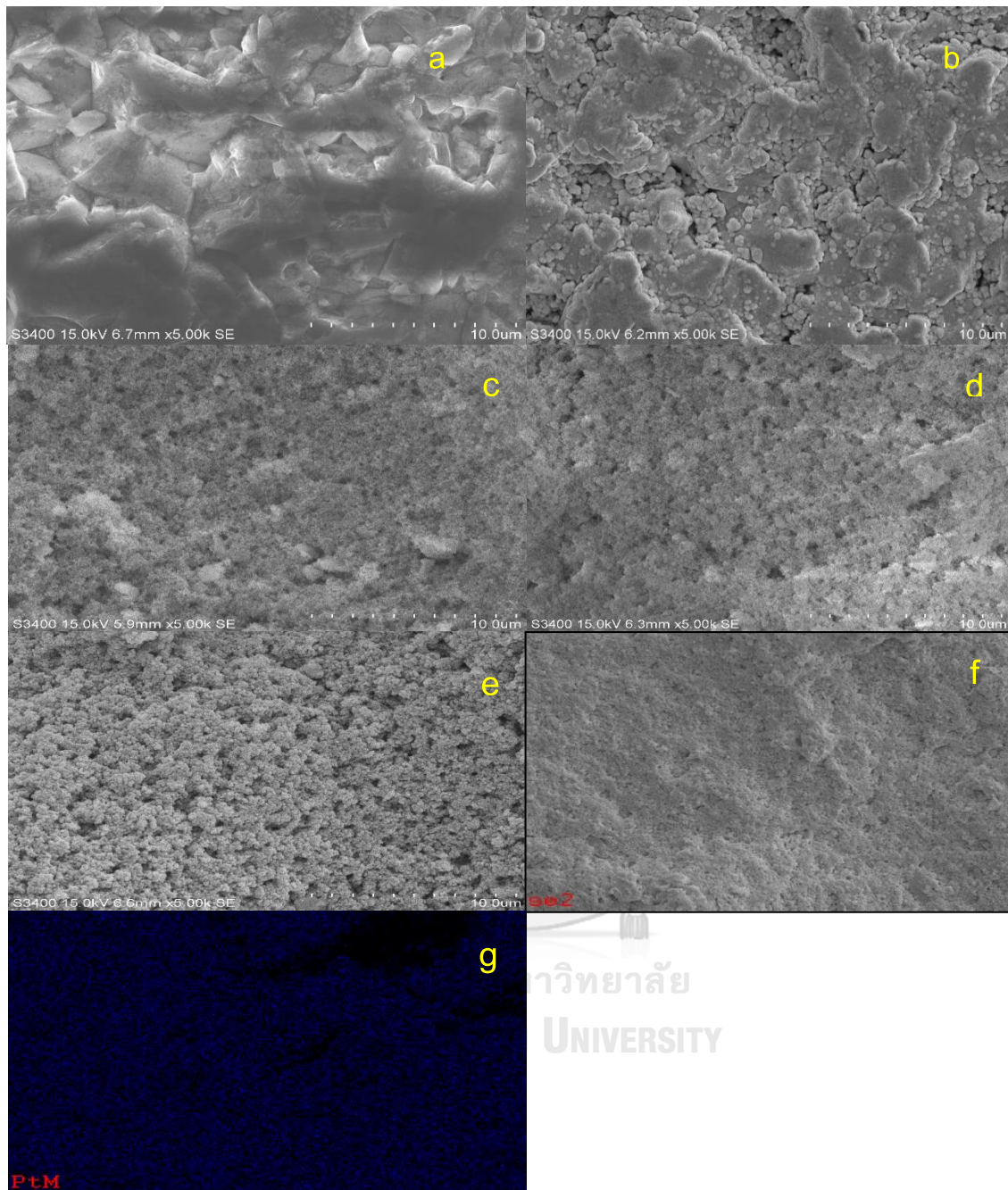
Figure 5. 2 Surface micrograph of α-Al$_2$O$_3$ disc (a), sputtered Au on α-Al$_2$O$_3$ disc (b) YSZ layer before (c), and, after (d) sintering, sputtered Pt (e) on YSZ and corresponding quantitative EDX maps: analyzed Pt layer (f), Pt (g).

The diffractogram of each layer was displayed in Figure 5.3. YSZ layer was observed in the reflection peaks for 30.0°, 34.9°, 50.2°, 59.6° and 62.5° that perform (111), (200), (220, (311) and (222) planes. These peaks were characteristic peak of cubic crystalline[106, 107]. In terms of sputtered Pt on the YSZ layer, show the reflection 2θ peaks at 38.6° and 46.6°, which correspond to (111) and (220) planes. The previous literature reported that peaks represent metallic Pt [108]. Also, the characteristic peak position of alumina substrate shifts due to the effect of YSZ layer coating on the substrate. Bragg's angle of alumina might be obscured; therefore, the angle measurements have been shifted.
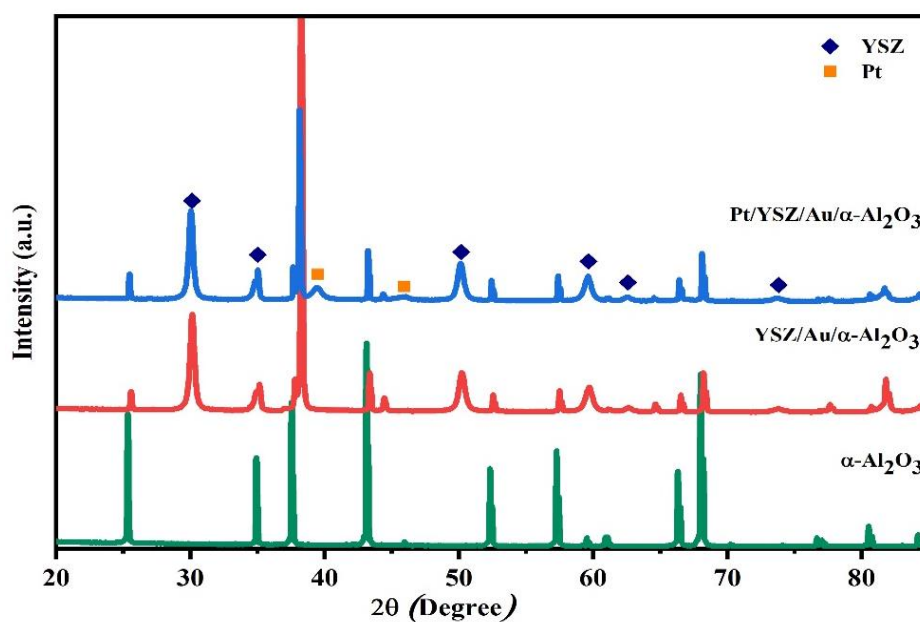
Figure 5. 3 XRD pattern of Al_2O_3 substrate, $YSZ/Au/Al_2O_3$, and Pt/ $YSZ/Au/Al_2O_3$.

5.3 Catalytic reaction test under open and closed-circuit condition

The catalytic propane oxidation on Pt/YSZ thin film was investigated under no applied external electric potential or current between 200-500 °C. The combustion curve of propane exhibits in Figure 5.4. The CO_2 formation rate increase as high temperature. This performance has behavior, according to Arrhenius's equation[44, 81].
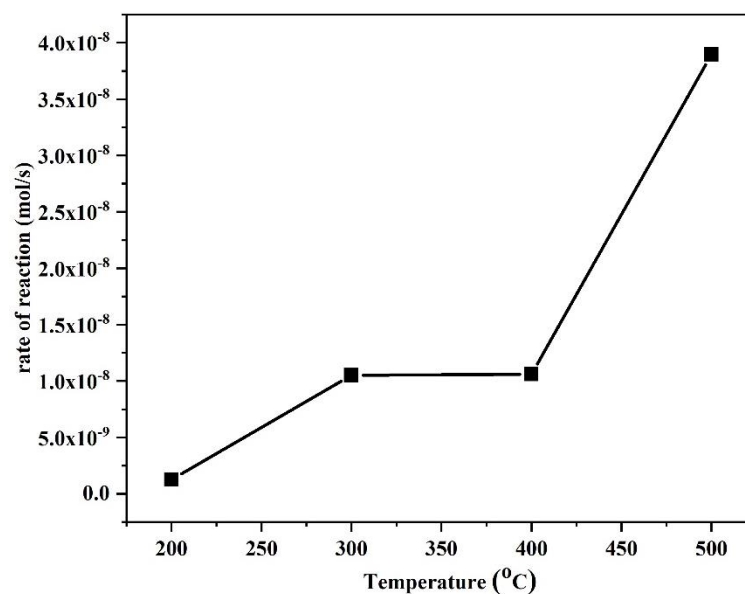
Figure 5. 4 Propane combustion curve versus temperature under open circuit condition.

The electrochemical promotion of propane oxidation on Pt/YSZ electrode was studied in the variation of applied potential cell and operating temperature. The reaction rate of propane combustion was shown in Figure 5.5. The combustion rate increase when the positive potential was applied between the quasi-reference gold electrode. Although the continuous increasing of CO_2 was detected in 300-500 °C, at 200 °C was hardly change. The rate enhancement ratio is compared between close to open circuit rate that indicated the sum of electrochemical reaction and electrochemical promotion effects. The ρ of propane oxidation shown in Figure 5.6 that increasing cell potential improves CO_2 production during polarization conditions. The NEMCA behavior exhibits electrophobic type according to previous reports[10, 12-14, 53, 93, 109]. The elecctrophobic was used to describe the migration of oxide ion from the solid electrolyte to TPB and the promotion of propane adsorption due to the generation of the effective double layer on a platinum surface. The maximum of ρ in this study observed at 400 °C and 1.0 V for applied potential. This value close to 3 and three times that of the unpromoted rate.
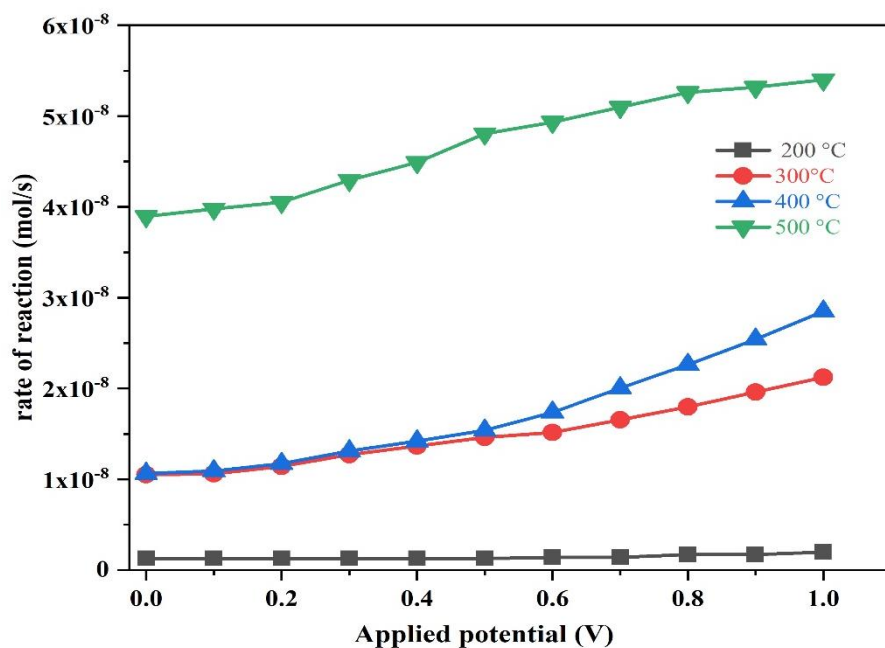
Figure 5. 5 *Effect of cell potential and temperature on CO_2 formation rate*
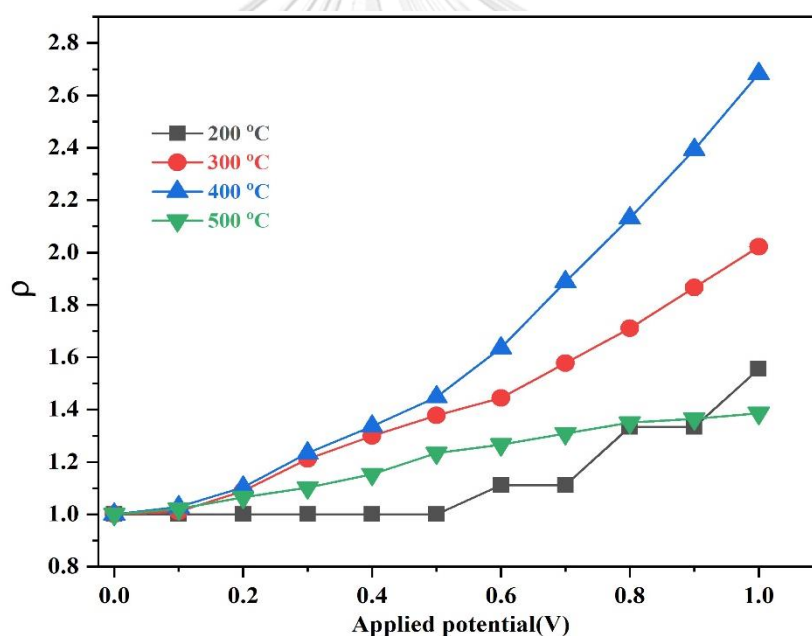
Figure 5. 6 Rate enhancement ratio, ρ, as function of cell potential and temperature.

Effect of applied potential and reaction temperature on the current of NEMCA thin film show in Figure 5.7. In 300-500 °C region, the current of cell vary on applied potential, but at 200 °C can hardly difference of current when increase potential. From Ohmic law, when increasing potential cause reducing the resistance and electron can

be mobile better than lower potential. At higher temperatures, oxide ion can transfer better than lower temperatures. Another thing, the resistance of solid electrolyte decreases at high temperature because O^{2-} was induced to oxide ion migration and caused the flow of ion in the YSZ layer[110]. For this reason, the current cell fluctuates with applied potential and temperature.
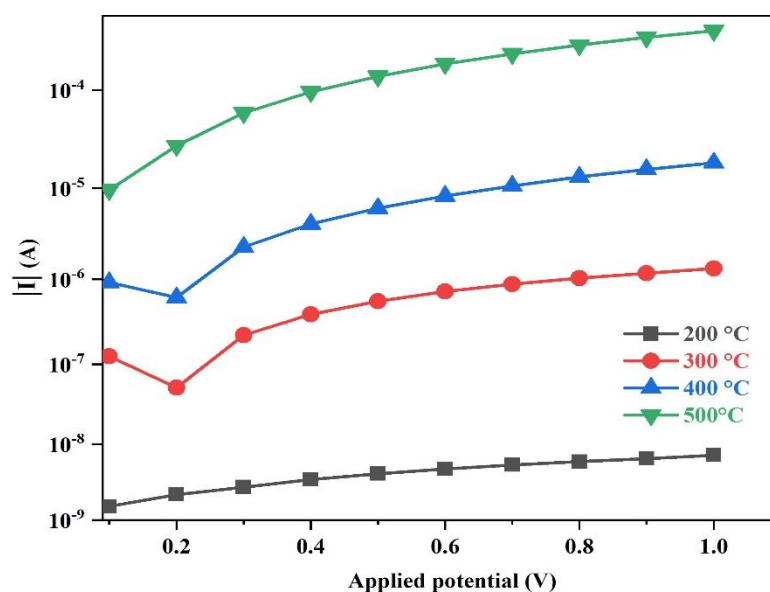
Figure 5. 7 Current of the cell as a function of applied potential and temperature.

The important parameter for considering the NEMCA effect is faradaic efficiency or Λ that indicates the effect of electrocatalytic reaction or electrochemical promotion. About Faradaic's law in terms of Λ demonstrate the rate of oxide ion that supplied to or migrate from catalyst surface[111]. Hence, Λ evinces ratio of CO_2 generation to oxygen ion flow on catalyst surface during anodic or cathodic polarization. For Pt/dip-coat YSZ electrode, the effect of anodic polarization and temperature was reported in Figure 5.8. Λ values in 300-500 °C are more significant than one that indicates clearly NEMCA phenomena. At 300 °C, h maximum Λ approximate 10,000 and was observed at applied potential of 0.2 V. Although at lower temperature and applied potential make more magnitude of Λ than higher temperature, the observation of NEMCA effect on

200°C show Λ values less than 1 which back spillover ion s are not migration in this condition. These results were consistent with previous researches by Tsiplakides, D. et al. [112] and Palermo, A. et al. [113]. In theory, the NEMCA effect needs small potential or current for generating the effective double layer on the working electrode.
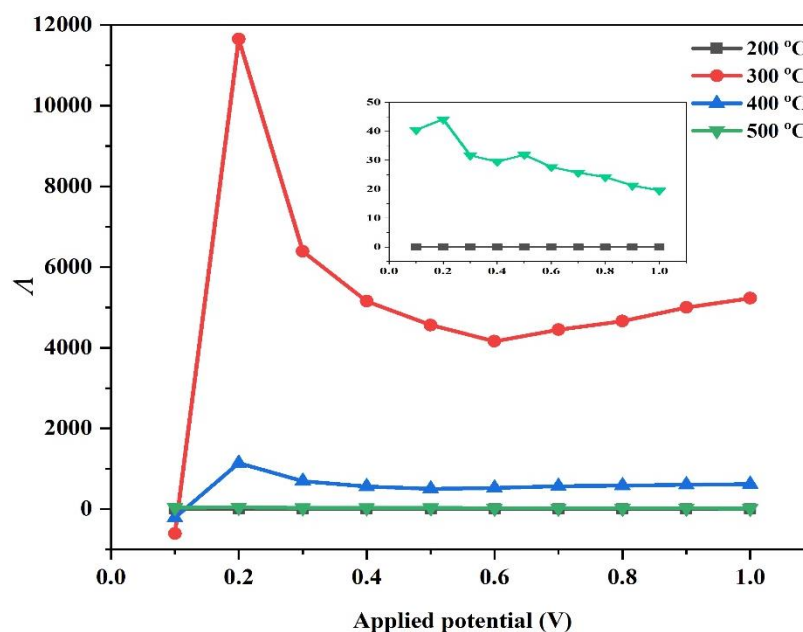
Figure 5. 8 Λ as a function of temperature and applied cell potential

The NEMCA effect on propane oxidation over Pt/dip-coated YSZ thin film can be detected in the temperature range from 300 to 500°C. Both ρ and Λ perform more one time that of open circuit rate. On the contrary, NEMCA cell at 200°C disappear the NEMCA effect due to the absence of oxide ion migration. Λ less than 1 was good evidence.

5.4 Comparison between fresh and used electrode
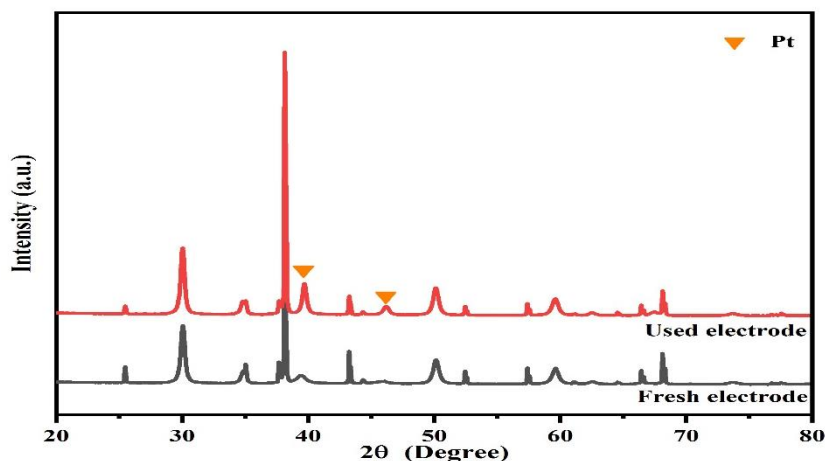
Figure 5. 9 XRD pattern of Pt/YSZ/Au on alumina disk, fresh electrode and

used electrode (operating temperature at 500 °C)

After the NEMCA experiment, the thin film electrode was analyzed and compared with the fresh electrode. Firstly. The XRD pattern of both electrodes display in Figure 5.9. The metallic Pt corresponds to 38.6° and 46.6° in the used electrode, which clearly observed to higher than the fresh electrode. The increased intensity of metallic Pt characteristic peak implied that Pt crystalline sizes are larger than Pt on fresh electrode. Secondly, the morphology of the catalyst electrode was studied by SEM. The microstructure of fresh and used Pt supported YSZ thin film at different magnifying power represents in Figure 5.10. For Figure 5.10 a) and b) can clearly distinguish between grain of Pt particle but, Figure 5.10 c) and d) show dissolved Pt grain and Pt particle agglomerate until larger than fresh sputtered Pt (in red circle). Lastly, Pt dispersion on YSZ thin film was determined by EDS mapping. As a result, the amount of Pt after propane oxidation reaction at 500 °C increased while the amounts of Zr and Y reduced. The possible way to explain that is the thermal sintering of Pt thin film. The thermal sintering might lead to deactivation of activity and catalytic performance of thin-film cells.
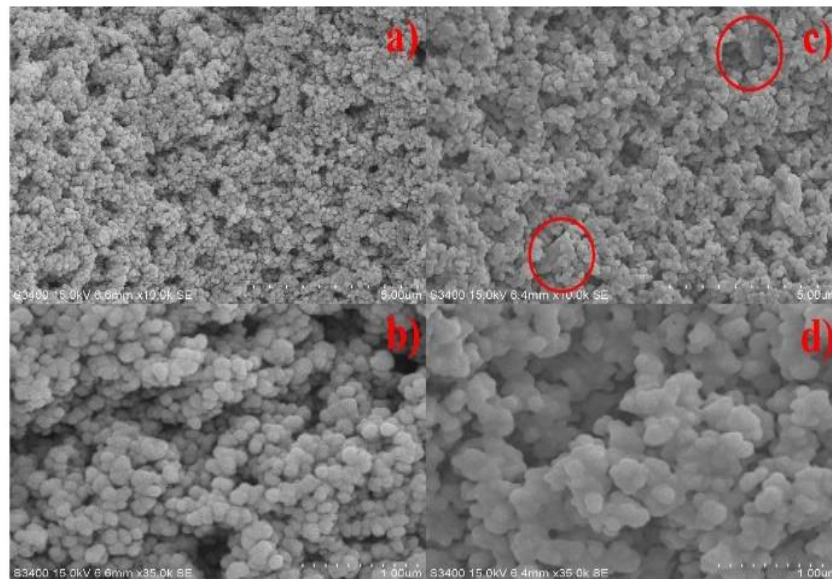
Figure 5. 10 Surface morphology of sputtered Pt/YSZ/Au on alumina substrate fresh electrode (a, b) and used electrode (c, d) at difference magnification

5.5 Problem and development for NEMCA thin film

In the application of Pt/dip-coated YSZ thin film has found difficult repeatability and reproductivity. In most cases, the NEMCA cell has poor conductivity; therefore, observation of NEMCA behavior cannot measure. The next factor, defective adhesion between dip-coated YSZ and their substrates, brings to uniform connectivity of counter electrode-solid electrolyte. Another, porous YSZ layer should be considered that porous structure has a lacking ionic conductivity. To solve this problem, the improvement of the dense layer of the YSZ layer is the first choice. In prior research reported that BICUVOX.10 is sintering aid for the YSZ system at low temperatures [102]. Second, the fabrication method for YSZ thin film was modified from dip coating to screen printing. For YSZ recipe was added with more amount of binder to increase the adhesion of the YSZ layer and connectivity of YSZ particle which was previously reported[114].

PART2: SYNTHESIS AND CHARACTERIZATION OF COPPER DOPED BISMUTH VANADATE COMPOUND ($Bi_2V_{0.9}Cu_{0.1}O_{5.35}$, BICUVOX.10) AS SINTERING ADDITIVE OF YSZ THIN FILM

5.6 Particles morphology of BICUVOX.10
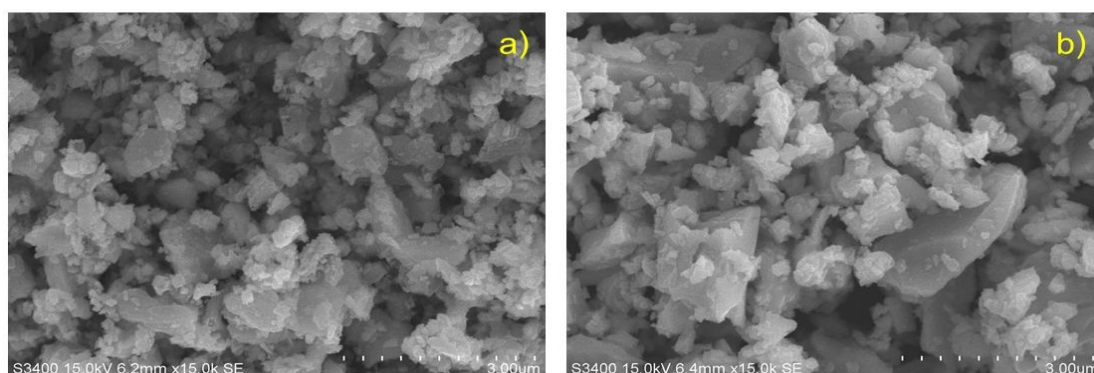
Figure 5. 11 SEM images of mixing starting material powder (a), and completely synthesized BICUVOX.10 powder (b).

Particle micrographs of raw material mixture powder and complete BICUVOX.10 synthesized powder shown in Figure 5.11. The particle sizes of mixing raw material were approximately 0.1-3.0 μm, which reduce from the initial size before ball mill at 10 μm (Figure 5.11a)). The small particles of starting material is believed to ensure a high γ' phase purity[115]. For complete synthesized BICUVOX.10 display in Figure 5.11b) that have a dense flake shape as well as previous reports[75, 116]. SEM determined particle size of BICUVOX.10 after attrition at 200 rpm for 24 hours. Particle distributions are the size in the range of 0.1-1.5 μm.

5.7 Chemical state and elemental composition of BICUVOX.10 powder

The chemical state of each element on synthesized powder was investigated by XPS analysis. XPS spectra are shown in Figure 5.12a) that record binding energy of Bi 4f, V 2p, O 1s, and Cu 2p. The characteristic binding energy of Bi 4f display in Figure 5.12b). The two symmetric peaks appear at 159.8 and 164.9 eV associated with Bi $4f_{7/2}$ and Bi $4f_{5/2}$ terms, respectively, and according to the trivalent oxidation state of Bi ion

[117, 118]. For vanadium, V $2p_{1/2}$ and V $2p_{3/2}$ was detected at 523.9 eV and 516.7 eV referred to vanadium pentavalent species (Figure 5.12c))[117, 119]. While XPS spectra of O 1s in BICUVOX.10 sample exhibit in Figure 5.12d). The obvious asymmetric peak of O 1s was segregated into two elements. The two types of oxygen bonding state were determined, at a binding energy of 529.7, and 532 eV were assigned to lattice oxygen (O_{latt}) and adsorbed oxygen (O_{ads}) bonding states respectively[117-119]. Astounding, binding energy Cu disappear on the BICUVOX.10 sample surface that shows in Figure 5.12e). There are two possibilities: first Cu atom embedded into BICUVOX.10 clusters [120], and Cu concentration have a lower than XPS detection limit. As a result, binding energy in the Cu region is fragile [121]. Cu content in the BICUVOX.10 sample might have to use other elemental analyses for confirmation that there is copper in this structure.

EDS analysis was used to specify the elements that are a composition on the surface of the sample. In this analysis, there was a response to the question of the presence of Cu in synthetic powder. Figure 5.13a)-e) presents the EDS mapping of Bi, V, O, and Cu. As a result, there is clear evidence of Cu dispersion on the surface of the powder. The elements distribution is homogeneous and absence of elemental agglomeration or some area separation — however, EDS inaccurate method for analysis concentration of the chemical in the BICUVOX.10 sample. The amount of Cu from the EDS result performed an exaggerated high value.

ICP-OES is alternating technique that was accuracy analyze chemical component of synthesized powder. ICP-OES cannot analyze all elements, therefore some elements like oxygen derived from calculation Table 5.1 reported the concentration of the chemical composition of BICUVOX and compared the result among theory, ICP-OES, and EDS. Both of ICP-OES and EDS analysis show element concentration (except Cu) closed to theorem value that will indicate bulk properties different to surface properties.
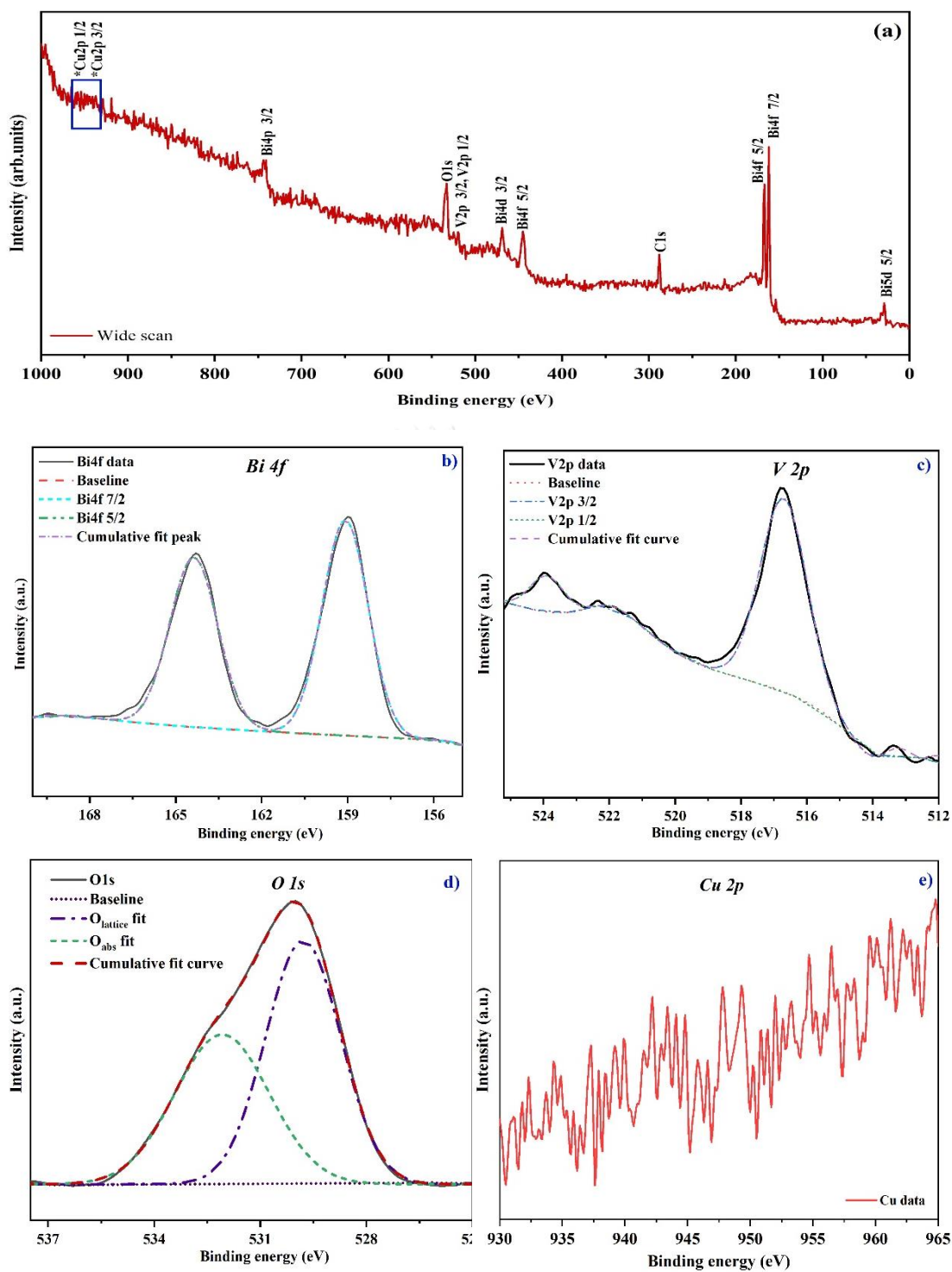
Figure 5. 12 *XPS survey spectra a), and high-resolution scan of the binding energy of Bi 4f, b), V 2p, c), O 1s, d) and Cu 2p, e) orbitals respectively.*
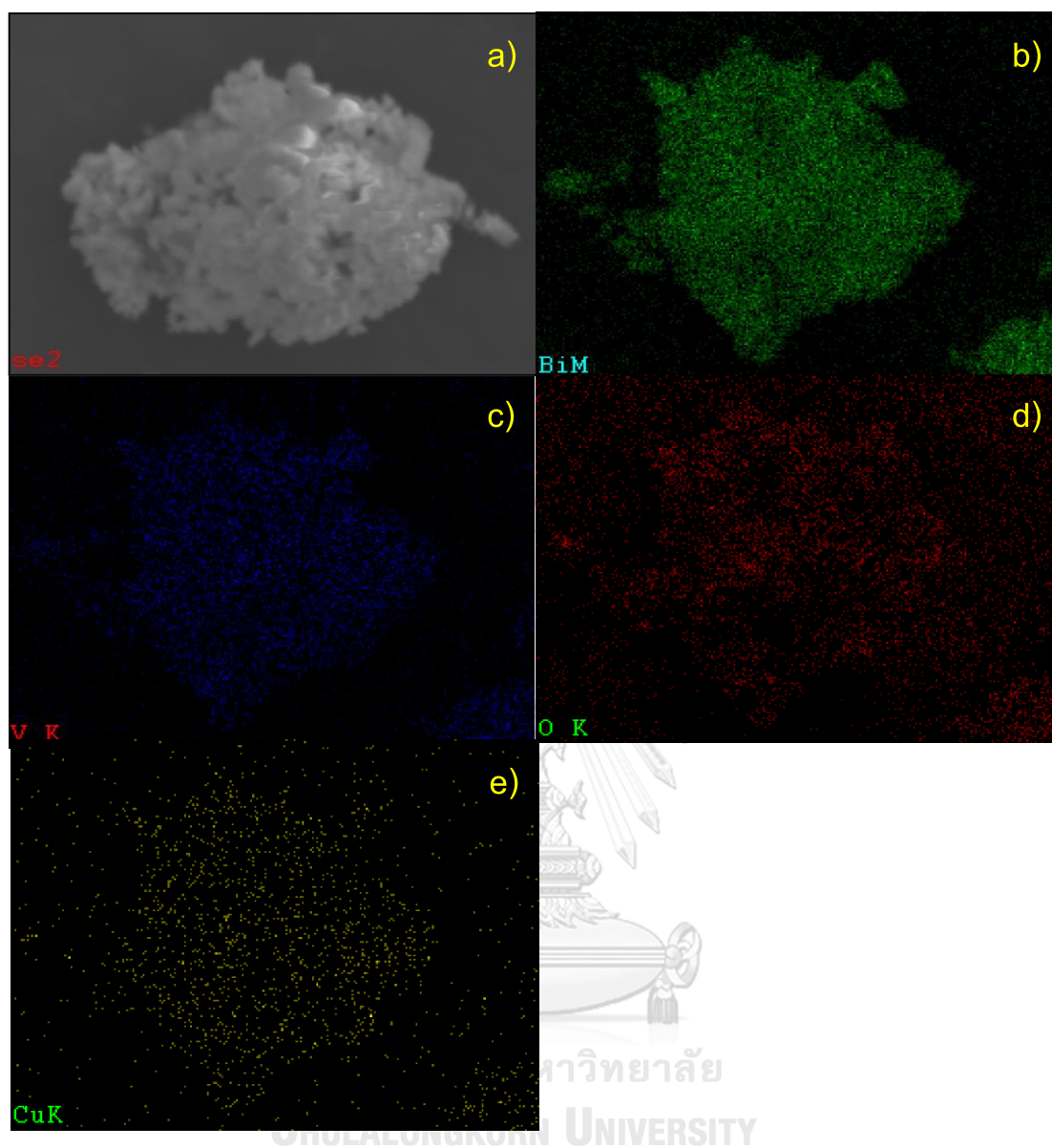
Figure 5. 13 Corresponding quantitative EDX area: analyzed BICUVOX.10 a), Bi, b), V,

c), O, d) and Cu, e)

Table 5. 1 Comparison concentration of elements in BICUVOX.10 in different method for determination

Element	Theory		ICP-OES		EDX mapping	
	%mole	Bi:V:Cu ratio	%mole	Bi:V:Cu ratio	%mole	Bi:V:Cu ratio
O	64.07		≈63.31*		71.00	
Bi	23.95	20: 9: 1	24.75	23.46:10.32:1	17.51	6.81:3.47:1
V	10.78		10.89		8.92	
Cu	1.2		1.06		2.57	

*derived from the calculation (differential between the amount of metal from ICP data)

5.8 Determination of structural and phase transition of BICUVOX.10

XRD investigated BICUVOX.10 structure formation. The diffractogram of each step of synthesis by solid-state reaction was displayed in Figure 5.14. First of all, starting material mixing by ball milling no signify BICUVOX.10 structure from the XRD pattern and also found a characteristic peak of Bi_2O_3 and $V_2O_{5,}$ which is an oxide precursor[122, 123]. The next, diffractogram of first calcine confirm solid-state reaction among Bi_2O_3, $V_2O_{5,}$ and CuO and born γ' phase of BICUVOX.10 structure as well previous work [73, 76]. Later, the second calcined process improves γ'-BICUVOX.10 phase which can see a sharp and higher peak in diffractogram. Finally, reducing the sizes of BICUVOX.10 does not make a difference in XRD pattern but, decreasing of intensity and broaden

peaks in diffractogram was obtain that indicated the crystalline size of BICUVOX.10 reduced.
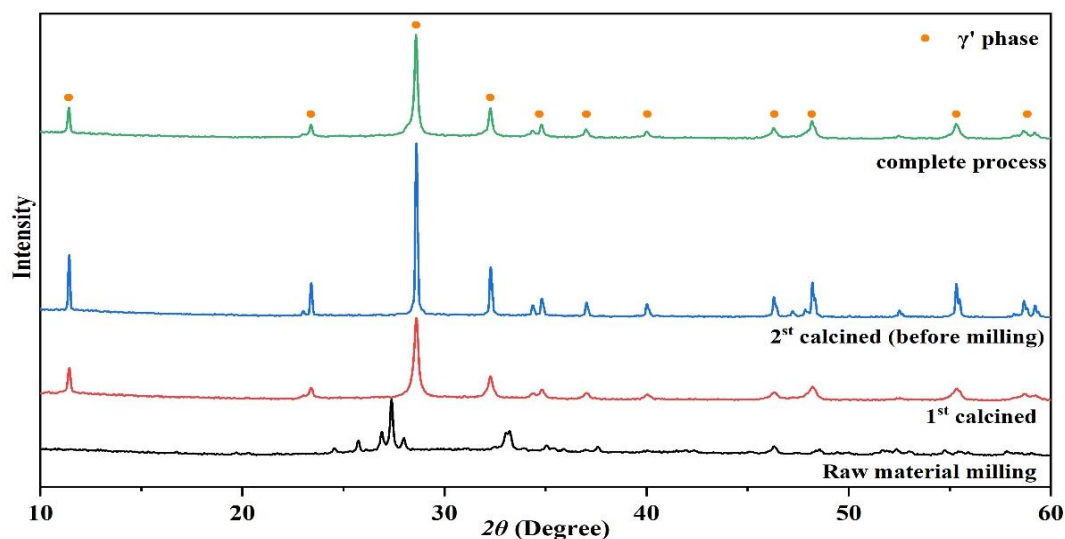
Figure 5. 14 XRD pattern of each synthesis step of BICUVOX.10 solid-state reaction: raw material milling, 1stcalcine, 2ndcalcine (before ball mill), and complete process.

Phase transition of BICUVOX.10 powder was evaluated by the DSC method. In this study, in an inert gas (N_2) and oxidizing gas (air) compare phase transition and stability of synthetic BICUVOX.10 powder. DSC curve of BICUVOX.10 in different gas atmosphere exhibit in Figure 5.15. Both DSC curves in N_2 and air show an endothermic peak at 459 and 466 °C, respectively, that refer to γ' to γ phase. Previous literature reports the range of phase transition temperature between 454-544°C. Phase transition of BICUVOX relates to the disorder of oxygen vacancies in the vanadate perovskite layer that arranges tetragonal structure when heating [124, 125]. The synthesized powder appears phase transition in this region. In both conditions, synthetic oxide powder is stable during thermal analysis at 600 °C [126].
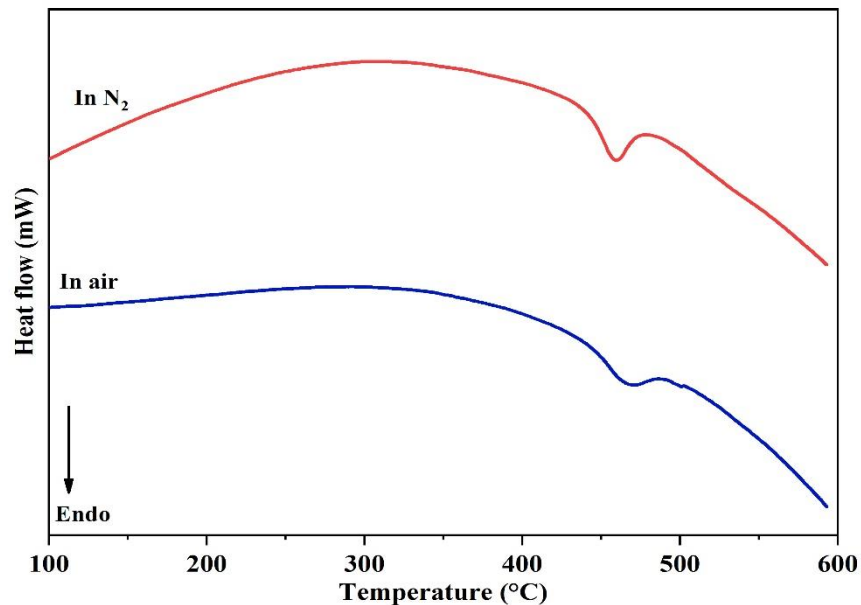
Figure 5. 15 The DSC curves of BICUVOX.10 powder in N_2 and air atmospheres during analysis.

PART3: FRABICATION OF YSZ-BICUVOX.10 THIN FILM VIA SCREEN PRINTING METHOD AND NEMCA OBSERVATION ON THIN FILM CELL

5.9 Morphology and structure of YSZ-BICUVOX.10 composite powders

In this work, addition BICUVOX.10 into YSZ powder was used as the physical mixing method. The microstructure of pure and blended BICUVOX.10/YSZ was shown in Figure 5.16. Pure YSZ is a size distribution in submicron and spherical shape (Figure 5.16a)). When increasing the amount of BICUVOX.10, the blended BICUVOX.10/YSZ composites are a perfectly homogeneous mixture due to ball milling that is mixing process while reducing the size of powders at the same time (Figure 5.16 b-e). BICUVOX.10 particles have been reduced sized near to YSZ particles.

In terms of phase and structure, change was evaluated by XRD. The diffractogram of pure cannot observe this structure in their composite. Pure BICUVOX.10 and their composite show in Figure 5.17. The XRD pattern of composites compare with pure YSZ that significant change characteristic peak of YSZ. The

composites were found a characteristic peak at 28.5°, which is evidence for the presence of BICUVOX.10 in ceramic powder.
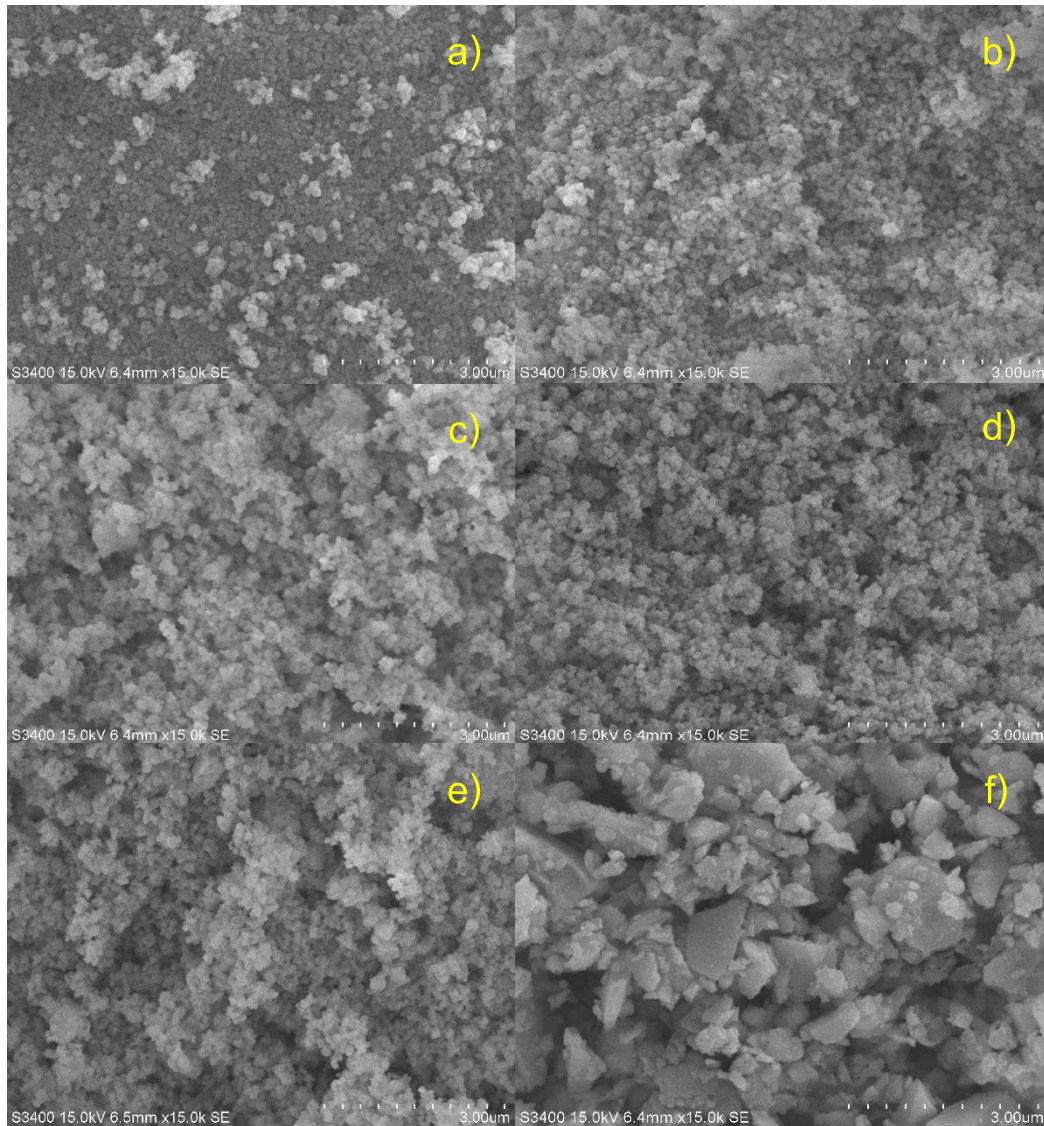
Figure 5. 16 Microstructure of pure YSZ, a), 1.5 % mole BICUVOX.10/YSZ, b), 2.5 % mole BICUVOX.10/YSZ, c), 3.5 % mole BICUVOX.10/YSZ, d), 4.5 % mole BICUVOX.10/YSZ, e), and pure BICUVOX.10, f).
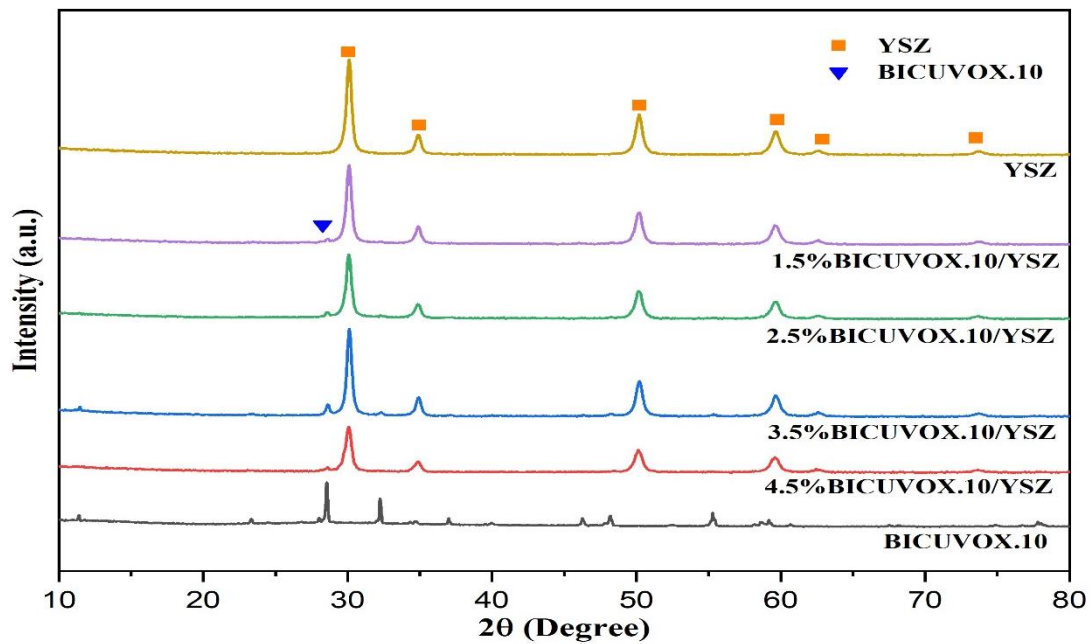
Figure 5. 17 XRD pattern of pure YSZ, 1.5 % mole BICUVOX.10/YSZ, 2.5 % mole BICUVOX.10/YSZ, 3.5 % mole BICUVOX.10/YSZ, 4.5 % mole BICUVOX.10/YSZ and Pure BICUVOX.10.

5.10 Characterization of BICUVOX.10/YSZ thin film

Microstructure of YSZ, BICUVOX.10/YSZ composite and BICUVOX.10 on top view display in fig.33. YSZ thin film performs porous structure and clearly void between YSZ particles that show in Figure 5.18a). For BICUVOX.10/YSZ composite thin film, increasing of BICUVOX.10 contents clearly agglomerate YSZ particle, which shows in Figure 5.18b-e, especially at 4.5% mole BICUVOX.10/YSZ the composite thin film can be observed evidently dissolving grain and agglomeration of large particles. Moreover, pure BICUVOX.10 obtain dense thin film on an alumina substrate, but BICUVOX.10 has a hole on film that is defect due to shrinkage of BICUVOX.10 much more than the substrate. Investigation of the amount of BICUVOX.10 in composite thin film surface by EDS that found BICUVOX.10 closed to starting composite powders (base on Bi content that is shown in Appendix D) For the top view of SEM images cannot proof the densification of YSZ by addition BICUVOX.10 compound. The cross-section area was examined. As a result, Figure 5.19 a)-b) shows the cross-section area of YSZ that still illustrates porous film. The next, 1.5% mole BICUVOX.10/YSZ thin-film was shown, in

Figure 5.19c)-d) that particles uniform agglomerate greater than pure YSZ. Later, 2.5% mole 3.5% mole BICUVOX.10/YSZ thin film display in Figure 5.19e)-f) and g)-h) respectively. The grain clearly dissolved, and particle connected. For 4.5% mole BICUVOX.10/YSZ thin film was shown, in Figure 5.18i)-j) that indicated fully grain diffusion. Hence, increasing the amount of BICUVOX.10 can improve the densification of YSZ thin film. Role of BICUVOX.10 acts as a grain connector that follows by a liquid phase mechanism [127-129]. At close to the melting point (approximately 887 °C), BICUVOX.10 can diffuse to void and cover it. The densification structure can be obtained in SEM images. Finally, BICUVOX.10 thin film formed dense film that can be seen in Figure 5.19k)-l).
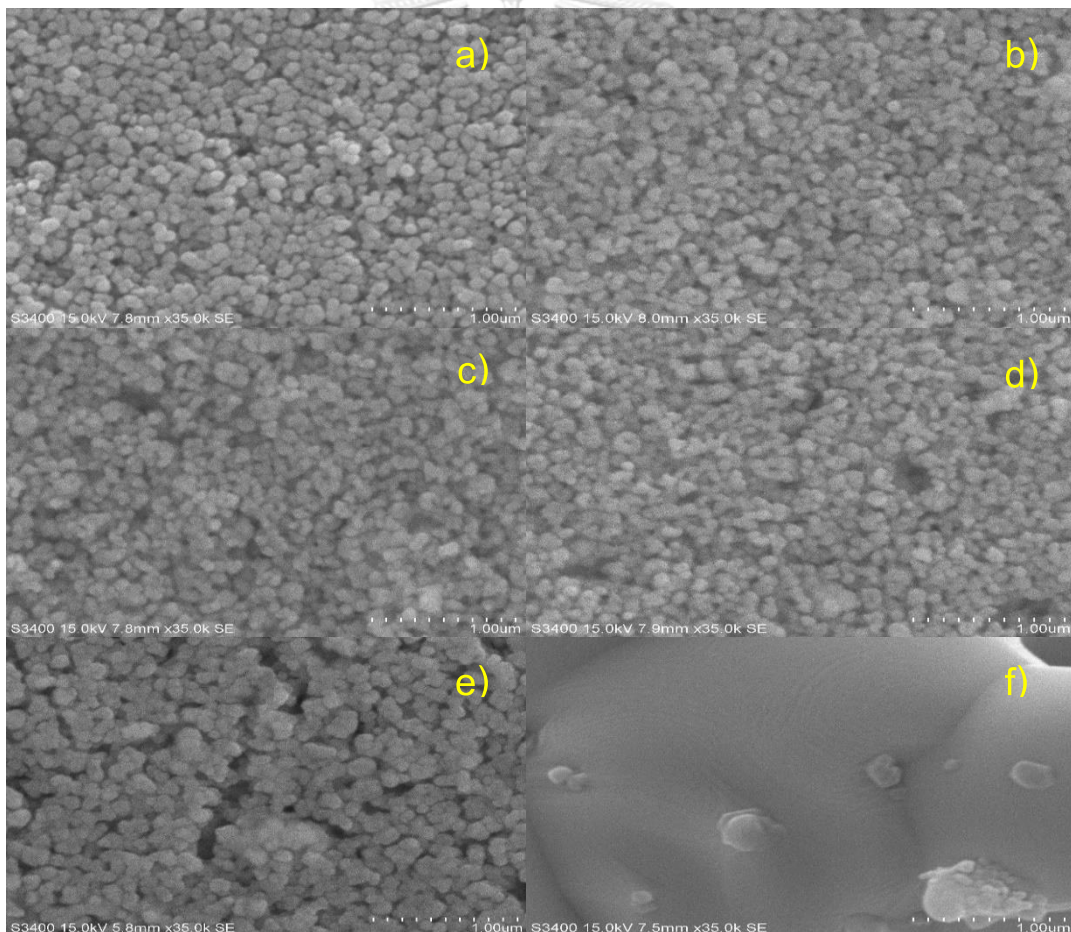
Figure 5. 18 Microstructure of thin-film (top view): pure YSZ, a), 1.5 % mole BICUVOX.10/YSZ, b), 2.5 % mole BICUVOX.10/YSZ, c), 3.5 % mole BICUVOX.10/YSZ, d), 4.5 % mole BICUVOX.10/YSZ, e) and pure BICUVOX.10, f).
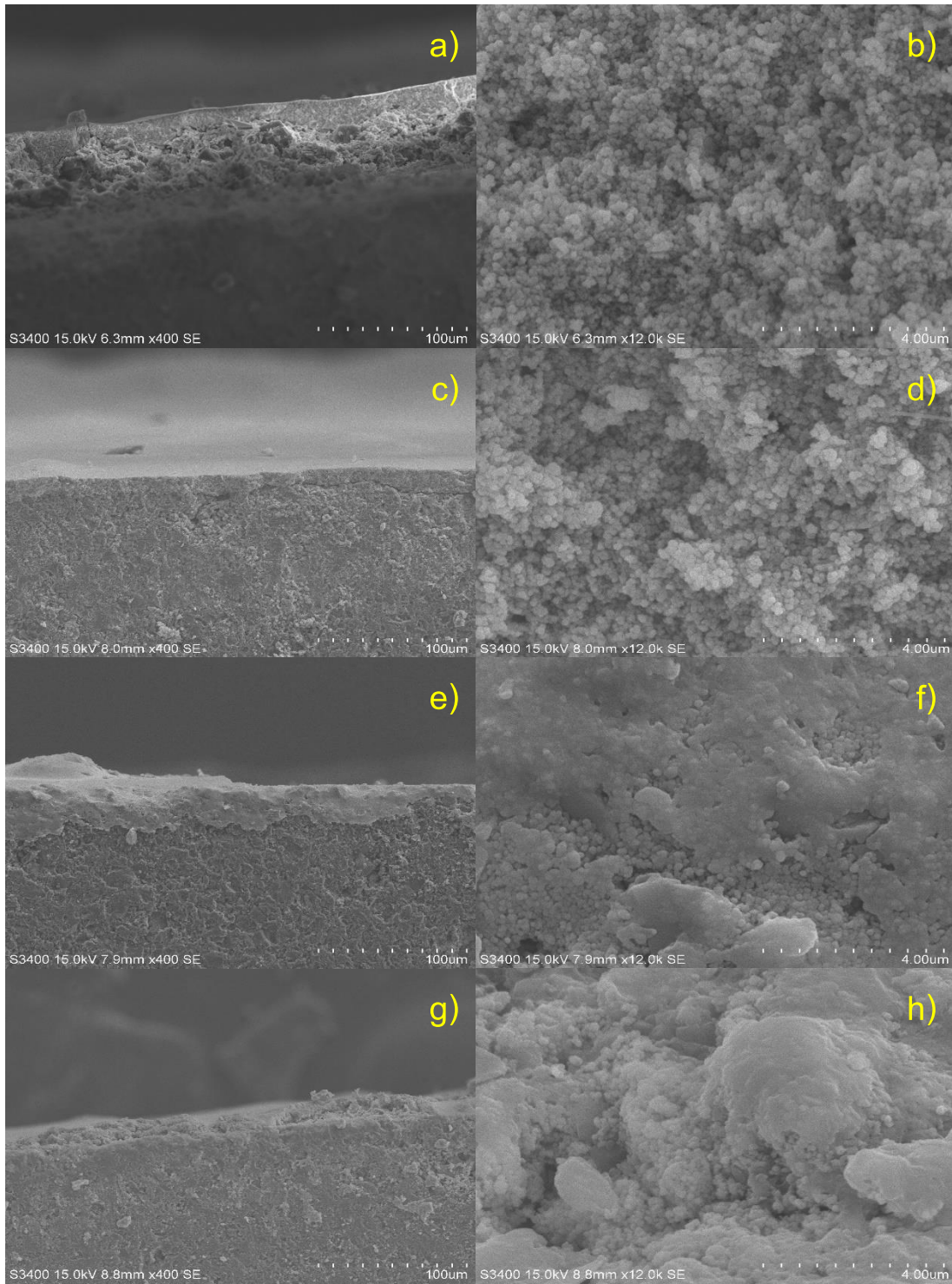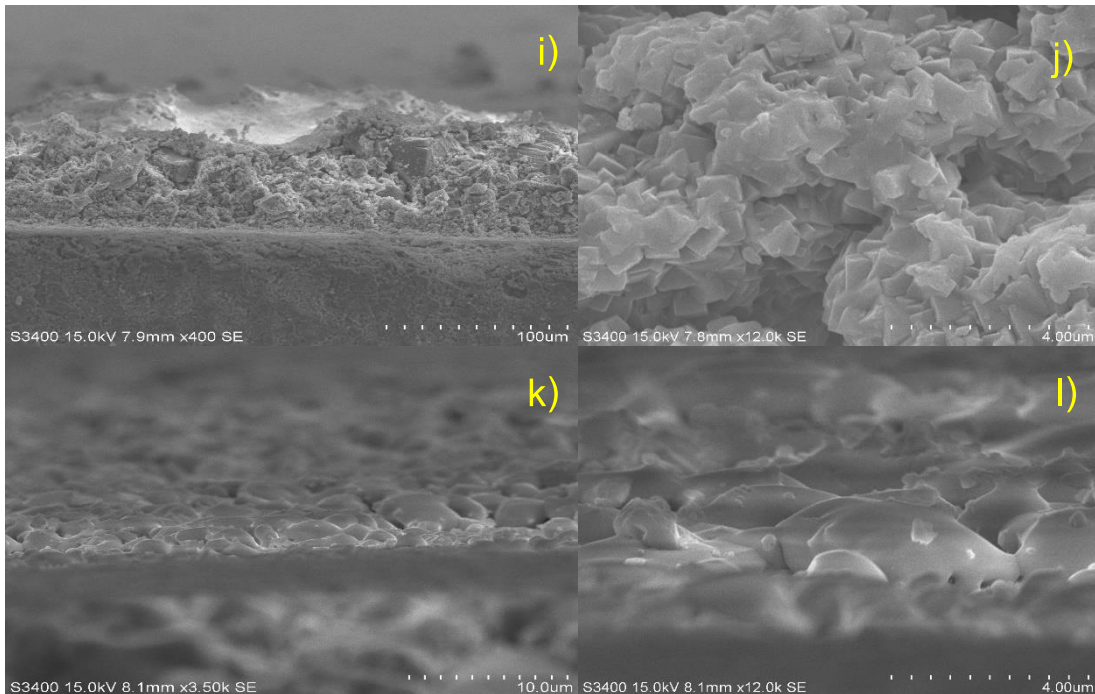
Figure 5. 19 Microstructure of thin film (cross-section view): pure YSZ, a)-b), 1.5 % mole BICUVOX.10/YSZ, c)-d), 2.5 % mole BICUVOX.10/YSZ, e)-f), 3.5 % mole BICUVOX.10/ YSZ, g)-h), 4.5 % mole BICUVOX.10/YSZ, i)-j), and pure BICUVOX.10, k)-l).

Observation of structural YSZ, BICUVOX.10/YSZ composite and BICUVOX.10 thin film on alumina substrate evaluate via XRD analysis. Diffractogram of BICUVOX.10/YSZ composite for all sintering aid concentration without an ambiguous reflection peak that indicates no formation of new species of a chemical compound from YSZ and BICUVOX.10 (Figure 5.20). Another thing, their composite thin films appear only characteristic peaks of YSZ as solid solution and alumina substrate as substrate. BICUVOX.10 in the composite film act as the only matrix that is low concentration. This is why the absence of characteristic peaks of BICUVOX.10 in all components, which accord to previous reports [98, 130, 131].
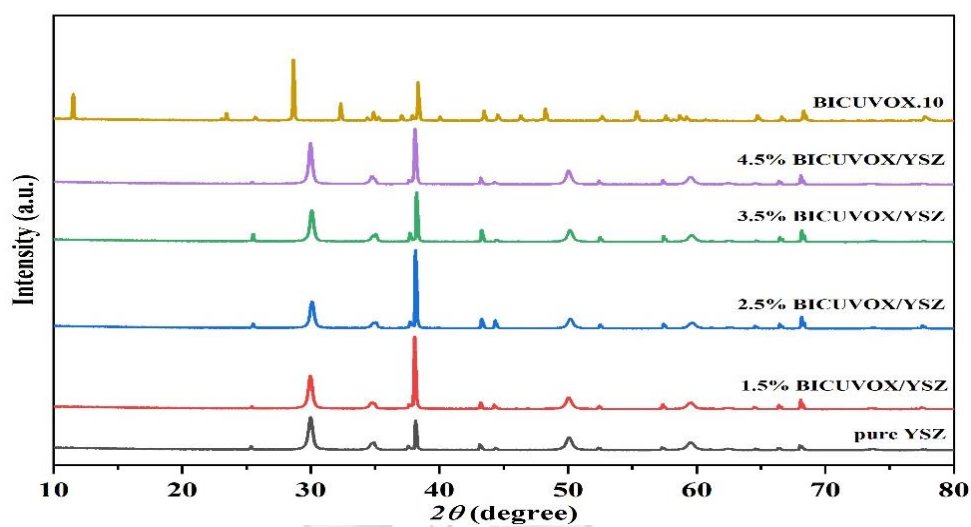
Figure 5. 20 *XRD pattern of* pure YSZ, 1.5 % mole BICUVOX.10/YSZ, 2.5 % mole BICUVOX.10/YSZ, 3.5 % mole BICUVOX.10/YSZ, 4.5 % mole BICUVOX.10/YSZ, and pure BICUVOX.10.

5.11 Catalytic propane oxidation under open and close circuit and observation of NEMCA behavior
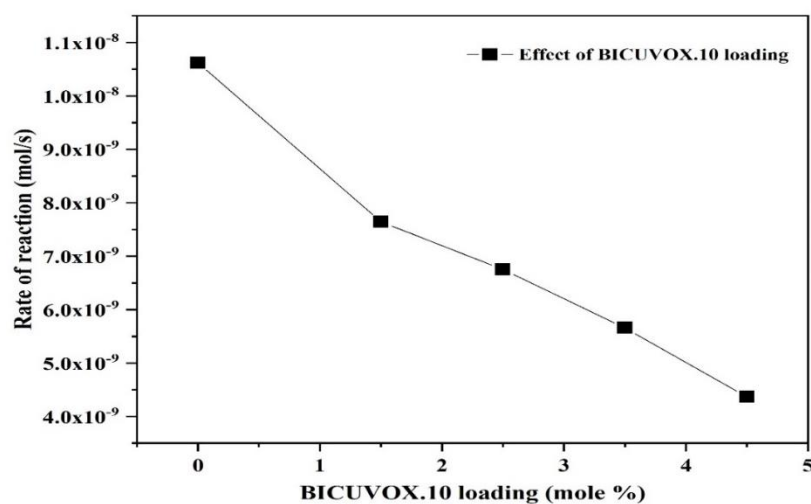
Figure 5. 21 Effect of BICUVOX.10 loading on rate of reaction at $400\,°C$

In the open-circuit condition, the effect of BICUVOX.10 concentrations were studied. Figure 5.21 displays the relation between the amount of sintering aid and the catalytic reaction rate. Increasing of BICUVOX.10 concentrations lead to reduce of reaction rate. For this reason, BICUVOX.10 increases the densified solid electrolyte layer and affects to decrease reaction area. SEM confirmed these results. In other words, lower Pt dispersion on YSZ thin film (YSZ act as support at the same time), decreasing of catalytic rate occurred.
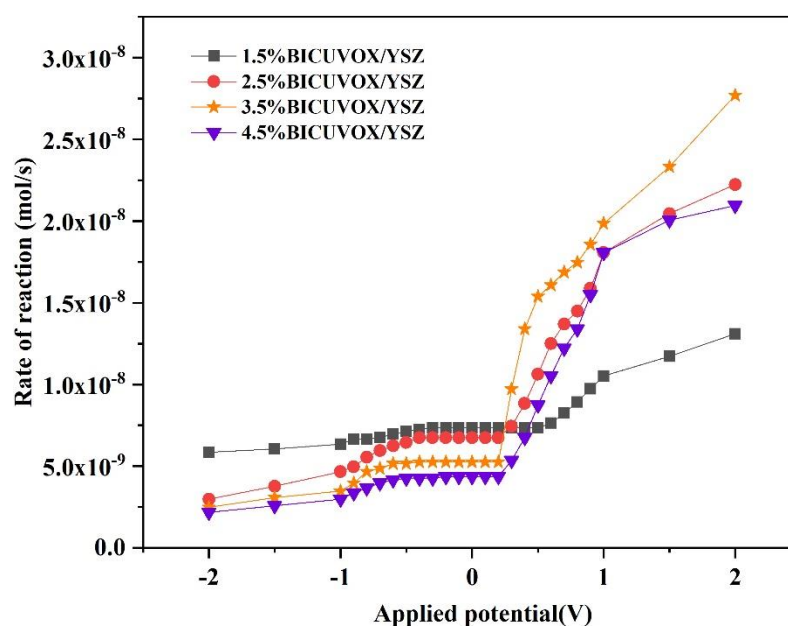
Figure 5. 22 Effect of applied potential and BICUVOX.10 loading on the rate of reaction at 400 °C.

The effect of applied potential was studied that varied potential range of -2.0 V to 2.0 V. Figure 5.22 was shown the reaction rate decease when applied negative potential. On the other hand, the reaction rate enhances beyond open-circuit conditions during anodic polarization. These results correspond to previous literature [12, 14, 53, 81, 82]. In positive applied potential, oxide ions migrate to fresh sputtered Pt and form an effective double layer on the catalyst surface. Because of this, induce adsorption of electron donor reactant (propane molecule) and bring to electrochemical promotion of

catalysis. Effect of sintering aid loading, increasing of loading improves the promotional reaction rate, but at 4.5% mole BICUVOX.10/YSZ depreciate the electrochemical promotional rate.
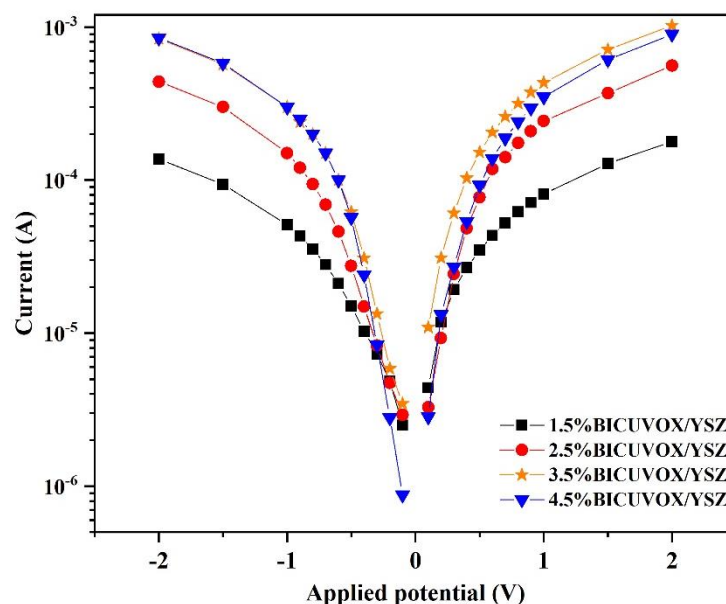
Figure 5.23 Effect of applied potential and BICUVOX.10 loading on cell current at 400 °C.

Effect of applied potential and on current of BICUVOX.10 loading on NEMCA thin film show Tafel curves in Figure 5.23. In anodic and cathodic polarization, increasing of applied potential improve current flow through thin-film cell From Ohmic law, when increasing of potential lead to decrease the resistance and electron can mobile better than lower potential. At high concentrations of BICUVOX.10 can produce dense YSZ layers more than lower content. This is why oxide ion can transfer in a dense structure better than a porous structure. Likewise, reaction rate result, Cell current dropdown with at 4.5% mole BICUVOX.10/YSZ thin-film cell. In this case, oxygen cannot diffuse to counter electrode enough (low oxygen reduction rate). Thus, cell current may be decreased. For this reason, the current of cells fluctuates with applied potential and structure of solid electrolytes. In prior research about NEMCA found that current is function with applied potential [12, 53, 64] as well as this work.
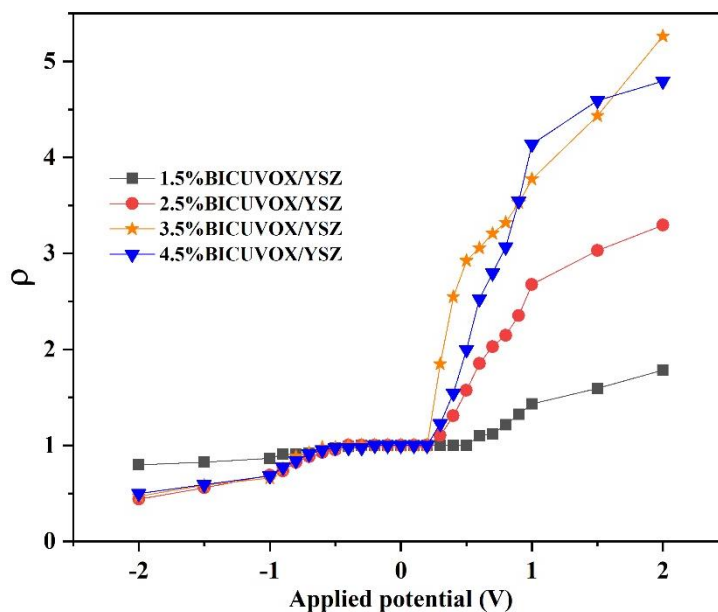
Figure 5. 24 Effect of applied potential and BICUVOX.10 loading on ρ at 400 $°C.$

Comparison between closed and opened circuit rates that represent in terms of the rate enhancement ratio. ρ is the sum of electrochemical reaction part and electrochemical promotion part. The ρ of propane oxidation shown in Figure 5.24 that anodic applied potential improve CO_2 formation while inhibition of CO_2 production during cathodic polarization. The NEMCA behavior exhibit electrophobic promotional type consistent with previous reports [10, 12-14, 53, 93, 109]. The elecctrophobic was used to descript the oxide pumping flow from the solid electrolyte to TPB and enhancement of propane adsorption due to an effective double layer from satisfied ion turn to platinum surface. The maximum of ρ close to 5 at 400 °C and 2.0 V for applied potential. This value assigns five times that of the open-circuit rate. For the effect of BICUVOX.10, loadings have the same tendency with the rate of reaction and cell current.
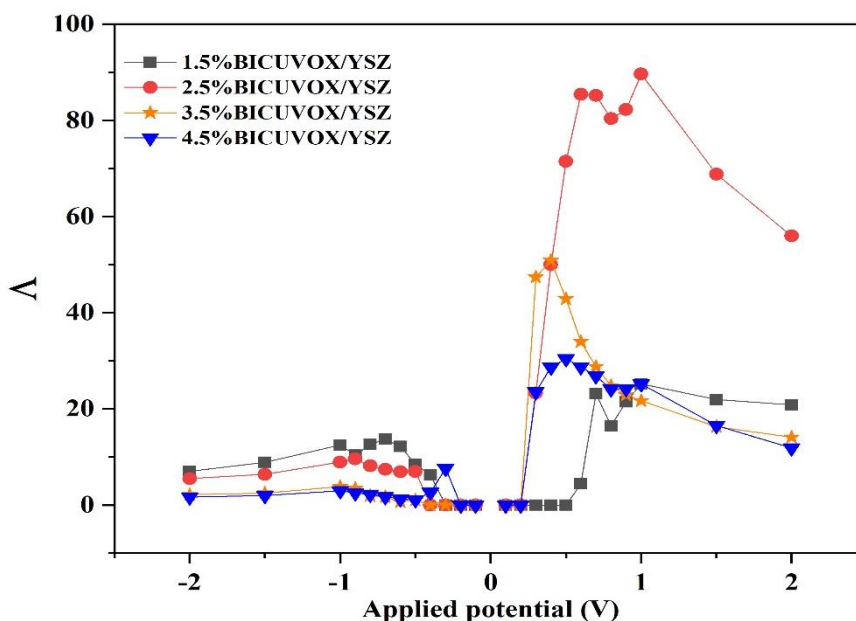
Figure 5. 25 Effect of applied potential and BICUVOX.10 loading on Λ at 400 $^{\circ}C$

The key factor for considering the magnitude of the NEMCA effect is Λ that indicates the effect of electrocatalytic reaction or electrochemical promotion. In this study, Pt/screen printing YSZ electrode, the effect of both positive and negative polarization, and sintering aid loading were reported in fig.5.25. Λ values in both anodic and cathodic regions are greater than one that indicates clearly the NEMCA phenomena. Nevertheless, Λ values in the cathodic polarization is less than in anodic polarization. Pt was used to quasi-reference, and the counter electrode replaced the gold electrode, which affects NEMCA observation. In cathodic polarization, oxide ion transfer from Pt electrode on the top layer to Pt electrode in the bottom layer leads to an effective double layer between the interface of Pt counter electrode and YSZ thin film. Retardation of decreasing reaction rate pathway has occurred that represent in Figure 5.26. Secondly, the Pt working electrode displays metallic Pt owning to oxide migration to the quasi-reference electrode in the application of cathodic potential [14]. Pt metallic is an active site for propane oxidation: thus, the reaction rate might slightly decrease

under the cathodic region. Maximum of Λ values closed to 90 was found that the addition 2.5% mole BICUVOX.10 and applied potential 1 V.

In this section, a problem encountered is low faradaic efficiency value due to the high value of cell current. Falgairette, C et al. [132] purpose oxygen storage in Pt/YSZ electrode. The four types were classified: first of all, the oxygen store at Pt/YSZ interface under polarization. Second, back-spillover species located between the catalyst surface gas-exposed interface. Third type cause of solid diffusion and related to the first species. Lastly, oxygen leaves from the solid electrolyte and form oxygen gas. In a possible pathway to explain is the oxide migrated from YSZ thin film classified two types: the first type generates the effective double layer lead to the induction of NEMCA phenomena. Latter type, oxide ion transfer to TPB, and desorb to oxygen gas at the catalyst surface.
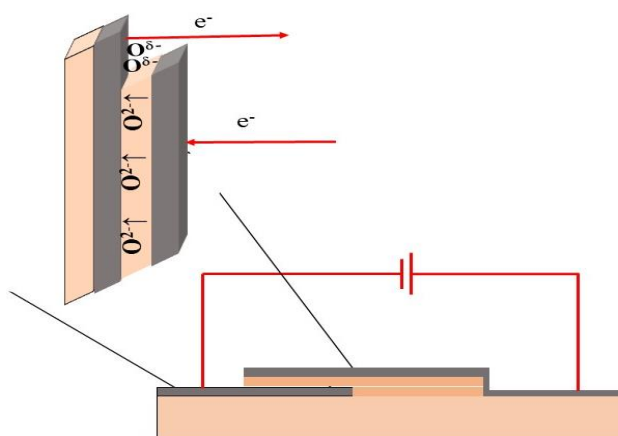
Figure 5. 26 Scheme of the possible pathway to the effective double-layer formation on the interface between Pt counter electrode and YSZ thin film under cathodic polarization

CHAPTER 6

CONCLUSIONS AND RECOMMENDATIONS

This chapter summarizes this work on the non-Faradaic electrochemical of catalytic activity (NEMCA) of propane oxidation over Pt/YSZ thin film electrode. The recommendations for toward studied are also elucidated in this chapter.

6.1 Conclusion

The catalytic propane oxidation over Pt/dip-coated YSZ thin film on alumina substrate was investigated under opened and closed circuit conditions. The NEMCA effect was clearly observed in the temperature range of 300-500 °C but, at 200 °C disappear NEMCA effect was confirmed by Λ value. Unfortunately, Pt/dip-coated YSZ thin film is difficult for repeatability and reproductivity due to low adhesion between the YSZ layer and the counter electrode. From previous kinds of literature, addition sintering aid into YSZ was reduced sintering temperature. In this work, copper doped bismuth vanadate (BICUVOX.10) was chosen because this compound can densify YSZ at target temperature (800°C). BICUVOX.10 was prepared by a solid-state reaction. The structural, chemical, and thermal properties were evaluated. As a result, their properties accorded with prior research. Next step, BICUVOX.10/YSZ composites were fabricated by screen printing method. Increasing the amount of BICUVOX.10 concentration enhances the densification of YSZ thin film. Another thing, addition of BICUVOX.10 no significant effect on the structure of YSZ. Catalytic measurement of Pt/ BICUVOX.10/YSZ composites thin-film under open circuit was found that decrease reaction rate when sintering aid increases concentration. Under polarization condition reaction rate and ρ exhibit electrophobic promotional type. Cell current increases when both cathodic and anodic polarization increase order. Lastly, Λ is greater than 1 that indicates the NEMCA phenomena. However, Λ values are lower than previous reports. The migration of oxide

ion between YSZ and BICUVOX.10 might cause desorption of oxide ion to oxygen gas. For this reason, Λ of Pt/BICUVOX.10-YSZ/Pt have a small magnitude.

6.2 Recommendation

In order to development of future work of NEMCA effect, some recommend, and suggestion derived from reading literature review or problem in this work:

1. The substrate might use a porous structure to solve in a blind spot; this is the area of the counter electrode.

2. Fabrication of YSZ layer by tape casting, then assemble with counter electrode by using organic binder and sinter at low temperature to improve adhesion between interface.

3. From 1., the counter electrode might use gold paste for improving heat resistance and protecting gold diffusion, which leads to the poor conductivity of the counter electrode.

4. Fabrication of bilayers of the solid electrolyte, the bottom layer produces a dense film to ion migration and top layer make a porous structure for the high dispersion of the metal catalyst electrode.

5. The other type of solid electrolyte might be used to replace YSZ; such as Gadolinium doped cerium oxide (GDC), $Ba(Zr_{0.1}Ce_{0.7}Y_{0.2})O_{3-\delta}$ or BZCY etc.

REFERENCES

[1.] Council, P. E. R., PROPANE: ENERGY FOR OUR PAST, PRESENT, AND FUTURE. In *https://pbpropane.com/Portals/0/Safety/download_9136-FL-15.pdf*, Council, T. P. E. R., Ed. Washington D.C., 2015; pp 1-2.

[2.] The National Renewable Energy Laboratory (NREL), A. N. L. o. T. U. S. D. o. E., Office of Energy Efficiency and Renewable Energy, Propane Basics. In *https://afdc.energy.gov/files/u/publication/propane_basics.pdf*, A National Laboratory of The U.S. Department of Energy, O. o. E. E. a. R. E., Ed. the U.S. Department of

Energy, Office of Energy Efficiency and Renewable Energy: Washington, District of Columbia, 2016; pp 1-4.

[3.] Billard, A.; Vernoux, P., Electrochemical catalysts for hydrocarbon combustion. *Topics in Catalysis* **2007**, *44* (3), 369-377.

[4.] Jones, J.; Ross, J. R. H., The development of supported vanadia catalysts for the combined catalytic removal of the oxides of nitrogen and of chlorinated hydrocarbons from flue gases. *Catalysis Today* **1997**, *35* (1), 97-105.

[5.] Wang, G.; You, R.; Meng, M., An optimized highly active and thermo-stable oxidation catalyst Pd/Ce–Zr–Y/Al$_2$O$_3$ calcined at superhigh temperature and used for C3H8 total oxidation. *Fuel* **2013**, *103*, 799-804.

[6.] Hicks, R. F.; Qi, H.; Young, M. L.; Lee, R. G., Effect of catalyst structure on methane oxidation over palladium on alumina. *Journal of Catalysis* **1990**, *122* (2), 295-306.

[7.] Abello, M. C.; Gomez, M. F.; Cadus, L. E., Selective oxidation of propane on MgO/γ-Al$_2$O$_3$-supported molybdenum catalyst: influence of promoters. *Catalysis Letters* **1998**, *53* (3), 185-192.

[8.] Peña, M. L.; Dejoz, A.; Fornés, V.; Rey, F.; Vázquez, M. I.; López Nieto, J. M., V-containing MCM-41 and MCM-48 catalysts for the selective oxidation of propane in gas phase. *Applied Catalysis A: General* **2001**, *209* (1), 155-164.

[9.] Vayenas, C. G.; Brosda, S.; Pliangos, C.; Bebelis, S., *Electrochemical Activation of*

Catalysis Promotion, Electrochemical Promotion, and Metal-Support Interactions. Kluwer Academic/Plenum Publishers: New york, 2001; p 10.

[10.] Kokkofitis, C.; Karagiannakis, G.; Zisekas, S.; Stoukides, M., Catalytic study and electrochemical promotion of propane oxidation on Pt/YSZ. *Journal of Catalysis* 2005, *234* (2), 476-487.

[11.] Bultel, L.; Vernoux, P.; Gaillard, F.; Roux, C.; Siebert, E., Electrochemical and catalytic properties of porous Pt–YSZ composites. *Solid State Ionics* 2005, *176* (7-8), 793-801.

[12.] Peng-ont, S.; Praserthdam, P.; Matei, F.; Ciuparu, D.; Brosda, S.; Vayenas, C. G., Electrochemical Promotion of Propane and Methane Oxidation on Sputtered Pd Catalyst-Electrodes Deposited on YSZ. *Catalysis Letters* 2012, *142* (11), 1336-1343.

[13.] Vernoux, P.; Gaillard, F.; Bultel, L.; Siebert, E.; Primet, M., Electrochemical Promotion of Propane and Propene Oxidation on Pt/YSZ. *Journal of Catalysis* 2002, *208* (2), 412-421.

[14.] Jiménez-Borja, C.; Delgado, B.; Díaz-Díaz, L. F.; Valverde, J. L.; Dorado, F., Enhancing the combustion of natural gas by electrochemical promotion of catalysis. *Electrochemistry Communications* 2012, *23*, 9-12.

[15.] Bumroongsakulsawat, P.; Yindee, S.; Vanalabhpatana, P.; Assabumrungrat, S., *High Faradaic Yields of Non-Faradaic Electrochemical Modification of Catalytic Activity of Propane Oxidation at Pt-YSZ*. 2016; Vol. 163, p E341-E343.

[16.] Pan, W. P.; Lü, Z.; Chen, K. F.; Zhu, X. B.; Huang, X. Q.; Zhang, Y. H.; Wei, B.; Su, W. H., Paper-Fibres Used as a Pore-Former for Anode Substrate of Solid Oxide Fuel Cell. *Fuel Cells* 2011, *11* (2), 172-177.

[17.] Di Bartolomeo, E.; Kaabbuathong, N.; Grilli, M. L.; Traversa, E., Planar electrochemical sensors based on tape-cast YSZ layers and oxide electrodes. *Solid State Ionics* 2004, *171* (3), 173-181.

[18.] de Lucas-Consuegra, A.; Dorado, F.; Jiménez-Borja, C.; Valverde, J. L., Electrochemical promotion of Pt impregnated catalyst for the treatment of automotive exhaust emissions. *Journal of Applied Electrochemistry* 2008, *38* (8), 1151-1157.

[19.]   Mizushima, Y.; Hori, M., Alumina aerogel for support of a methane combustion catalyst. *Applied Catalysis A: General* 1992, *88* (2), 137-148.

[20.] Vaidya, S. H.; Rode, C. V.; Chaudhari, R. V., Bimetallic Pt–Sn/γ-alumina catalyst for highly selective liquid phase hydrogenation of diethyl succinate to γ-butyrolactone. *Catalysis Communications* 2007, *8* (3), 340-344.

[21.] Colussi, S.; Gayen, A.; Llorca, J.; de Leitenburg, C.; Dolcetti, G.; Trovarelli, A., Catalytic Performance of Solution Combustion Synthesized Alumina- and Ceria-Supported Pt and Pd Nanoparticles for the Combustion of Propane and Dimethyl Ether (DME). *Industrial & Engineering Chemistry Research* 2012, *51* (22), 7510-7517.

[22.] Liu, Y.-M.; Cao, Y.; Yan, S.-R.; Dai, W.-L.; Fan, K.-N., Highly Effective Oxidative Dehydrogenation of Propane Over Vanadia Supported on Mesoporous SBA-15 Silica. *Catalysis Letters* 2003, *88* (1), 61-67.

[23.] Kokkofitis, C.; Karagiannakis, G.; Stoukides, M., Electrochemical promotion in O^{2-} cells during propane oxidation. *Topics in Catalysis* 2007, *44* (3), 361-368.

[24.] Sprio, S.; Guicciardi, S.; Bellosi, A.; Pezzotti, G., Yttria-stabilized zirconia films grown by radiofrequency magnetron sputtering: Structure, properties and residual stresses. *Surface and Coatings Technology* 2006, *200* (14), 4579-4585.

[25.] Hobein, B.; Tietz, F.; Stöver, D.; Čekada, M.; Panjan, P., DC Sputtering of yttria-stabilised zirconia films for solid oxide fuel cell applications. *Journal of the European Ceramic Society* 2001, *21* (10), 1843-1846.

[26.] Heiroth, S.; Lippert, T.; Wokaun, A.; Döbeli, M.; Rupp, J. L. M.; Scherrer, B.; Gauckler, L. J., Yttria-stabilized zirconia thin films by pulsed laser deposition: Microstructural and compositional control. *Journal of the European Ceramic Society* 2010, *30* (2), 489-495.

[27.] Chen, F.; Liu, M., Preparation of yttria-stabilized zirconia (YSZ) films on $La_{0.85}Sr_{0.15}MnO_3$ (LSM) and LSM–YSZ substrates using an electrophoretic deposition (EPD) process. *Journal of the European Ceramic Society* 2001, *21* (2), 127-134.

[28.] Zhou, W.; Shi, H.; Ran, R.; Cai, R.; Shao, Z.; Jin, W., Fabrication of an anode-supported yttria-stabilized zirconia thin film for solid-oxide fuel cells via wet powder

spraying. *Journal of Power Sources* **2008**, *184* (1), 229-237.

[29.] Matsuzaki, Y.; Hishinuma, M.; Yasuda, I., Growth of yttria stabilized zirconia thin films by metallo-organic, ultrasonic spray pyrolysis. *Thin Solid Films* **1999**, *340* (1), 72-76.

[30.] Chen, K.; Lü, Z.; Ai, N.; Huang, X.; Zhang, Y.; Xin, X.; Zhu, R.; Su, W., Development of yttria-stabilized zirconia thin films via slurry spin coating for intermediate-to-low temperature solid oxide fuel cells. *Journal of Power Sources* **2006**, *160* (1), 436-438.

[31.] Hui, R.; Wang, Z.; Yick, S.; Maric, R.; Ghosh, D., Fabrication of ceramic films for solid oxide fuel cells via slurry spin coating technique. *Journal of Power Sources* **2007**, *172* (2), 840-844.

[32.] Kim, J. C.; Lee, D. Y.; Kim, H.-R.; Lee, H.-W.; Lee, J.-H.; Son, J.-W., Surface modification of anode substrate via nano-powder slurry spin coating for the thin film electrolyte of solid oxide fuel cell. *Thin Solid Films* **2011**, *519* (8), 2534-2539.

[33.]   Gurauskis, J., Deposition Via Dip Coating Technique of Dense Yttrium Stabilized Zirconia Layers. *International Journal of Applied Ceramic Technology* **2013**, *10* (1), 79-86.

[34.] Wang, Z.; Sun, K.; Shen, S.; Zhou, X.; Qiao, J.; Zhang, N., Effect of co-sintering temperature on the performance of SOFC with YSZ electrolyte thin films fabricated by dip-coating method. *Journal of Solid State Electrochemistry* **2009**, *14* (4), 637-642.

[35.] Lei, L.; Bai, Y.; Liu, Y.; Liu, J., An Investigation on Dip-Coating Technique for Fabricating Anode-Supported Solid Oxide Fuel Cells. *International Journal of Applied Ceramic Technology* **2015**, *12* (2), 351-357.

[36.] Schlupp, M. V. F.; Prestat, M.; Martynczuk, J.; Rupp, J. L. M.; Bieberle-Hütter, A.; Gauckler, L. J., Thin film growth of yttria stabilized zirconia by aerosol assisted chemical vapor deposition. *Journal of Power Sources* **2012**, *202*, 47-55.

[37.] Shim, J. H.; Chao, C.-C.; Huang, H.; Prinz, F. B., Atomic Layer Deposition of Yttria-Stabilized Zirconia for Solid Oxide Fuel Cells. *Chemistry of Materials* **2007**, *19* (15), 3850-3854.

[38.] Diehl, F.; Barbier, J.; Duprez, D.; Guibard, I.; Mabilon, G., Catalytic oxidation of heavy hydrocarbons over Pt/Al_2O_3. Influence of the structure of the molecule on its reactivity. *Applied Catalysis B: Environmental* **2010**, *95* (3), 217-227.

[39.] A. Wierzbicki, T.; Lee, I.; K. Gupta, A., *Combustion of propane with Pt and Rh catalysts in a meso-scale heat recirculating combustor*. 2014; Vol. 130, p 350–356.

[40.] Postole, G.; Nguyen, T.-S.; Aouine, M.; Gélin, P.; Cardenas, L.; Piccolo, L., Efficient hydrogen production from methane over iridium-doped ceria catalysts synthesized by solution combustion. *Applied Catalysis B: Environmental* **2015**, *166-167*, 580-591.

[41.] Lee, J. H.; Trimm, D. L., Catalytic combustion of methane. *Fuel Processing Technology* **1995**, *42* (2), 339-359.

[42.] Sabatini, S.; Kil, I.; Dekar, J.; Hamilton, T.; Wuttke, J.; Smith, M. A.; Hoffman, M. A.; Onori, S., A New Semi-Empirical Temperature Model for the Three Way Catalytic Converter. *IFAC-PapersOnLine* **2015**, *48* (15), 434-440.

[43.] Williams, S.; Hu, L.; Nakazono, T.; Ohtsubo, H.; Uchida, M., Oxidation Catalysts for Natural Gas Engine Operating under HCCI or SI Conditions. *SAE International Journal of Fuels and Lubricants* **2008**, *1*, 326-337.

[44.] Enterkin, J. A.; Setthapun, W.; Elam, J. W.; Christensen, S. T.; Rabuffetti, F. A.; Marks, L. D.; Stair, P. C.; Poeppelmeier, K. R.; Marshall, C. L., Propane Oxidation over Pt/SrTiO$_3$ Nanocuboids. *ACS Catalysis* **2011**, *1* (6), 629-635.

[45.] Stoukides, M.; Vayenas, C. G., The effect of electrochemical oxygen pumping on the rate and selectivity of ethylene oxidation on polycrystalline silver. *Journal of Catalysis* **1981**, *70* (1), 137-146.

[46.] Vayenas, C. G.; Bebelis, S.; Yentekakis, I. V.; Tsiakaras, P.; Karasali, H.; Karavasilis, C., Catalytic and Electrocatalytic Reactions in Solid Electrolyte Cells: The Nemca Effect. *Materials Science Forum* **1991**, *76*, 141-148.

[47.] Vayenas, C. G.; Bebelis, S.; Neophytides, S., non-Faradaic electrochemical modification of catalytic activity (NEMCA). *Journal of Physical Chemistry* **1988**, *92*.

[48.] Vayenas, C. G.; Bebelis, S.; Neophytides, S.; Yentekakis, I. V., non-Faradaic electrochemical modification of catalytic activity (NEMCA) in solid electrolyte. *Appiled Physical A* **1989**, *49*.

[49.] Vayenas, C. G., Promotion, Electrochemical Promotion and Metal–Support Interactions: Their Common Features. *Catalysis Letters* **2013**, *143* (11), 1085-1097.

[50.] Vayenas, C. G.; Brosda, S.; Pliangos, C., Rules and Mathematical Modeling of Electrochemical and Chemical Promotion. *Journal of Catalysis* **2001**, *203* (2), 329-350.

[51.] Brosda, S.; Vayenas, C. G., Rules and Mathematical Modeling of Electrochemical and Classical Promotion. *Journal of Catalysis* **2002**, *208* (1), 38-53.

[52.] Anastasijevic, N. A., NEMCA—From discovery to technology. *Catalysis Today* **2009**, *146* (3), 308-311.

[53.] Peng-ont, S.; Souentie, S.; Assabumrungrat, S.; Praserthdam, P.; Brosda, S.; Vayenas, C. G., Electrochemical promotion of propane oxidation over Pd, Ir, and Ru catalyst-electrodes deposited on YSZ. *Ionics* **2013**, *19* (12), 1705-1714.

[54.] de Lucas-Consuegra, A.; Dorado, F.; Valverde, J. L.; Karoum, R.; Vernoux, P., Low-temperature propene combustion over Pt/K-βAl$_2$O$_3$ electrochemical catalyst: Characterization, catalytic activity measurements, and investigation of the NEMCA effect. *Journal of Catalysis* **2007**, *251* (2), 474-484.

[55.] Bebelis, S.; Vayenas, C. G., Non-faradaic electrochemical modification of catalytic activity 6. Ethylene epoxidation on Ag deposited on stabilized ZrO$_2$. *Journal of Catalysis* **1992**, *138* (2), 588-610.

[56.] Theleritis, D.; Souentie, S.; Siokou, A.; Katsaounis, A.; Vayenas, C. G., Hydrogenation of CO$_2$ over Ru/YSZ Electropromoted Catalysts. *ACS Catalysis* **2012**, *2* (5), 770-780.

[57.] Bebelis, S.; Karasali, H.; Vayenas, C. G., Electrochemical promotion of CO2 hydrogenation on Rh/YSZ electrodes. *Journal of Applied Electrochemistry* **2008**, *38* (8), 1127-1133.

[58.] Neophytides, S.; Vayenas, C. G., Non-faradaic electrochemical modification of catalytic activity: 2. The case of methanol dehydrogenation and decomposition on Ag. *Journal of Catalysis* **1989**, *118* (1), 147-163.

[59.] Salazar, M.; Smotkin, E. S., Electrochemically promoted olefin isomerization reactions at polymer electrolyte fuel cell membrane electrode assemblies. *Journal of Applied Electrochemistry* **2006**, *36* (11), 1237-1240.

[60.] Yiokari, C. G.; Pitselis, G. E.; Polydoros, D. G.; Katsaounis, A. D.; Vayenas, C. G.,

High-Pressure Electrochemical Promotion of Ammonia Synthesis over an Industrial Iron Catalyst. *The Journal of Physical Chemistry A* **2000**, *104* (46), 10600-10602.

[61.] Giddey, S.; Badwal, S. P. S.; Kulkarni, A., Review of electrochemical ammonia production technologies and materials. *International Journal of Hydrogen Energy* **2013**, *38* (34), 14576-14594.

[62.] Chiang, P.-H.; Eng, D.; Stoukides, M., Electrocatalytic nonoxidative dimerization of methane over Ag electrodes. *Solid State Ionics* **1993**, *61* (1), 99-103.

[63.] Vayenas, C.; Koutsodontis, K., *Non-Faradaic electrochemical activation of catalysis*. 2008; Vol. 128, p 182506.

[64.] Zagoraios, D.; Athanasiadi, A.; Kalaitzidou, I.; Ntais, S.; Katsaounis, A.; Caravaca, A.; Vernoux, P.; Vayenas, C., Electrochemical Promotion of methane oxidation over nanodispersed Pd/Co$_3$O$_4$ catalysts. *Catalysis Today* **2019**.

[65.] Marnellos, G., Catalytic studies in electrochemical membrane reactors. *Solid State Ionics* **2004**, *175* (1-4), 597-603.

[66.] Kaloyannis, A.; Vayenas, C., *Non-Faradaic Electrochemical Modification of Catalytic Activity : 12. Propylene Oxidation on Pt*. 1999; Vol. 182, p 37–47.

[67.] Kaloyannis, A.; Vayenas, C. G., Non-faradaic electrochemical modification of catalytic activity: 11. Ethane oxidation on Pt. *Journal of Catalysis* **1997**, *171* (1), 148-159.

[68.] Tsampas, M. N.; Sapountzi, F. M.; Vernoux, P., Applications of yttria stabilized zirconia (YSZ) in catalysis. *Catalysis Science & Technology* **2015**, *5* (11), 4884-4900.

[69.] Preux, N.; Rolle, A.; Vannier, R. N., 12 - Electrolytes and ion conductors for solid oxide fuel cells (SOFCs). In *Functional Materials for Sustainable Energy Applications*, Kilner, J. A.; Skinner, S. J.; Irvine, S. J. C.; Edwards, P. P., Eds. Woodhead Publishing: 2012; pp 370-401.

[70.] Chroneos, A.; Yildiz, B.; Tarancón, A.; Parfitt, D.; A Kilner, J., *Oxygen Diffusion in Solid Oxide Fuel Cell Cathode and Electrolyte Materials: Mechanistic Insights from Atomistic Simulations*. 2011; Vol. 4.

[71.] Cambridge, U. o. Fuel Cells. https://www.doitpoms.ac.uk/tlplib/fuel-cells/printall.php (accessed 1 March).

[72.] Abraham, F.; Debreuille-Gresse, M. F.; Mairesse, G.; Nowogrocki, G., Phase transitions and ionic conductivity in $Bi_4V_2O_{11}$ an oxide with a layered structure. *Solid State Ionics* **1988**, *28-30*, 529-532.

[73.] Cho, H.; Sakai, G.; Shimanoe, K.; Yamazoe, N., Preparation of BiMeVO x (Me = Cu, Ti, Zr, Nb, Ta) compounds as solid electrolyte and behavior of their oxygen concentration cells. *Sensors and Actuators B-chemical - SENSOR ACTUATOR B-CHEM* **2005**, *109*, 307-314.

[74.] Joubert, O.; Jouanneaux, A.; Ganne, M., Crystal structure of low-temperature form of bismuth vanadium oxide determined by rietveld refinement of X-ray and neutron diffraction data (α - $Bi_4V_2O_{11}$). *Materials Research Bulletin* **1994**, *29* (2), 175-184.

[75.] Sabolsky, E. M.; Razmyar, S.; Sabolsky, K., Microstructural, electrical, and mechanical characterization of $Bi_2Cu_{0.1}V_{0.9}O_{5.35}$ (BICUVOX) ceramics fabricated from co-precipitated precursor powders. *Journal of Materials Science* **2013**, *48* (2), 733-743.

[76.] Simner, S. P.; Suarez-Sandoval, D.; Mackenzie, J. D.; Dunn, B., Synthesis, Densification, and Conductivity Characteristics of BICUVOX Oxygen-Ion-Conducting Ceramics. *Journal of the American Ceramic Society* **1997**, *80* (10), 2563-2568.

[77.] Pernot, E.; Anne, M.; Bacmann, M.; Strobel, P.; Fouletier, J.; Vannier, R. N.; Mairesse, G.; Abraham, F.; Nowogrocki, G., Structure and conductivity of Cu and Ni-substituted $Bi_4V_2O_{11}$ compounds. *Solid State Ionics* **1994**, *70-71*, 259-263.

[78.] Skinner, S. J.; Kilner, J. A., Oxygen ion conductors. *Materials Today* **2003**, *6* (3), 30-37.

[79.] Stoukides, M.; Vayenas, C. G., Solid-electrolyte-aided study of the ethylene oxidation on polycrystalline silver. *Journal of Catalysis* **1981**, *69* (1), 18-31.

[80.] Fee, M. A. Electrochemical Investigation of Thin Nickel, Copper and Silver Films Interfaced with Yttria-Stabilized Zirconia University of Ottawa, Ottawa, 2013.

[81.] Lizarraga, L.; Guth, M.; Billard, A.; Vernoux, P., *Electrochemical catalysis for propane combustion using nanometric sputtered-deposited Pt films*. 2010; Vol. 157, p 61-65.

[82.] Peng-ont, S. ELECTROPROMOTED PROPANE OXIDATION ON SPUTTER-

DEPOSITED Pd, Ir, Ru, AND Cu CATALYST-ELECTRODES ON YSZ AND MODIFICATION OF Pd CATALYST WITH MnxOy INTERLAYER FOR FURTHER IMPROVEMENT. Disteration, Chulalongkorn University, Bangkok, 2013.

[83.] Taroco, H. A.; Santos, J. A. F.; Domingues, R. Z.; Matencio, T., Ceramic Materials for Solid Oxide Fuel Cells In *Advances in Ceramics - Synthesis and Characterization, Processing and Specific Applications* Sikalidis, C., Ed. Intecth: Brasil, 2011; p 26.

[84.] Wang, Z.; Sun, K.; Shen, S.; Zhang, N.; Qiao, J.; Xu, P., Preparation of YSZ thin films for intermediate temperature solid oxide fuel cells by dip-coating method. *Journal of Membrane Science* 2008, *320* (1-2), 500-504.

[85.] Von Dollen, P.; Barnett, S., A Study of Screen Printed Yttria-Stabilized Zirconia Layers for Solid Oxide Fuel Cells. *Journal of the American Ceramic Society* 2005, *88* (12), 3361-3368.

[86.] Somalu, M. R.; Yufit, V.; Shapiro, I. P.; Xiao, P.; Brandon, N. P., The impact of ink rheology on the properties of screen-printed solid oxide fuel cell anodes. *International Journal of Hydrogen Energy* 2013, *38* (16), 6789-6801.

[87.] Tikkanen, H.; Suciu, C.; Wærnhus, I.; Hoffmann, A. C., Examination of the co-sintering process of thin 8YSZ films obtained by dip-coating on in-house produced NiO–YSZ. *Journal of the European Ceramic Society* 2011, *31* (9), 1733-1739.

[88.] Sumi, H.; Shimada, H.; Sato, K.; Hashida, T., Estimation of micro-size defects in electrolyte thin-film by X-ray stress measurement for anode-supported solid oxide fuel cells. *Mechanical Engineering Journal* 2016.

[89.] Kim, S.-D.; Lee, J.-J.; Moon, H.; Hyun, S.-H.; Moon, J.; Kim, J.; Lee, H.-W., Effects of anode and electrolyte microstructures on performance of solid oxide fuel cells. *Journal of Power Sources* 2007, *169* (2), 265-270.

[90.] Matei, F.; Jiménez-Borja, C.; Canales-Vázquez, J.; Brosda, S.; Dorado, F.; Valverde, J. L.; Ciuparu, D., Enhanced electropromotion of methane combustion on palladium catalysts deposited on highly porous supports. *Applied Catalysis B: Environmental* 2013, *132-133*, 80-89.

[91.] Tsampas, M. N.; Sapountzi, F. M.; Boréave, A.; Vernoux, P., Isotopical labeling

mechanistic studies of electrochemical promotion of propane combustion on Pt/YSZ. *Electrochemistry Communications* **2013**, *26*, 13-16.

[92.] Souentie, S.; Lizarraga, L.; Papaioannou, E. I.; Vayenas, C. G.; Vernoux, P., Permanent electrochemical promotion of C_3H_8 oxidation over thin sputtered Pt films. *Electrochemistry Communications* **2010**, *12* (8), 1133-1135.

[93.] Bebelis, S.; Kotsionopoulos, N., Non-faradaic electrochemical modification of the catalytic activity for propane combustion of Pt/YSZ and Rh/YSZ catalyst-electrodes. *Solid State Ionics* **2006**, *177* (26), 2205-2209.

[94.] Marwood, M.; Vayenas, C. G., Electrochemical Promotion of Electronically Isolated Pt Catalysts on Stabilized Zirconia. *Journal of Catalysis* **1997**, *168* (2), 538-542.

[95.] Tsampas, M. N.; Vernoux, P., Chapter 11 - Electrochemical Promotion of Catalysis for Automotive Post-Treatment and Air Cleaning. In *New and Future Developments in Catalysis*, Suib, S. L., Ed. Elsevier: Amsterdam, 2013; pp 281-302.

[96.] Shi, J. L.; Yen, T. S.; Schubert, H., Effect of small amounts of additives on the sintering of high-purity Y-TZP. *Journal of Materials Science* **1997**, *32* (5), 1341-1346.

[97.] Bowen, C.; Ramesh, S.; Gill, C.; Lawson, S., Impedance spectroscopy of CuO-doped Y-TZP ceramics. *Journal of Materials Science* **1998**, *33* (21), 5103-5110.

[98.] Yang, F., Effects of ZnO Sintering Additive on the Sintering Behavior and Conductivity of YSZ Solid Electrolyte. *International Journal of Electrochemical Science* **2017**, *12*, 8295-8305.

[99.] Lewis, G. S.; Atkinson, A.; Steele, B. C. H., Cobalt additive for lowering the sintering temperature of yttria-stabilized zirconia. *Journal of Materials Science Letters* **2001**, *20* (12), 1155-1157.

[100.] Kim, H. LOW TEMPERATURE SINTERING OF NANOSIZED CERAMIC POWDER:YSZ-BISMUTH OXIDE SYSTEM. The Ohio State University, Columbus, Ohio, 2004.

[101.] Takahashi, T.; Esaka, T.; Iwahara, H., Conduction in Bi_2O_3-based oxide ion conductors under low oxygen pressure. I. Current blackening of the Bi_2O_3-Y_2O_3 electrolyte. *Journal of Applied Electrochemistry* **1977**, *7* (4), 299-302.

[102.] Nagao, M.; Kobayashi, K.; Hibino, T., Low-temperature Sintering of Yttria-stabilized Zirconia Using Bismuth–Vanadium Oxide as a Sintering Aid at 800 °C. *Chemistry Letters* **2014**, *43*, 1887-1889.

[103.] Christian, C.; Amine, B.; Caroline, P., 3 Polyvinyl Butyral. In *Handbook of Thermoplastics, Second Edition*, 2015.

[104.] Cui, Q.; Dong, X.; Wang, J.; Li, M., Direct fabrication of cerium oxide hollow nanofibers by electrospinning. *Journal of Rare Earths* **2008**, *26* (5), 664-669.

[105.] He, S.; He, H.; Li, Y.; Wang, D., Effects of maleic anhydride grafted polyethylene on rheological, thermal, and mechanical properties of ultra high molecular weight polyethylene/poly(ethylene glycol) blends. *Journal of Applied Polymer Science* **2015**, *132* (43).

[106.] Muccillo, R.; de Florio, D.; Muccillo, E., Equimolar Yttria-Stabilized Zirconia and Samaria-Doped Ceria Solid Solutions. *Ceramics* **2018**, *1*, 343-352.

[107.] Zalga, A.; Abakevičienė, B.; Zarkov, A.; Beganskienė, A.; Kareiva, A.; Tamulevičius, S., On the Properties of Yttria-Stabilized Zirconia Thin Films Prepared by Sol-Gel Method. *Materials Science* **2011**, *17*.

[108.] Beck, G.; Fischer, H.; Mutoro, E.; Srot, V.; Petrikowski, K.; Tchernychova, E.; Wuttig, M.; Rühle, M.; Luerßen, B.; Janek, J., Epitaxial Pt(111) thin film electrodes on YSZ(111) and YSZ(100) — Preparation and characterisation. *Solid State Ionics* **2007**, *178* (5), 327-337.

[109.] Kambolis, A.; Lizarraga, L.; Tsampas, M. N.; Burel, L.; Rieu, M.; Viricelle, J. P.; Vernoux, P., Electrochemical promotion of catalysis with highly dispersed Pt nanoparticles. *Electrochemistry Communications* **2012**, *19*, 5-8.

[110.] Kang, M.; Fang, J.; Li, S.; Liu, T.; Wang, C.; Tan, L., Effect of Electrode Morphology on the Electrochemical Performance of Pt/YSZ Electrodes. *International Journal of Electrochemical Science* **2013**, *8*, 12757-12768.

[111.] Bachmann, C. Kinetic, electrochemical and spectroscopic investigation of the oxidation of CO and C_2H_4 on YSZ-supported metal model electrodes. Universitätsbibliothek, Gießen, 2015.

[112.] Tsiplakides, D.; Vayenas, C. G., Temperature Programmed Desorption of Oxygen from Ag Films Interfaced with Y_2O_3-Doped ZrO_2. *Journal of Catalysis* **1999**, *185* (2), 237-251.

[113.] Palermo, A.; Tikhov, M. S.; Filkin, N. C.; Lambert, R. M.; Yentekakis, I. V.; Vayenas, C. G., Electrochemical promotion of NO reduction by CO and by propene. In *Studies in Surface Science and Catalysis*, Hightower, J. W.; Nicholas Delgass, W.; Iglesia, E.; Bell, A. T., Eds. Elsevier: 1996; Vol. 101, pp 513-522.

[114.] Somalu, M. R.; Yufit, V.; Brandon, N. P., The effect of solids loading on the screen-printing and properties of nickel/scandia-stabilized-zirconia anodes for solid oxide fuel cells. *International Journal of Hydrogen Energy* **2013**, *38* (22), 9500-9510.

[115.] Zhang, T.; ma, J.; Kong, L. B., Mechanochemical synthesis of nano-sized $Bi_2V_{0.9}Cu_{0.1}O_{5.35}$ powders. *Journal of Materials Research - J MATER RES* **2006**, *21*, 71-74.

[116.] Khaerudini, D. S.; Guan, G.; Zhang, P.; Abudula, A., Oxide ion conductors based on niobium-doped bismuth vanadate: conductivity and phase transition features. *Ionics* **2016**, *22* (1), 93-97.

[117.] Kong, D.; Qi, J.; Liu, D.; Zhang, X.; Pan, L.; Zou, J., Ni-Doped $BiVO_4$ with V^{4+} Species and Oxygen Vacancies for Efficient Photoelectrochemical Water Splitting. *Transactions of Tianjin University* **2019**, *25* (4), 340-347.

[118.] Merupo, V.-I.; Velumani, S.; Ordon, K.; Errien, N.; Szade, J.; Kassiba, A.-H., Structural and optical characterization of ball-milled copper-doped bismuth vanadium oxide ($BiVO_4$). *CrystEngComm* **2015**, *17* (17), 3366-3375.

[119.] Mali, S. S.; Park, G. R.; Kim, H.; Kim, H. H.; Patil, Jyoti V.; Hong, C. K., Synthesis of nanoporous $Mo:BiVO_4$ thin film photoanodes using the ultrasonic spray technique for visible-light water splitting. *Nanoscale Advances* **2019**, *1* (2), 799-806.

[120.] Jiang, F.; Zhou, R.; Yao, Z.; Du, Y.; Xu, J.; Yang, P.; Wang, C., Facile Fabrication of Pt-Cu Nanoclusters-Decorated Porous Poly(5-cyanoindole) with High Electrocatalytic Activity. *International Journal of Electrochemical Science* **2011**, *6*.

[121.] Lan, Y.-Q.; Li, J.-S.; Dong, H.-Q.; Li, S.-L.; Li, R.-H.; Bao, J.; Dai, Z., Polyoxometalate-assisted green fabrication of Pd nanoparticles/reduced graphene oxide

nanocomposite with enhanced methanol-tolerance for the oxygen reduction reaction. *New J. Chem.* **2015**, *40*.

[122.] He, R.; Zhou, J.; Fu, H.; Zhang, S.; Jiang, C., Room-temperature in situ fabrication of Bi_2O_3/g-C_3N_4 direct Z-scheme photocatalyst with enhanced photocatalytic activity. *Applied Surface Science* **2017**.

[123.] Zhang, Y.; Zheng, J.; Wang, Q.; Hu, T.; Meng, C., Hydrothermal synthesis of vanadium dioxides/carbon composites and their transformation to surface-uneven V_2O_5 nanoparticles with high electrochemical properties. *RSC Advances* **2016**, *6* (96), 93741-93752.

[124.] Murasheva, V. V.; Poletaeva, N. A.; Fortalnova, E. A.; Safronenko, M. G.; Politova, E. D.; Kurilkin, V. V.; Venskovskii, N. U., Phase formation of BICUVOX solid solutions. *Russian Journal of Inorganic Chemistry* **2010**, *55* (12), 1867-1873.

[125.] Politova, E. D.; Fortalnova, E. A.; Poletaeva, N. A.; Kaleva, G. M.; Mosunov, A. V.; Safronenko, M. G.; Venskovskii, N. U., Ferroelectric Phase Transitions in Ionic Conducting BICUVOX Ceramics. *Ferroelectrics* **2009**, *379* (1), 35-42.

[126.] PaŚciak, G.; Chmielowiec, J.; Chan, S. H., Thermal and structural study of BIVOX undoped and doped with La in various atmosphere toward applications in IT-SOFC. *Ceramics International* **2014**, *40* (7, Part A), 8969-8974.

[127.] Batista, R. M.; Muccillo, E. N. S., Densification and grain growth of 8YSZ containing NiO. *Ceramics International* **2011**, *37* (3), 1047-1053.

[128.] Jamil, S. M.; Dzarfan Othman, M. H.; Rahman, M. A.; Jaafar, J.; Ismail, A. F.; Mohamed, M. A., Role of lithium oxide as a sintering aid for a CGO electrolyte fabricated via a phase inversion technique. *RSC Advances* **2015**, *5* (72), 58154-58162.

[129.] Lee, J.-A.; Lee, H.-C.; Heo, Y.-W.; Lee, J.-H.; Kim, J.-J., Effect of Li doping on sintering characteristics and microstructural behavior of yttria-stabilized zirconia. *Ceramics International* **2016**, *42* (15), 17339-17346.

[130.] Ahmad, S. I.; Mohammed, T.; Bahafi, A.; Suresh, M. B., Effect of Mg doping and sintering temperature on structural and morphological properties of samarium-doped ceria for IT-SOFC electrolyte. *Applied Nanoscience* **2017**, *7* (5), 243-252.

[131.] Ahn, C.-W.; Song, H.-C.; Park, S.-H.; Nahm, S.; Uchino, K.; Priya, S. J.; Lee, H.-G.; Kang, N.-K., Low temperature sintering and piezoelectric properties in $Pb(Zr_xTi_{1-x})O_3$-$Pb(Zn_{1/3}Nb_{2/3})O_3$-$Pb(Ni_{1/3}Nb_{2/3})O_3$ ceramics. *Japanese Journal of Applied Physics* **2005**, *44*, 1314-1321.

[132.] Falgairette, C.; Jaccoud, A.; Fóti, G.; Comninellis, C., The phenomenon of "permanent" electrochemical promotion of catalysis (P-EPOC). *Journal of Applied Electrochemistry* **2008**, *38* (8), 1075-1082.
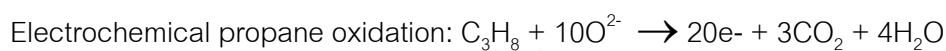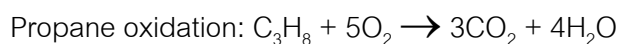
APPENDICES

APPENDIX A

CALCULATION FOR THE RATE ENHANCEMENT RATIO AND

FARADAIC EFFICIENCY

In this work, total reaction consists catalytic and electrochemical part:

Propane oxidation: $C_3H_8 + 5O_2 \longrightarrow 3CO_2 + 4H_2O$

Electrochemical propane oxidation: $C_3H_8 + 10O^{2-} \longrightarrow 20e- + 3CO_2 + 4H_2O$

Follow equation 2.4 and 2.5 in chapter 2

The rate enhancement ratio, ρ

$$\rho = \frac{r}{r_0}$$

Where r = the electrochemically promoted catalytic rate (close circuit)

r_0 = the catalytic rate at unpromoted condition (open circuit)

The faradaic efficiency, Λ

$$\Lambda = \frac{r-r_0}{(I/nF)} \cong \frac{\Delta r}{(I/nF)}$$

where I is the applied current

n is the charge of the sacrificed ions (in YSZ case, n = 2)

F is Faraday's constants (96485 C/mol)

For example, NEMCA of propane oxidation on Pt/dip-coated YSZ thin-film cell was observed at 400 $^{\circ}$C and applied potential between Pt and Au electrode at 0.2 V.

Feed inlet gas C_3H_8 16.67 cm^3/min, O_2 25 cm^3/min and He 58.33 cm^3/min

No catalyst (thermal, support and counter effect) can obtain CO_2 concentration = 0.043 %vol.

At open circuit condition can obtain CO_2 concentration = 0.150 %vol.

At close circuit condition (applied potential = 0.2 V) can obtain CO_2 concentration = 0.161 %vol., and record cell current = 6.15×10^{-7} A (6.15×10^{-7} C/s)

$$r_0 = \frac{\frac{0.150}{100} \times (16.67+25+58.33) \frac{cm^3}{min} \times \frac{1min}{60\ s} \times 10^5 Pa}{8314000 \frac{cm^3 Pa}{K\ mol} \times (400+273.15)K} = 1.06216 \times 10^{-8}\ mole/s$$

$$r = \frac{\frac{0.161}{100} \times (16.67+25+58.33) \frac{cm^3}{min} \times \frac{1min}{60\ s} \times 10^5 Pa}{8314000 \frac{cm^3 Pa}{K\ mol} \times (400+273.15)K} = 1.17135 \times 10^{-8}\ mole/s$$

Therefore, the rate enhancement ratio, ρ

$$\rho = \frac{1017135 \times 10^{-8} \frac{mol}{s}}{1.06216 \times 10^{-8} \frac{mol}{s}} = 1.102804$$

and the faradaic efficiency, Λ at cell current = 6.15×10^{-7} C/s

$$\Lambda = \frac{\frac{10}{3}\left(\left(1.17135 \times 10^{-7}\right) - \left(1.06216 \times 10^{-7}\right)\right) \frac{mol}{s}}{\dfrac{6.15 \times 10^{-7} \frac{C}{s}}{96485 \frac{C}{mol}}} = 1142$$

88

APPENDIX B

CACULATION FOR METAL CONCENTRATION IN SYTHESIZED

BICUVOX.10 POWDER

ICP-OES analyzed metal concentration and calculated by standard calibration method. This experiment generates three metals standard calibration curves including bismuth (Bi), vanadium (V), and copper (Cu). The standard calibration curves of each metal display in Figure B.1-3.
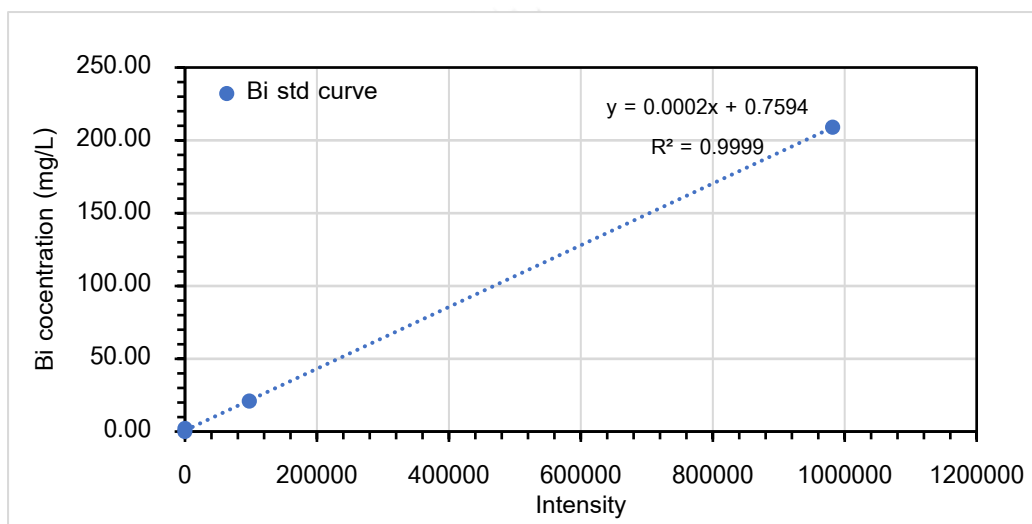

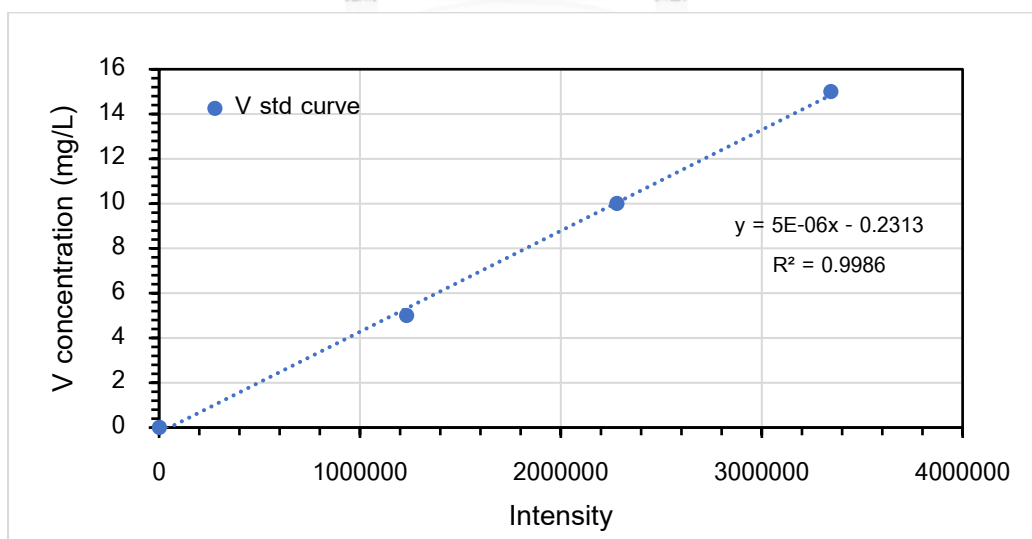*Figure B. 1* Standard calibration curve of Bi^{3+} from ICP-OES analysis.

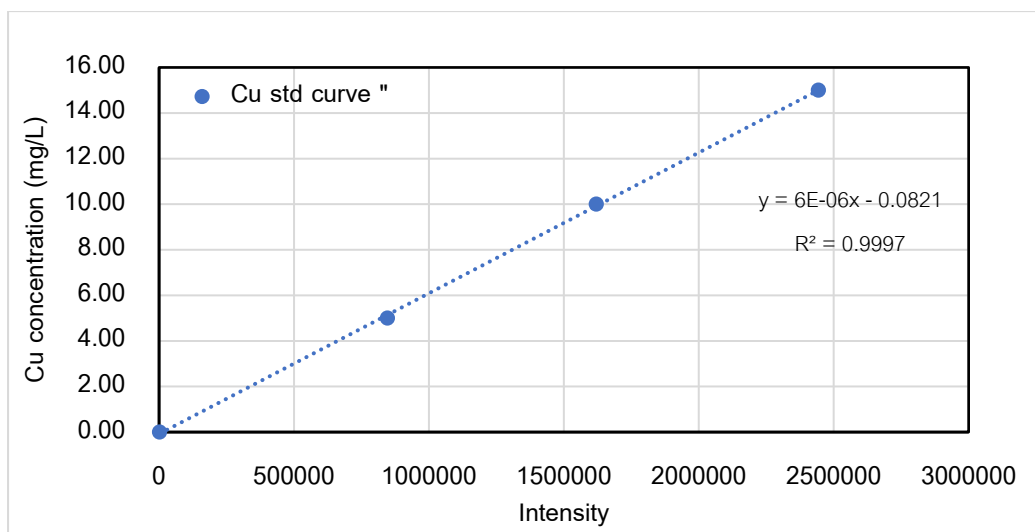*Figure B. 2* Standard calibration curve of V^{5+} from ICP-OES analysis.

Figure B. 3 Standard calibration curve of Cu^{2+} from ICP-OES analysis.

For example, 0.01109 g. of BICUVOX.10 powder was dissolved and made up the volume by 5%v/v of HNO_3 solution in a 100 ml volumetric flask.

From ICP-OES result, Bi^{3+} obtain intensity = 411926,

$$V^{5+} \text{obtain intensity} = 1906302.9$$

$$\text{And } Cu^{2+} \text{obtain intensity} = 186735.6$$

Calculate the concentration of each metal follows the linear equation in fig. 43-45

For Bi^{3+} case,

$$\left[Bi^{3+}\right]=0.0002\left(411926\right)+0.7594=83.1446 \ \frac{mg}{l}$$

Therefore, 0.01109 g. of BICUVOX.10 powder have Bi^{3+}:

$$Bi= \frac{\left(83.1446 \ \frac{mg}{l}\right) \times \left(100 \ ml\right)}{\left(\frac{1000 \ mg}{1 \ g}\right) \times \left(\frac{1000ml}{1 \ l}\right)} = 0.00832 \text{ g of Bi}$$

$$\%Bi= \frac{0.00832 \text{ g of Bi}}{0.01109 \text{ g of BICUVOX.10}} \times 100 = 74.97\% \text{ of Bi}$$

In the case of V^{5+},

$$[V^{5+}] = \left(\left(5 \times 10^{-6} \right) \times 1906302.9 \right) - 0.2313 = 9.300 \; \frac{mg}{l}$$

Therefore, 0.01109 g. of BICUVOX.10 powder have V^{5+}:

$$V = \frac{\left(9.300 \; \frac{mg}{l} \right) \times \left(100 \; ml \right)}{\left(\frac{1000 \; mg}{1 \; g} \right) \times \left(\frac{1000 \; ml}{1 \; l} \right)} = 0.000930 \; g \; of \; V$$

$$\%V = \frac{0.000930 \; g \; of \; V}{0.01109 \; g \; of \; BICUVOX.10} \times 100 = 8.39\% \; of \; V$$

In the case of Cu^{2+},

$$[Cu^{2+}] = \left(\left(6 \times 10^{-6} \right) \times 186735.6 \right) - 0.0821 = 1.0383 \; \frac{mg}{l}$$

Therefore, 0.01109 g. of BICUVOX.10 powder have Cu^{2+}:

$$Cu = \frac{\left(1.0383 \; \frac{mg}{l} \right) \times \left(100 \; ml \right)}{\left(\frac{1000 \; mg}{1 \; g} \right) \times \left(\frac{1000 \; ml}{1 \; l} \right)} = 0.00010383 \; g \; of \; Cu$$

$$\%Cu = \frac{0.00010383 \; g \; of \; Cu}{0.01109 \; g \; of \; BICUVOX.10} \times 100 = 1.0383\% \; of \; Cu$$

Table B. 1 Elemental analysis data from ICP-OES and EDS mapping

Element	Theory	ICP-OES	EDS mapping
	% mass	% mass	% mass
O	15.401	N/A	20.992±2.321
Bi	75.206	73.590±2.392	67.595±2.055
V	8.249	8.490±0.339	8.394±0.597
Cu	1.143	0.953±0.0336	3.018±0.626

APPENDIX C

TGA-DTG of screen printing YSZ thin film
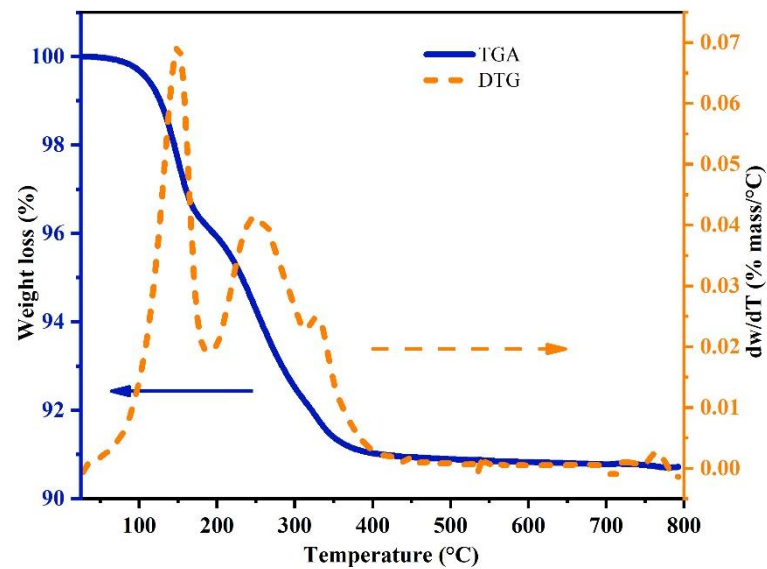

Figure C. 1 TGA and DTG curve for thermal analysis of screen printing YSZ thin film

TGA analyzes the thermal degradation of screen printing film that shows in Figure C.1. The organic ingredients decomposed below the sintering temperature that confirms that the YSZ and their composites thin-film without the organic compound in structure similar to the discussion in topic 5.1.

APPENDIX D
EDS mapping of YSZ/BICUVOX.10

EDS mapping used for the analysis of element dispersion on YSZ/BICUVOX.10 screen printing thin-film. The results are shown in Table D.1-4 that is higher of Bi, V, and Cu dispersion concentration to the additional amount of BICUVOX.10 increase.

Table D. 1 *Element dispersion on 1.5% mole BICUVOX.10/YSZ*

Element	Wt%	At%
OK	17.03	53.82
YL	12.42	07.07
ZrL	67.68	37.53
BiM	01.40	00.34
VK	00.39	00.39
CuK	01.08	00.86
Matrix	Correction	ZAF

Table D. 2 *Element dispersion on 2.5% mole BICUVOX.10/YSZ*

Element	Wt%	At%
OK	19.76	58.53
YL	12.00	06.39
ZrL	64.51	33.51
BiM	02.52	00.57
VK	00.45	00.42
CuK	00.76	00.57
Matrix	Correction	ZAF

Table D. 3 Element dispersion on 3.5% mole BICUVOX.10/YSZ

Element	Wt%	At%
OK	16.07	52.36
YL	11.96	07.01
ZrL	66.02	37.73
BiM	03.72	00.93
VK	00.68	00.70
CuK	01.55	01.27
Matrix	Correction	ZAF

Table D. 4 Element dispersion on 4.5% mole BICUVOX.10/YSZ

Element	Wt%	At%
OK	18.24	56.29
YL	10.86	06.03
ZrL	64.33	34.82
BiM	04.44	01.05
VK	00.77	00.75
CuK	01.37	01.06
Matrix	Correction	ZAF

VITA

NAME   Wanchana Lelalertsupakul

DATE OF BIRTH   13 October 1994

PLACE OF BIRTH   Bangkok

INSTITUTIONS ATTENDED   Department of Industrial Chemistry, Faculty of Applied
                        Science, NorthKing Mongkut,s University Technology of
                        North Bangkok

HOME ADDRESS   34, Besides Somdet Phra Pinklao Hospital 15 Alley, Soi
                        Taksin 22, Somdet Phra Chao Taksin Road, Bukkhalo
                        Subdistrict, Thonburi District, Bangkok

PUBLICATION   Wanchana Lelalertsupakul, Palang Bumroongsakulsawat,
                        "Non-Faradaic Electrochemical Modification of Catalytic
                        Activity (NEMCA) of propane oxidation at Pt/YSZ thin film on
                        α-alumina", Proceeding of The Pure and Applied Chemistry
                        International Conference 2019, BITEC, Bangna, Bangkok,
                        Thailand, February 7th-8th, 2019